MicroRNA-223-mediated neutrophilic inflammation in Community Acquired Pneumonia

Inaugural-Dissertation
to obtain the academic degree
Doctor rerum naturalium (Dr. rer. nat.)
submitted to the Department of Biology, Chemistry and Pharmacy of Freie Universität Berlin

by

MS Cengiz Gökeri

2019

Commencement of doctoral studies: April 2015

Completion of doctoral studies: June 2019

Supervisors: Dr.-Ing. Geraldine Nouailles & Prof. Dr. Martin Witzenrath

Undertaken at: Charité – Universitätsmedizin Berlin, Division of Pulmonary Inflammation

1st Reviewer: Prof. Dr. Martin Witzenrath

2nd Reviewer: Prof. Dr. Rupert Mutzel

Date of defense: 17.09.2019

Deutsch: Ich erkläre, dass ich diese Arbeit selbst verfasst und keine anderen als die angegebenen Quellen und Hilfsmittel benutzt habe.

English: I hereby declare that I have authored this thesis independently and have not used sources other than those that have been declared.

Cengiz Gökeri

Berlin, den 13.06.2019

Table of contents

1. Introduction

1.1. Community Acquired Pneumonia

Community Acquired Pneumonia (CAP) remains one of the foremost causes of lethality worldwide, with an estimated 1.6 million deaths provoked by its leading causative pathogen, *Streptococcus pneumoniae* (S. pn.) [1]. In fact, according to the Institute for Health Metrics and Evaluation, lower respiratory tract infections remain in the top 4 causes of global mortality [2] (depicted in Fig. 1). Although every individual is potentially susceptible to the development of pneumonia, major groups at risk include individuals with weakened, suppressed or absent immunity, such as children below the age of 5 and the elderly [3], asplenic individuals [3], human immunodeficiency virus (HIV) patients [4], individuals with respiratory, renal or metabolic comorbidities and chronic obstructive pulmonary disease (COPD) patients undertaking inhaled medications such as corticosteroids [5].

CAP is described as an acute infection of the lower respiratory tract with early symptoms including cough, fever and new focal chest signs [3] such as reduced expansion of the chest, reduced entry of air and bronchial breathing [6]. Upon the initiation of pneumococcal pathogenesis, a typical virulence feature of S. pn. is the ability to breach the epithelial-endothelial lung barrier through the transformation of epithelial cells (EpiC), which may result in systemic disease that may lead to sepsis and the spread of bacteria into secondary lymphoid organs [7].

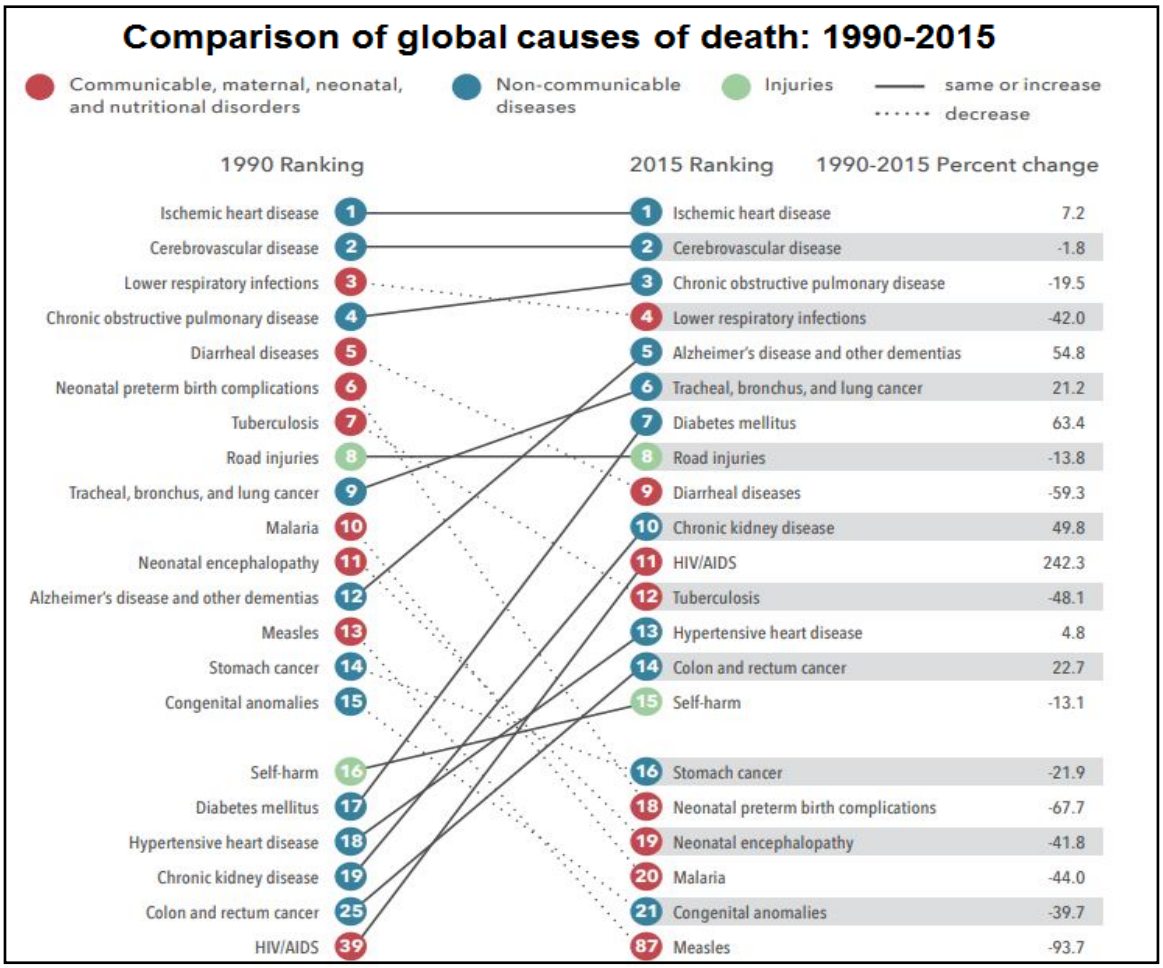

Figure 1. Incidences of global mortality rates from 1990-2015 (adapted from IHME, 2016) [2].

1.1.1. CAP – antibiotic therapy

Despite a general consensus of prominent governmental and independent bodies including the National Institute for Clinical Excellence, British Thoracic Society and American Thoracic Society recommending the use of β-lactam antibiotics to manage pneumococcal disease in CAP patients [8, 9], identifying the causative pathogen in a short time frame remains challenging [8]. Clinical studies have shown that the importance of early antibiotic treatment (commenced less than 4 hours following hospital admission) should not be underestimated or disregarded, with reduced in-hospital mortality [10, 11] and length of stay [10] exhibited in early treated patients a grave indicator of the significance of quick intervention. Hence, customized and rapid treatment strategies for critically ill patients, coupled to the development of cutting edge diagnostic and prognostic markers, of paramount importance.

1.1.2. CAP – vaccination strategies

Pneumococci account for around 50% of bacterial septicemia cases in asplenic patients [12]. Comprised of encapsulated and unencapsulated variants [13], more than 90 capsular serotypes have been identified [14]. While the polysaccharide capsule represents a major virulence factor for the bacteria to evade host immunity, its immunogenicity has helped in the development of a 23-valent pneumococcal polysaccharide vaccine (PPCV23) which covers serotype-sensitive protection of 88% of bacteremic pneumococcal infections in the USA and 96% of those in the UK [13]. In fact, cases of invasive pneumococcal disease (IPD) in children decreased dramatically from 95 per 100,000 in 1998 (pre-introduction of the 7-valent pneumococcal conjugate vaccine (PCV7)) to only 2 per 100,000 in 2016 (depicted in Fig. 2) [15], indicating the substantial impact of the pneumococcal vaccine. However, the ability of S. pn. to undergo horizontal gene transfer, coupled to the widespread geographical and temporal distribution of the various serotypes, have hindered universal vaccine development strategies [13] offering global protection.

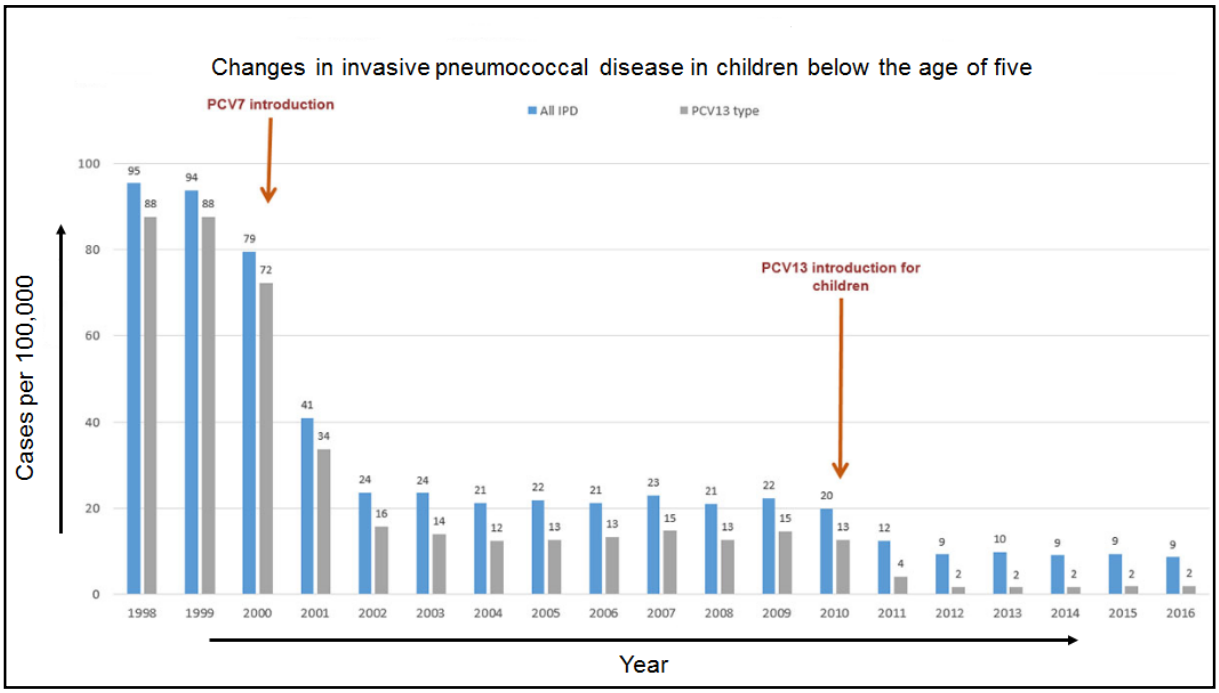

Figure 2. Impact of pneumococcal vaccine introduction on IPD rates in children in the US (adapted from CDC – Surveillance and Reporting) [15].

1.2. *Streptococcus pneumoniae*

S. pn. (or pneumococci) are classified as Gram-positive diplococci that are causative for various conditions ranging from relatively mild respiratory tract infections to severe pneumonia and septicemia [12]. Depending on the serotype, pneumococci may either colonize the upper respiratory tract, leading to carriage of the bacteria, or infiltrate the lower respiratory tract which may result in IPD - features adopted to ensure the viability and effective transmission of the pathogen [16].

1.2.1. Structural components and virulence of *Streptococcus pneumoniae*

1.2.1.1. Immune evasion and adherence

Colonizing serotypes of S. pn. are specialized in resisting classical host defense mechanisms of the upper airways such as the mucus layer. A common trait harbored by colonizing S. pn. is the possession of a large negatively charged polysaccharide capsule that is utilized by the pathogen to repel the host mucopolysaccharide that contains like-charged sialic acid residues, thereby resisting being trapped in the thick mucus layer [17]. Whilst the capsule is protective against mucociliary clearance, it creates unfavorable conditions for bacterial adherence to the host nasopharynx; hence S. pn. have developed the ability to alter their capsule composition – termed phase variation – to overcome this obstacle [18]. The capsule offers further protection to S. pn. by means of evading phagocytosis by neutrophils and macrophages and also neutrophil-mediated neutrophil extracellular traps (NETs) capture [19].

Lipoteichoic acid (LTA), an amphiphilic cell wall constituent expressed in most Gram-positive bacteria [20], is a major virulence factor for S. pn. serotype 4 (TIGR4)-mediated pathogenesis and structural changes to the bacterial surface may allow incorporation of cationic D-alanine into the LTA as a mechanism to repel cationic antimicrobial peptides (AMPs) utilized by neutrophils for antimicrobial defense [19].
Choline-binding proteins such as the pneumococcal surface protein (Psp)A and PspC bulge from the bacterial cell wall through the capsular surface and yield virulence by obstructing host anti-bacterial defense [21]. PspA has been

demonstrated to inhibit activation of factor B-mediated complement in vivo, while also inhibiting C3b deposition and processing in vitro [22]. Although the exposure of the PspA N-terminal at the surface renders the protein as an immunogen and has been described to generate protective antibodies [21], certain S. pn. serotype 2 strains such as D39, may thwart the actions of protective immunoglobulins generated against PspA [23]. While PspC has been described widely to be important in complement evasion and critical for bacterial virulence, sepsis and colonization, the degree of mortality in mice upon infection with PspC-deficient pneumococci varies depending on the serotype utilized for infection. Intranasal challenge with PspC-deficient TIGR4 improved survival of MF1 mice by more than 75% compared to wild-type TIGR4 infection, whereas mortality rates remain unchanged in MF1 mice upon intranasal challenge with wild-type and PspC-deficient D39 [24].

Pneumococcal surface antigen (Psa)A is another surface protein that has been described as an adhesin [25] and immunogen capable of being utilized as a possible vaccine candidate [26], whilst its prime function is to serve as a manganese transporter [27]. Manganese is a crucial cofactor in S. pn. metabolism, regulating processes such as glycolysis, gluconeogenesis and peptide cleavage [25]. S. pn. PsaA-mutant strains display reduced adherence to type II pneumocytes relative to wild-type D39 [28], while the role of PsaA in pneumococcal-associated virulence and mortality varies with different S. pn. serotypes; mice infected with PsaA-deficient TIGR4 exhibited 100% survival compared to WT TIGR4 infection, however no difference in virulence was observed for WT and PsaA-deficient D39 [27]. Pneumococci also express other adhesins on their outer surface (depicted in Fig. 3) to allow for binding to host cells, leading to colonization and virulence [29].

1.2.1.2. Proteolytic enzymes and toxins

Alpha-enolase (Eno) was identified as a 47 kilodalton (kDa) pneumococcal surface protein capable of binding human plasminogen, thereby enabling bacteria to possess proteolytic properties that promote bacterial invasion and spread [29]. Neuraminidase

(NanA) is an enzyme that targets sialic acid cleavage from the host glycocalyx and mucin, paving the way for the bacteria to adhere and colonize the upper respiratory tract, however it has also been described to be essential for the viability of the pathogen in the blood after intranasal inoculation [30].

Autolysin (LytA) is an enzyme located in the bacterial cell wall that functions to trigger autolysis of the microbe, releasing cytoplasmic toxins such as pneumolysin (Ply) and other bacterial products that augment inflammation, while also containing immunogenic features [31]. It has also been reported, however, that Ply release is not entirely dependent on the activity of autolysin [32].

Amongst the multiple virulence factors harbored by S. pn., Ply acts as the major constituent involved in pneumococcal pathogenesis [33]. Upon its release from the cell wall due to the actions of bacterial autolysin [13], high concentrations of the exotoxin may induce irreversible pore formation resulting in dissolution of various cell types including innate immune cells, platelets and also epithelial and endothelial cells; thereby paving the way for extra-pulmonary dissemination and persistence of S. pn. [34]. Lower Ply concentrations are rendered sub-lethal and pore formation may be subject to repair, albeit at the expense of triggering hyper-reactivity of innate cells and platelets, which may play a part in the pathogenesis of organ dysfunction [34].

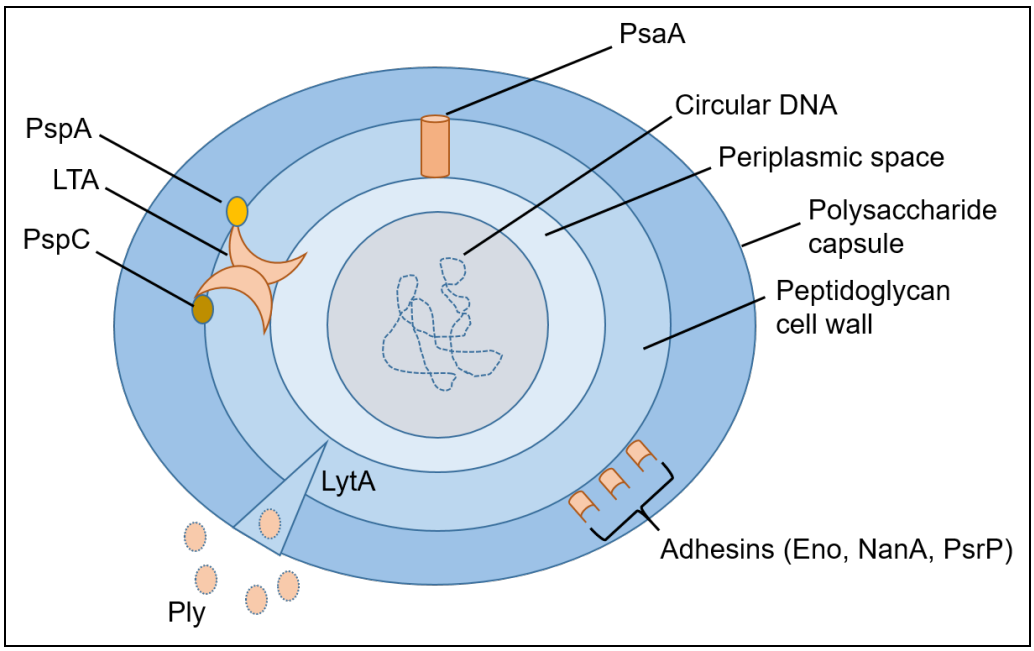

Figure 3. Structure and virulence factors harbored by pneumococci (adapted from van der Poll & Opal, 2009) [16]. PsaA: Pneumococcal surface antigen A, PspA: Pneumococcoal surface protein A,

PspC: Pneumococcal surface protein C, LTA: Lipoteichoic acid, LytA: Autolysin, Ply: Pneumolysin, Eno: Alpha-enolase, NanA: Neuraminidase, PsrP: Pneumococcal serine-rich repeat protein.

1.2.2. Innate immune recognition of *Streptococcus pneumoniae*.

Pneumococcal pathogenesis is initiated upon adhesion of the microbe to the host epithelia, which triggers the start of the antimicrobial response against infiltrating bacteria [35]; depicted in Fig. 4. Containing the growth of pulmonary infiltrating bacteria relies on the recognition of various bacterial motifs, termed pathogen-associated molecular patterns (PAMPs), by host pathogen recognition receptors (PRRs) found on innate immune and epithelial cells [36]. Most prominent surface PRRs comprise toll-like receptors (TLRs), scavenger receptors and C-type lectins [37], which function to recognize various PAMPs such as surface lipids and lipoproteins [37], diacylglycerides [38] and β-glucan [39], respectively. Intracellular PRRs comprise TLRs, nucleotide oligomerization domain (NOD)-like receptors (NLRs), and retinoic acid-inducible gene-I (RIG-I)-like receptors (RLRs), which are responsible for the endosomal/lysosomal recognition of bacterial and viral nucleic acids, cytoplasmic recognition of bacterial peptidoglycans and viral nucleic acids, respectively [37].

TLRs are well established to be of paramount importance for innate recognition of invading pathogens, either through receptors located on the plasma membrane (TLR1, -2, -4, -5 and -6) or in endosomes (TLR3, -7, -8 and -9). Upon recognition of bacterial motifs such as S. pn. cell wall constituents including lipoproteins signal through TLR2 ligation whereas the exotoxin Ply has been reported to signal via TLR4 [33] and to activate the NLR family, pyrin domain-containing (NLRP)3 inflammasome [40]. As a consequence of ligand-receptor ligations, adaptor molecules such as myeloid differentiation primary response (MyD)88, TIR-domain-containing adapter-inducing interferon-β (TRIF) and TRIF-related adaptor molecule (TRAM) signal the activation of the transcriptional mediators nuclear factor ‘kappa-light-chain-enhancer’ of activated B-cells (NF-κB) and/or interferon-regulatory factor (IRF)3/7 which drive inflammation [33, 41], as depicted in Fig. 4.

Upon recognition of bacterial motifs and PRR-PAMP mediated NF-κB signaling, the release of inflammatory mediators such as interleukin (IL)-1β, IL-6, interferon (IFN)-α/β, tumor necrosis factor (TNF)-α and inflammatory chemokines such as CXC chemokine ligand (CXCL)1, CXCL5 and CC chemokine ligand (CCL)2 ensue, resulting in activation of the acute-phase immune response, stimulation of immune and non-immune cells in the vicinity, and recruitment of neutrophils (PMN) and other inflammatory innate leukocytes [36, 33, 42].

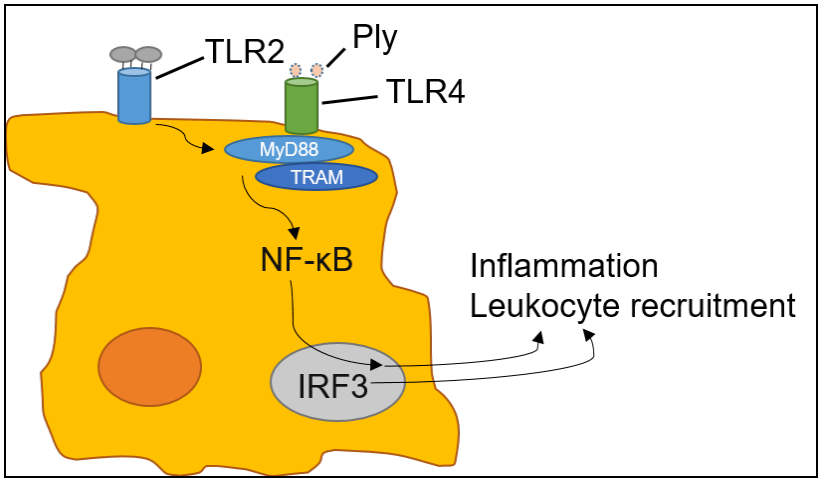

Figure 4. Bacterial sensing and initiation of the immune response to S. pn. (adapted from Whitsett & Alenghat, 2014) [43]. TLR: Toll-like receptor, Ply: Pneumolysin, MyD88: Myeloid differentiation primary response 88, TRAM: TRIF-related adaptor molecule. NF-κB: Nuclear factor 'kappa-light-chain-enhancer' of activated B cells, IRF3: Interferon regulatory factor.

1.3. The respiratory system and pulmonary defense

The upper respiratory tract (nasal passages), conducting airways (larynx, trachea, bronchi, bronchioles, terminal bronchioles) and lower respiratory tract (alveolar ducts, alveoli) collectively assemble the respiratory system which facilitates gaseous exchange and immune defense against invading pathogens [44]. The immune defense properties of the respiratory tract are mediated by non-specific and anatomical features coupled to more specific mechanisms [45]. Non-specific protection against particulate matter and invading pathogens include mucus production and mucociliary clearance in the conducting and upper airways, while

reflexes such as coughing aid in the expulsion of matter if the preceding features were inadequate [45]. Pathogen-specific mechanisms include the production of secretory immunoglobulin (Ig)A, which is initially produced as a polymeric immunoglobulin by sub-epithelial plasma cells and shuttled across airway epithelia by the polymeric immunoglobulin receptor (pIgR), whereby it gets processed to the secretory component [46]. Upon being processed, secretory IgA mediates protection through immune exclusion and hinders breach of the epithelia by the pathogen [45]. If the aforementioned features are evaded and microparticles or pathogens reach the lower respiratory tract, a more specific response ensues due to the presence and stimulation of phagocytes and immune cells such as alveolar macrophages and alveolar epithelial cells, triggering phagocytosis of pathogens and leukocyte recruitment [45].

1.3.1. Conducting airways – composition and immune defense mechanisms

The upper conducting airways of the respiratory tract are composed of submucosal glands and goblet cells [45], Clara cells [45], ciliated columnar and cuboidal epithelia [44] and nonciliated club cells [44]. Goblet cells in the larger airways are responsible for mucus production, while nonciliated Clara cells take up the role in bronchioles [45]. Submucosal glands located in the bronchi generate serous and mucous secretions to protect against microparticles and pathogens [45] while ciliated epithelia control the movement of mucus along the airways [47]. The adsorptive properties of mucus aids in the generation of a highly anti-microbial composition of host molecules including defensins, cathelicidins, lactoferrin, lysozyme and surfactant proteins [45]. Club cells are the prominent cell type in the bronchiolar epithelium, capable of secreting anti-inflammatory and immunomodulatory proteins and cytochrome P450 enzymes important in detoxification [44].

1.3.2. The alveolus – composition and immune defense mechanisms

The alveolus, depicted in Fig. 5, is an elastic structure consisting of alveolar macrophages (AM), endothelial cells, and alveolar epithelial cell (AEC) type I and

AECII. The proximity of AECI and AECII to endothelial cells of the pulmonary vasculature allows for efficient gaseous exchange and the surfactant layer produced by AECII provides the appropriate surface tension within the alveolus, while also contributing to antimicrobial defense [43]. AECs are connected to one another and to AM by connexin 43 (Cnx43) that allows for intracellular communication between adjacent cells [48]; thereby regulating the inflammatory response in sync following pathogenic stimulus [49].

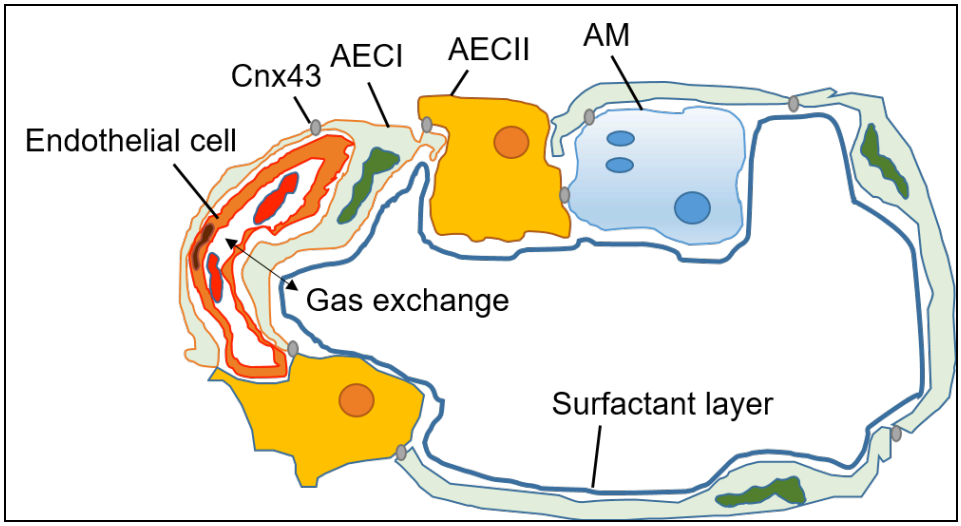

Figure 5. Structure of the alveolus (adapted from Whitsett & Alenghat, 2014) [43]. AEC: Alveolar epithelial cell, AM: Alveolar macrophage, Cnx43: Connexin 43.

1.4. Cellular immune response to *Streptococcus pneumoniae*

1.4.1. Alveolar macrophages

AM, previously described to originate from hematopoietic monocyte precursors [50], have in recent years been demonstrated to be seeded prenatally in the lungs as fetal monocytes that later develop into long-lived mature AM postnatally upon exposure to granulocyte-macrophage colony-stimulating factor (GM-CSF) [51]. GM-CSF, originally described as a growth factor aiding neutrophilic and macrophagic proliferation and differentiation [52], has been shown to be crucial for macrophage-

mediated surfactant clearance [53]. Amongst the various cell types in the lungs, AM are one of the first phagocytes to come into contact with lung infiltrating bacteria [54]. While they play an important role in the very early hours of inflammation, it has been accepted that they possess limited capacity to clear bacterial infections on their own [55], making it crucial for other innate leukocyte populations to supplement the fight against invading bacteria. Of the several effector functions of AM, one of the most significant features they possess is the capacity to produce CXCL1, a potent inflammatory chemokine that binds to its corresponding receptor, CXC chemokine receptor (CXCR)2, that is expressed by PMN and signals their chemotaxis to the lungs [56]. Other important effector functions of AM during the early response to S. pn. include the release of TNF-α [55] and activation of the NLRP3 inflammasome to release the potent pro-inflammatory cytokine IL-1β [40]. While pro-inflammatory cytokine secreting AM can be classed as the “classical” M1 macrophages, “alternatively activated” M2 macrophages are involved in tissue repair [57].

1.4.2. Inflammatory monocytes / macrophages

Another important player in response to bacterial lung infections are inflammatory monocyte/macrophages (iM), which can be divided into subpopulations of “patrolling monocytes” expressing low levels of Ly6C that probe the vasculature and take part in early inflammatory responses and tissue repair (58), and recruited monocytes expressing high levels of Ly6C (Ly6C^{hi} iM), which migrate from the blood to the lungs in a CC receptor (CCR)2-dependent fashion [59] upon the release of CCL2 by epithelial, endothelial or monocytic cells [60]. In resting conditions, monocytes in the circulation serve to monitor the presence of PAMPs while also restoring macrophage and dendritic cell (DC) populations. However, upon the detection of PAMPs and ligation of the TLRs they possess, they are able to differentiate into a pro-inflammatory phenotype whereby they infiltrate tissues to exert their effector functions which include phagocytosis, production of pro-inflammatory cytokines, myeloperoxidase (MPO) and superoxide [61]. Ly6C^{hi} iM have also been described to differentiate to patrolling monocytes (Ly6C^{lo}) or alternative macrophages during sterile inflammation and post *Staphylococcus aureus* (*S. aureus*) skin infection in vivo (58).

1.4.3. Dendritic cells

DC link the innate and adaptive immune responses in the lungs and are comprised of conventional and plasmacytoid subsets that have distinct functions and surface markers [62]. Lung DC have the capacity to produce IL-23 [63] which results in the expansion of the pool of IL-17 producing T helper (Th)17 cells important for bacterial clearance [62] and also in the stimulation of innate lymphoid cell (ILC)3 to release IL-17 and IL-22 [64]. DC also provide the necessary costimulatory molecules while engaging with naïve T cells to trigger their differentiation into T helper cells [65].

1.4.4. Neutrophils (PMN)

PMN are polymorphonuclear phagocytes that are of paramount importance in the immune response to bacterial lung infections due to the fact that they are recruited in high numbers very early after infection [66]. The lifespan of PMN in the circulation has been a topic of vigorous debate; while early work described PMN to have a short half-life of around 8 hours in humans [67], more recent findings using heavy water (^2H_2O) labeling suggested a surprisingly extended median half-life of 3.8 days in healthy volunteers [68]. Follow up studies using similar techniques later point towards the original finding of a circulating half-life of less than a day [69], which is a more physiologically compatible time frame considering the strong inflammatory properties of PMN [70]. PMN are generated in the bone marrow [70] from a common myeloid progenitor shared with macrophages and under influence of transcription and growth factors [71]. Granulocyte colony-stimulating factor (G-CSF) is a major driver of granulopoiesis and has been shown to be a survival factor for PMN progenitors in resting conditions, while it also serves to act as a stimulus for proliferation and survival of granulocytes following infection [72]. Recombinant G-CSF was initially approved in the US in the 1980s for clinical application directed towards small cell lung cancer patients receiving intensive chemotherapy; henceforth successfully restoring extensive chemotherapy-linked neutropenia [73]. Cellular sources of G-CSF include hematopoietic cells such as macrophages and monocytes [74], stromal cells

such as fibroblasts [74] and non-hematopoietic cells such as endothelial cells, which have been described to be a major source of G-CSF in vivo following lipopolysaccharide (LPS) stimulation [75], triggering the important switch from steady state to emergency granulopoiesis through MyD88-mediated TLR signaling [75]. Additionally, the discovery of CXCL-chemokines over recent decades has helped further understand mechanisms of PMN recruitment in response to inflammation. CXCL1, part of a subset of seven ELR motif chemokines that agonistically bind to their associated chemokine receptors CXCR1 and CXCR2 [76], is synthesized as a monomeric or dimeric protein, both of which are capable of potent CXCR2 stimulation and activation [77]. Basal levels of CXCL1 are negligible during resting conditions, however spike up following infection [77]. Cellular sources of CXCL1 include alveolar macrophages and airway epithelial cells [78], whilst expression levels are higher in murine hematopoietic cells than non-hematopoietic cells following influenza infection [79]. CXCL2 is secreted by various pulmonary cellular sources, although it is predominantly produced by alveolar macrophages [80]. CXCL2 binds to its shared receptor, CXCR2, with higher affinity than CXCL1, however CXCL2 levels are retained in the pulmonary space and act locally while CXCL1 may selectively transit through the vasculature and into the circulation [80]. Furthermore, CXCL1 and 2 inhibition alone may not affect PMN recruitment into alveolar spaces, whilst dual inhibition of the chemokines leads to reduced PMN influx, indicating multiple synergistic mechanisms of pulmonary PMN recruitment [81]. Indeed, in recent years, CXCL5 has also been described as a potent PMN chemotactic factor. Bone marrow resident cell-derived CXCL5 has been described to be important in regulating PMN homeostasis in the bone marrow, with inhibition of its receptor, CXCR2, resulting in PMN hyperplasia and retention in the bone marrow [82]. The source of CXCL5 in the blood is primarily from platelets under resting conditions, while pulmonary AECII are the exclusive cell type that produce CXCL5 in the lungs [82]. Furthermore, in chronic lung infections, epithelial-derived CXCL5 has been shown to be produced following the induction of TLR2 signaling, leading to pulmonary PMN recruitment into bronchoalveolar spaces, and abrogation of the CXCL5/CXCR2 axis protects against PMN-mediated pathology following *Mycobacterium tuberculosis* (Mtb) infection in mice [36].

Upon infectious stimuli, PMN respond by extravasating into the inflamed tissue via expressed adhesins such as lymphocyte function-associated antigen (LFA)-1, macrophage-1 antigen (Mac-1) and the $\alpha_4\beta_1$ integrin found on the surface of PMN [83]. TNF-α, produced by lung resident cells following infection, activates the endothelium to express the complementary surface adhesins allowing tethering and rolling of PMN along the activated vasculature [84]. The initial contact between the PMN and activated endothelium activates the integrins to establish a stronger interaction that allows for leukocyte crawling and eventual extravasation with the help of morphological polarization of the PMN [84]. Such interactions involve P-selectin glycoprotein ligand (PSGL)-1, LFA-1 and Mac-1 on the PMN surface binding with P-selectin, intercellular adhesion molecule (ICAM)1/2 and ICAM-1 on the activated endothelium respectively [85]. Once infiltrated into the inflamed tissue, PMN possess several effector functions to kill bacteria, including production of reactive oxygen species (ROS) via the nicotinamide adenine dinucleotide phosphate reduced (NADPH) oxidase system [86], release of azurophilic granules containing lysosomal enzymes [87], and the release of NETs; a meshwork released by PMN that is composed of DNA and histones, elastase and MPO [88]. The transcriptional master regulator of PMN is microRNA-223 (miR-223), which controls the normal maturation and activation of PMN, and also regulates myeloid progenitor proliferation via targeting the transcription factor myocyte enhancer factor (Mef)2c [89].

1.5. MicroRNAs in immunobiology

MicroRNAs (miRNAs) are short (18-22 nucleotides in length) regulatory, non-coding, endogenous RNAs that are expressed in plants and animals [90]. The prime function of miRNAs is to target untranslated regions (UTRs) of messenger RNAs (mRNAs) for degradation or inhibition of translation [91], making miRNAs crucial regulators of gene expression. The presence of a wide and abundant reservoir of miRNAs implicate their roles in regulating a broad range of physiological and pathological conditions including cellular development, differentiation, cancer, autoimmunity and cardiovascular and inflammatory diseases [92].

1.5.1. miR-223 biogenesis

The miR-223 gene locus lies on the X-chromosome and its expression is driven by the action of activating/inhibitory transcription factors [93], as depicted in Fig. 6. Activating myeloid transcription factors such as CCAAT Enhancer Binding Protein (C/EBP)α and PU.1 [93] bind to the miR-223 promoter to trigger transcription of the primary miR-223 transcript (pri-miR-223) by RNA polymerase (Pol)II. The primary transcript is processed by the microprocessor complex, which contains the enzymes Drosha and DiGeorge syndrome critical region (DGCR)8, to a precursor miRNA (pre-miR-223) in the nucleus before being shuttled to the cytoplasm by exportin 5. The cytoplasmic miR-223 precursor is further processed by the enzyme Dicer to generate a double-stranded miRNA duplex, which can then separate into single strands and get incorporated into the RNA-induced silencing complex (RISC). Once incorporated into RISC, miR-223 can target mRNAs for degradation by binding to complementary seed sequences in the 3' untranslated region (UTR). Nuclear factor 1 A-type (NFI-A) acts as the inhibitory transcription factor that competes with cEBPα to bind to the miR-223 promoter in the absence of stimulation, however following a stimulus such as retinoic acid, cEBPα displaces NFI-A from the promoter and triggers the expression of miR-223. Once expressed, miR-223 directly targets NFI-A mRNA for inhibition of translation and hence reduced NFI-A protein [94, 95].

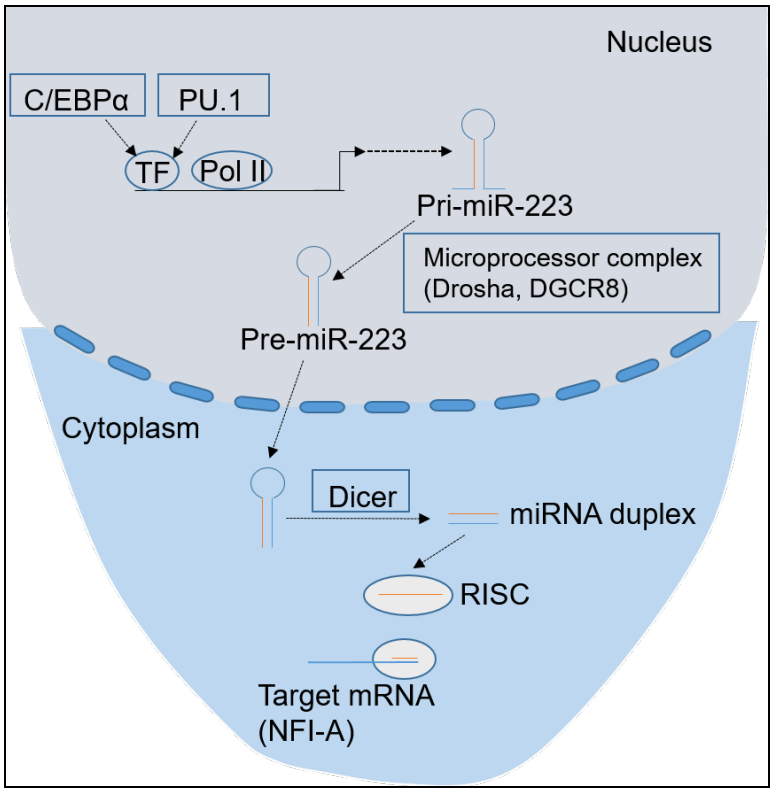

Figure 6. miR-223 biogenesis in the nucleus under influence of activating/inhibitory transcription factors (adapted from Mehta & Baltimore 2016 and Fazi et al. 2005) [94, 95]. C/EBPα: CCAAT enhancer binding protein, PU.1: Spi-1 transcription factor, TF: Transcription factor, Pol II: RNA polymerase II, DGCR8: DiGeorge syndrome critical region 8, RISC: RNA-induced silencing complex, NFI-A: Nuclear factor 1 A-type, pri-miR-223: Primary transcript of miR-223, pre-miR-223: Precursor of miR-223.

1.5.2. miR-223 functions in neutrophil biology

miR-223 is a master regulator of hematopoietic cells, with its expression almost entirely localized in bone barrow cells [90]. miR-223 is expressed at relatively low levels in hematopoietic stem cells and granulocyte progenitors, with its expression increasing steadily along the stages of PMN development and differentiation; bone marrow neutrophils (BM-PMN) express moderate levels of miR-223 whilst highest expression levels can be quantified in mature peripheral blood PMN [89]. miR-223 was characterized to promote differentiation and inhibit myeloid progenitor proliferation through targeting of the transcription factor Mef2c, which promotes mitotic activation and proliferation of myeloid progenitors [89]. Peritoneal PMN in miR-223 knockout (miR-223$^{-/-}$) mice were shown to exhibit enhanced respiratory

burst following phorbol myristate acetate (PMA) stimulation, while miR-223$^{-/-}$ mice presented enhanced neutrophilic infiltration in the lungs, coupled to enhanced liver hemorrhage and hepatocyte necrosis following endotoxin challenge [89]. Peripheral blood PMN in miR-223$^{-/-}$ mice also presented a hypersegmented morphology compared to WT mice [89], implicating the role of miR-223 not only in the differentiation of myeloid cells, but also in maintaining normal maturity and preventing neutrophil hyperactivation. Moreover, miR-223 has been described to be released by PMN in microvesicles, which can be taken up by epithelial cells to dampen ventilator-induced lung injury (VILI)-associated inflammation by targeting Poly(ADP-ribose) polymerase (PARP)1, which regulates NF-κB-directed inflammation [96], making miR-223 an anti-inflammatory molecule in the context of acute lung injury (ALI). The anti-inflammatory properties of miR-223 also apply for the functional role of PMN in a chronic lung infection setting. It has been demonstrated that miR-223$^{-/-}$ mice display exacerbated PMN-mediated pulmonary inflammation whilst miR-223 dampens neutrophilic pulmonary inflammation through the direct targeting of chemokines CXCL2, CCL3 and IL-6 in myeloid cells of Mtb-infected mice [97].

1.5.3. miR-223 in cancer

miR-223 has been described to play different roles in various oncological regulatory processes, hence it is referred to as an oncogenic microRNA (oncomiR) [98]. miR-223 has been shown to directly target p120, a tumor suppressor gene that maintains cell adhesion and regulates E-cadherin stability, hence prompting enhanced β-catenin signaling linked to epithelial-mesenchymal transition (EMT) in LoVo cells (a human colon cancer cell line); an indication of carcinogenic transformation [99].

miR-223 has also been implicated as having tumor suppressor properties, as shown to be expressed in lower levels in breast cancer tissues and cells, while also targeting the expression of stromal interaction molecule (STIM)1, which controls transforming growth factor (TGF)-β-mediated proliferation and EMT in breast cancer [100].

Furthermore, miR-223 can target cell cycle progression in acute myeloid leukemia (AML), through regulating the expression and negative feedback loop involving E2F Transcription Factor (E2F)1 and c/EBPα [101]. E2F1 induces C/EBPα expression, which is a trigger for miR-223 generation, however in the absence of miR-223, E2F1-mediated cell cycle progression is not targeted, hence proliferation cannot be halted [101].

1.5.4. miR-223 potential as a circulating biomarker

In recent years, miRNAs have been described to circulate in human plasma in a stable state, identifying them as strong potential candidates for prognostic biomarkers in various diseases including cancer [102]. miRNAs in the circulation may be in the form of microvesicles [103] or vesicle-free complexes coupled to Argonaute 2, both of which are protected from plasma RNase activity [104]. miR-223 levels were found to be lower in sera of hepatocellular carcinoma (HCC) patients, compared to sera from healthy patients [105]; a finding mirrored in respective liver biopsy samples. miR-223 was also found to be upregulated in sera of non-small cell lung cancer (NSCLC) patients, compared to cancer-free control group [106]. It is, however, important to state that different studies have made use of different ways to quantify miRNAs in sera, including normalizing the expression to other circulating miRNAs or spiking in exogenous non-human miRNAs [98]. Additionally, the variation of gene expression amongst different demographic populations further complicates analyses [107], making it necessary to perform more standardized methodology for effective evaluation of results in the field of circulating nucleic acid biomarkers.

2. Aims of the study

MicroRNAs are short non-coding RNA molecules that are abundant in variety across animal and plant species. The prime function of microRNAs is to bind complimentary sequences on the 3' end of messenger RNA untranslated regions, targeting the degradation or inhibition of translation of messenger RNAs. While microRNAs have been described to play important roles in gene silencing, development/inhibition of a variety of cancer types and autoimmune diseases, and the control of cellular migration, proliferation and differentiation, the precise role exerted by microRNAs in pulmonary acute lung infections remains to be elaborated. Our study was designed to elucidate the role of microRNA-223, a master regulator of neutrophil function and maturation, in response to intranasal *Streptococcus pneumonia* infection in C57BL/6J wild-type and microRNA-223 knockout mice. Pneumonia is characterized by vast numbers of neutrophils migrating into the alveolar spaces and lung tissue which help clear bacteria by phagocytosis and additional inflammatory effector functions, making them crucial effector cells in the immune response to pneumococci. An imbalanced immune response, however, could lead to excessive cellular inflammation which is harmful to the host. Hence, understanding migration patterns and effector functions of neutrophils in the absence of microRNA-223 expression is crucial to elucidate the significance of microRNA-223 in neutrophilic inflammation in the lungs

3. Materials and methods

3.1. Materials

See Appendix 1: Materials

3.2. Methods

3.2.1. Mice and study approval

All mice used in the study were 8-10 weeks old females (18-22 g). Wild-type (WT) C57BL/6J mice were obtained from the Research Facilities for Experimental Medicine (FEM), Berlin, Germany or Charles River Laboratories, Sulzfeld, Germany, while miR-223$^{-/-}$ mice were obtained from the breeding facility of the CharitéCrossOver (CCO), Berlin, Germany. Mice were kept under Specific Pathogen Free (SPF) conditions at the in-house animal facility of Charité – Universitätsmedizin Berlin in Berlin, Germany, and treated in complete accordance and compliance with the local institution (Charité – Universitätsmedizin Berlin), governmental body (Landesamt für Gesundheit und Soziales Berlin) and the Federation of European Laboratory Animal Science Associations to ensure minimal stress and discomfort of mice throughout the study.

3.2.2. Bacteria and intranasal infection of mice

A day prior to infection, WT bacteria (S. pn. serotype 2; D39 WT) were plated onto BD™ Columbia Agar with 5% Sheep Blood and allowed to grow for 9 hours at 37ºC. Ply-deficient pneumococci (D39 Δply) were plated on Columbia Agar with 5% Sheep Blood containing 100 ng erythromycin and were also incubated at 37ºC for 9 hours. Single colonies were then transferred to Todd Hewitt Broth medium supplemented with 0.5% yeast (THY) and 10% heat-inactivated fetal calf serum (FCS), the optical

density at 600 nm (OD_{600}) adjusted to 0.03-0.04 and kept on ice. The following day, bacteria were grown to mid-log phase (OD_{600} of 0.35), centrifuged at 2000xg for 10 minutes without breaks (Heraeus Instruments, Megafuge 1.0R) and washed with pre-warmed sterile phosphate-buffered saline (1x PBS). The concentration was adjusted to $2.5x10^8$/ml and mice were infected intranasally at an infectious dose of $5x10^6$ colony forming units (CFU) in 20 µl 1x PBS. Control mice received 20 µl sterile 1x PBS intranasally.

3.2.3. Monitoring, weighing and temperature recording

Starting at 24 hours p.i., mice were observed at 12-hour intervals for their reactions to external stimuli and general behavior, while self-isolation, difficulty breathing, or any other pathological signs were graded based on humane end-point criteria. Mice were then weighed and changes to body temperature were recorded. Mice that met the humane end-point criteria were sacrificed as described in 3.2.4.

3.2.4. Anesthesia, organ preparation and sampling

3.2.4.1. Sacrificing of mice, collecting blood and performing bronchoalveolar lavage

At the corresponding analysis time points, mice were anesthetized by intraperitoneal administration of ketamine (80 µg/g of body weight) and xylazine (25 µg/g of body weight). Upon loss of pedal withdrawal reflexes, blood was drawn into Ethylenediaminetetraacetic acid (EDTA) capillary blood collection tubes from the vena cava and the mice were sacrificed by exsanguination. The trachea was freed and the lungs were flushed twice with 0.8 ml 1x PBS (containing protease inhibitor) through the trachea to obtain bronchoalveolar lavage (BAL).

3.2.4.2. Blood sampling

Blood leukocyte counts and frequencies from collected EDTA-blood were determined using the scil Vet ABC Hematology Analyzer. Aliquots from the same EDTA-blood samples were spared for CFU determination and the remainder centrifuged (2000xg for 10 minutes 4ºC) to obtain plasma, which was later stored in -80ºC for future analyses of plasma proteins, alveolar-endothelial barrier integrity, and cytokine/chemokine analysis.

3.2.4.3. Isolation of BAL cells and fluid

An aliquot of BAL was spared for bacterial load determination (3.2.6) while the remainder was centrifuged (470xg for 5 minutes, 4ºC). The supernatant (BAL fluid; BALF) was collected and stored in -80ºC for future analyses (determination of alveolar-endothelial barrier integrity, chemokine concentrations, inflammatory cytokine concentrations) while the pellet containing BAL cells (BALC) was resuspended in PBS + 0.5% Bovine Serum Albumin (BSA) (FACS buffer) and kept on ice for cell surface staining of innate leukocytes.

3.2.4.4. Isolation of lungs

Lungs were isolated by an incision in the chest, beginning at the xiphoid and extending to the neck with surgical scissors. The ribs were cracked left and right of the ribcage and lifted. To diminish the number of blood lymphocytes, lungs were perfused through the right heart ventricle with 5 ml chilled 1x PBS. A lobe of the lung was excised and placed in a gentleMACS^{TM} M Tube containing 1 ml TRIzol reagent and immediately homogenized using the gentleMACS^{TM} Dissociator (program – RNA 01.01) and stored at -80ºC for future analysis of miR-223 and gene expression via quantitative polymerase chain reaction (qPCR). The left lung piece was excised and placed inside a tissue culture dish containing 6 ml Complete Roswell Park Memorial Institute medium (cRPMI; RPMI 1640 supplemented with 10% FCS (heat-

inactivated), 1% 4-(2-hydroxyethyl)-1-piperazineethanesulfonic acid (HEPES) buffer, 1% L-glu) supplemented with 2 mg DNase I and 6.4 mg collagenase type II and kept on ice. The remainder of the lungs were excised and placed in gentleMACS™ M Tubes containing 1 ml 1x PBS (containing protease inhibitor) for bacterial load determination and future proteomic analyses.

3.2.4.5. Processing of lung tissue for flow cytometric analysis

Lung pieces designated for flow cytometric analysis were excised and minced manually in a tissue culture dish containing cRPMI supplemented with DNase I and collagenase II, as described in 3.2.4.4. Following fine mincing of the lungs, the suspension, contained in a 15 ml tube, was placed in a 37ºC water bath and incubated for 30 minutes for the enzymatic digestion to commence. After 30 minutes, the minced lung suspension was then pressed using a syringe plunger through a pre-wetted 100 µm filter into a 50 ml tube. The filter was washed with FACS buffer and the resulting suspension was centrifuged (470xg for 5 minutes, 4ºC). The supernatant was discarded and the pellet was resuspended in 2 ml red blood cell lysis buffer to clear erythrocytes. Following 2 minutes of exposure to the lysis buffer, the reaction was stopped by addition of 10 ml FACS buffer and centrifuged again (470xg for 5 minutes, 4ºC). The supernatant was discarded and the lung cells resuspended in 500 µl of FACS buffer and kept on ice until stained for flow cytometric analysis.

3.2.4.6. Isolation and processing of spleen

The spleen was exposed, excised and cut in half. One half of the spleen was placed in gentleMACS™ M Tubes containing 1 ml 1x PBS (containing protease inhibitor) and homogenized for bacterial load determination and future proteomic analyses. The other half of the spleen was placed in a 15 ml tube with 2 ml FACS buffer on ice. The half spleen was then pressed using a syringe plunger through a 70 µm filter into a petri dish and the cell suspension transferred into a 15 ml tube. The petri dish and

the 70 µm filter were washed with 10 ml FACS buffer and transferred into the same 15 ml tube. The cell suspension was centrifuged (470xg for 5 minutes, 4ºC), supernatant discarded, and the pellet resuspended in 2 ml red blood cell lysis buffer to clear erythrocytes. Following 2 minutes of exposure to the lysis buffer, the reaction was stopped by addition of 10 ml FACS buffer and centrifuged again (470xg for 5 minutes, 4ºC). The supernatant was discarded and the spleen cells resuspended in 1-5x10^7 cells/ml of FACS buffer until stained for flow cytometric analysis.

3.2.4.7. Preparation of lungs for histopathological analysis

Mice were anesthetized as previously described in 3.2.4 and upon loss of pedal withdrawal reflexes, blood was collected through the vena cava. The trachea was freed from tissue and loosely fixed with a surgical knot. Immediately after the final breath, the tracheal knot was tightened to keep lungs inflated. The lungs were isolated by an incision in the chest, beginning at the xiphoid and extending to the neck with surgical scissors. The ribs were cracked left and right of the ribcage and lifted. The heart and thymus were removed with care to avoid touching the lungs with surgical instruments. The trachea was cut upstream of the surgical knot, lifted and the tissue underneath the rib cage excised. The lungs were pulled underneath the rib cage by holding the trachea and placed in a histological cassette. The cassette, containing the isolated lungs, was placed in 4% formalin solution and kept in the dark for 24 hours at room temperature before being processed. Lungs were analyzed for edema, hemorrhages, neutrophilic infiltration and lymphocytic cuff formation.

3.2.5. Determination of bacterial burden in the lungs and secondary lymphoid organs

Lungs and spleen collected in gentleMACS^{TM} M Tubes were homogenized using the gentleMACS^{TM} Dissociator (program – protein 01.01). Homogenized lung and spleen suspensions, collected blood samples and BALC were serially diluted in 1x PBS,

plated onto Columbia Agar with 5% Sheep Blood and incubated for 24 hours at 37ºC under 5% carbon dioxide (CO_2) prior to CFU counting.

3.2.6. Isolation, infection and stimulation of murine and human primary cells

3.2.6.1. Isolation of murine bone marrow neutrophils

Mice were anesthetized as described in 3.2.4 and upon loss of pedal withdrawal reflexes, mice were sacrificed by exsanguination. The femur and tibia were stripped away of the skin and carefully cleared of remaining tissue and joints to isolate intact bones. Using a 20 ml syringe and a cannula (26 G), the bones were flushed with 1x PBS into a 50 ml centrifuge tube containing 2 ml MACS buffer (PBS + 0.5% BSA + 2 mM EDTA). The suspension containing total bone marrow cells was centrifuged (470xg for 5 minutes, 4ºC), followed by discarding of the supernatant and resuspension of the pellet in 2 ml red blood cell lysis buffer. Following 2 minutes of exposure to the lysis buffer, bone marrows cells cleared of erythrocytes were washed with 1x PBS, a 100 µl aliquot was removed and stored on ice to later check for purity of isolation via flow cytometry, and the remainder was centrifuged (470xg for 5 minutes, 4ºC). The supernatant was discarded and the pellet resuspended in 5 ml MACS buffer. An aliquot of total bone marrow cells was diluted 1:10 in trypan blue and total bone marrow cells were counted using a hemocytometer. Upon determining the total cell count, bone marrow cells were centrifuged (470xg for 5 minutes, 4ºC) and the supernatant discarded. The pellet was resuspended in 200 µl MACS buffer per 10^8 cells and incubated with 50 µl biotinylated monoclonal antibody (mAb) against Ly6G per 10^8 cells for 10 minutes at 4ºC. Next, 150 µl of MACS buffer was added to the cell suspension, followed by addition of 100 µl of anti-biotin microbeads per 10^8 cells to capture biotinylated cells by positive selection. The cell suspension was briefly vortexed and incubated for 15 minutes at 4ºC, followed by washing with MACS buffer and centrifugation (470xg for 5 minutes, 4ºC). The supernatant was discarded and the pellet was resuspended in 500 µl MACS buffer per 10^8 cells. For magnetic separation of biotinylated bone marrow cells, a pre-cooled LS column was placed in the magnetic field of a MidiMACS Separator and the column was rinsed

with 3 ml of MACS buffer. The bone marrow cell suspension was passed through a 30 µm pre-separation filter and into the LS column, followed by 3 repeats of washing with 3 ml MACS buffer. Labeled $Ly6G^+$ bone marrow cells were positively selected to be retained in the column due to magnetic pull, whereas non-labeled cells pass through the column as a flowthrough. The non-labeled negatively selected bone marrow cells were collected into a 15 ml tube and a 100 µl aliquot was removed and stored on ice to later check for purity of isolation via flow cytometry. Following collection of the negative fraction, the LS column containing $Ly6G^+$ bone marrow PMN was removed from the MidiMACS Separator and placed on a 15 ml tube away from magnetic force. 5 ml MACS buffer were added onto the column and the magnetically labeled bone marrow PMN were immediately flushed out by firmly pushing the plunger of a syringe into the column. An aliquot of eluted bone marrow PMN was diluted 1:10 in trypan blue and counted using a hemocytometer. The remainder was centrifuged (470xg for 5 minutes, 4ºC) and the supernatant discarded. The pellet was resuspended with the buffer/medium of choice at the desired cellular concentration for functional studies.

3.2.6.2. Isolation of murine pulmonary epithelial cells

Mice were anesthetized as previously described in 3.2.4 and upon loss of pedal withdrawal reflexes, mice were euthanized by exsanguination. The trachea was freed from tissue and loosely fixed with a surgical knot before cutting open the diaphragm to expose the thoracic compartment. The lungs were perfused through the right heart ventricle with chilled 10 ml Hank's Balanced Salt Solution (HBSS) -Ca^{2+} -Mg^{2+}, followed by removal of the heart and thymus. Next, 1.5 ml of dispase were applied into the lungs through the trachea using a 2 ml syringe, followed by immediate application of 0.5 ml pre-warmed 1% low melt agarose. The syringe used for agarose application was kept fixed on the trachea for 5 minutes to allow the agarose to solidify and prevent the discharge of dispase out of the lungs. Following 5 minutes of incubation, the cannula was dispensed and the lungs were isolated by making an incision underneath the rib cage to release the lungs, followed by pulling out the lungs underneath the rib cage by holding the trachea. The lungs were dipped in 2 separate vials containing ice cold HBSS and then placed inside a 15 ml tube

containing 2 ml dispase after carefully removing the trachea. The lungs were then incubated for 10 minutes at 37ºC before being placed in a petri dish containing 10 ml Dulbecco's Modified Eagle Medium (DMEM) supplemented with 10% FCS (heat-inactivated), 1% L-glutamine (L-glu), 1% penicillin/streptomycin (P/S), 25 mM HEPES and 100 units of DNase I. Lungs were mechanically processed to a single cell suspension by means of manual mincing of the lungs using blunt forceps until translucent branches of the lungs became visible. Using an 18 gauge cannula, the digested lung suspension was drawn into a syringe, ejected back into the petri dish, and repeated 3 times to further disrupt any remaining large pieces of lung tissue. The digested lung suspension was then passed through a pre-wetted 100 µm filter into a 50 ml tube and the petri dish was washed with DMEM medium before supplementing the digested cell suspension to ensure maximal cellular recovery. Digested lung cells were then passed through a pre-wetted 70 µm filter into a new 50 ml tube and centrifuged (470xg for 5 minutes, 4ºC). The supernatant was carefully removed and centrifuged once more (470xg for 5 minutes, 4ºC) to ensure minimal loss of cells. The pellets from the consecutive centrifugation steps were combined and exposed to red blood cell lysis solution for 2 minutes to clear of erythrocytes. The erythrolysis reaction was stopped by washing with epithelial MACS buffer (eMACS buffer; 1x PBS supplemented with 3% FCS (heat-inactivated) and 10 mM EDTA) and the cells were passed through a pre-wetted MACS pre-separation filter (30 µm) into a new tube before being centrifuged (470xg for 5 minutes, 4ºC). After discarding the supernatant, the pellet was resuspended in 10 ml eMACS buffer. A 100 µl aliquot was removed and stored on ice to later check for purity of isolation via flow cytometry, while another aliquot was diluted 1:10 in trypan blue in order to count lung cells using a hemocytometer. After determination of the total lung cell count, the cell suspension was centrifuged (470xg for 5 minutes, 4ºC), the supernatant was discarded, and the pellet was resuspended in 100 µl eMACS buffer per 10^7 cells. Next, total lung cells were stained with 10 µl of biotinylated monoclonal antibodies (mAbs) for negative selection against cluster of differentiation (CD)31 (tagging monocytes, thrombocytes, granulocytes, endothelial cells), CD16/32 (tagging natural killer (NK) cells, PMN, eosinophils, AM, monocytes and B cells), and CD45 (hematopoietic cells) per 10^7 lung cells, vortexed, and incubated for 15 minutes at room temperature. During the incubation time, MagniSort Streptavidin Negative Selection Beads were thoroughly vortexed and 10 µl beads per 10^7 lung cells were

added into a 2 ml microcentrifuge tube and washed with 1 ml eMACS buffer prior to being placed on a DynaMag-2 magnet for 5 minutes to magnetically attract streptavidin beads to the surface of the microcentrifuge tube. The eMACS buffer was removed after 5 minutes of incubation and the microcentrifuge tube was displaced away from the magnetic field. The washing step was repeated 2 more times before resuspending the beads in 100 µl eMACS buffer per 10^7 cells. After 15 minutes of incubation with biotinylated negative selection mAbs, lung cells were washed with eMACS buffer and centrifuged (470xg for 5 minutes, 4ºC). The supernatant was discarded and the cell pellet was resuspended in 100 µl eMACS buffer per 10^7 cells. The equal volumes of beads solution and biotinylated lung suspension were mixed inside the 2 ml microcentrifuge tube containing the beads by gentle pipetting and incubated at room temperature for 5 minutes to allow for biotin-streptavidin binding. Next, the beads/cells mix was topped up to 2 ml with eMACS buffer and split into two 2 ml microcentrifuge tubes and placed on the DynaMag-2 magnet for 5 minutes to allow for magnetic separation. The supernatant was carefully removed without disturbing the magnetically attached beads and collected into a 15 ml centrifuge tube. The beads were then washed 2 more times with eMACS buffer as previously described and the supernatant carefully removed and collected into the same 15 ml centrifuge tube which contained enriched negatively selected murine pulmonary epithelial cells. 100 µl aliquots of the positive fraction (biotinylated cells in streptavidin beads) and the negative fraction (enriched in pulmonary epithelial cells) were removed and stored on ice to later check for purity of isolation via flow cytometry. Finally, an aliquot of the negatively selected cells was diluted 1:10 in trypan blue and counted using a hemocytometer prior to centrifugation (470xg for 5 minutes, 4ºC). The supernatant was removed and the pellet containing negatively selected murine pulmonary epithelia was resuspended in $8x10^5$ cells/ml of DMEM + 10% FCS + 1% L-glu + 1% P/S + 25 mM HEPES and seeded on a 48 well tissue culture dish at a density of $2x10^5$ cells per 250 µl volume and incubated at 37ºC + 5% CO_2. The medium was replaced with fresh pre-warmed medium in the following 2 days post-isolation, while on the third day post-isolation, cells were washed with pre-warmed 1x PBS and resuspended in DMEM + 2% FCS + 1% L-glu medium. Murine pulmonary epithelial cells were ready to infect or stimulate on day 4 post-isolation.

3.2.6.3. Co-isolation of murine pulmonary epithelial cells and lung neutrophils

Mice were anesthetized as previously described in 3.2.4 and upon loss of pedal withdrawal reflexes, mice were euthanized by exsanguination. The trachea was freed from tissue and loosely fixed with a surgical knot before cutting open the diaphragm to expose the thoracic compartment. The lungs were perfused through the right heart ventricle with chilled 5 ml of 1x PBS followed immediately by 2 ml dispase. Then, the heart and thymus were removed and an 18 gauge cannula was inserted into the trachea and the loose surgical knot tightened. Next, BAL was performed as previously described in 3.2.4 followed by application of 0.7 ml dispase and 0.5 ml 1% low melt agarose, delivered via the same cannula fixed on the trachea. The syringe used for agarose application was kept fixed on the trachea for 5 minutes to allow the agarose to solidify and prevent the discharge of dispase out of the lungs. Following 5 minutes of incubation, the cannula was dispensed and the lungs were isolated by making an incision underneath the rib cage to release the lungs, followed by pulling out the lungs underneath the rib cage by holding the trachea. The lungs were dipped in 2 separate vials containing ice cold 1x PBS and then placed inside a petri dish containing digestion medium (herein referred to as the lung digest dish) containing MACS buffer supplemented with 6.4 mg collagenase type II and 2 mg DNase I per lung. The tissue was minced thoroughly within the digest dish using blunt ended scalpels until translucent branches of the lungs became visible, and the processed lungs were incubated at 37ºC in a shaker with an orbital speed of 125 rpm for 30 minutes. Next, using an 18 gauge cannula, the digested lung suspension was drawn into a syringe, ejected back into the lung digest dish, and repeated 3 times to further disrupt any remaining large pieces of lung tissue. The digested lung suspension was then passed through a 70 µm filter pre-wetted with MACS buffer into a 50 ml tube and the digest dish was washed 3 times with MACS buffer to ensure maximal cellular recovery. The lung suspension was centrifuged (470xg for 5 minutes, 4ºC) and the supernatant discarded. The pellet was resuspended in red blood cell lysis solution for 2 minutes to clear erythrocytes. The erythrolysis reaction was stopped by washing with MACS buffer and the cells were passed through another pre-wetted 70 µm filter into a new tube before being centrifuged (470xg for 5 minutes, 4ºC). After discarding the supernatant, the pellet was resuspended in 10 ml MACS buffer. A 100 µl aliquot

was removed and stored on ice to later check for purity of isolation via flow cytometry, while another aliquot was diluted 1:10 in trypan blue in order to count digested lung cells using a hemocytometer. After determination of the total lung cell count, the cell suspension was centrifuged (470xg for 5 minutes, 4ºC), the supernatant was discarded, and the pellet was resuspended in 100 µl MACS buffer per 10^7 cells. Next, total lung cells were stained with 10 µl of biotinylated monoclonal antibodies (mAbs) against Ly6G per 10^7 cells to label PMN, vortexed and incubated for 15 minutes at room temperature. Meanwhile, 10 µl MagniSort Negative Selection Beads per 10^7 cells were added into a 2 ml microcentrifuge tube containing 1 ml MACS buffer and washed 3 times in the presence of a magnetic field, as described previously in 3.2.6.2. prior to resuspending the beads in 100 µl MACS buffer per 10^7 cells. Upon completion of the incubation time, biotinylated lung cells were washed with MACS buffer, centrifuged (470xg for 5 minutes, 4ºC), the supernatant discarded and the pellet resuspended in 100 µl MACS buffer per 10^7 cells. The resuspended cellular pellet was transferred to the beads solution and the mixture incubated for 5 minutes to allow for biotin-streptavidin binding. The mixture was topped up to 2 ml with MACS buffer, separated into equal volumes in another microcentrifuge tube, and placed on the DynaMag-2 for magnetic separation as previously described in 3.2.6.2. Biotinylated PMN were positively selected towards the magnet whereas all non-Ly6G expressing cells remained in the negative fraction supernatant. The supernatant was carefully removed into a 15 ml centrifuge tube and 2 additional washing steps were performed as previously described in 3.2.6.2. The positive fraction containing biotinylated $Ly6G^+$ PMN was washed with MACS buffer and a 100 µl aliquot was stored on ice to later check for purity of isolation via flow cytometry. The positive fraction was then centrifuged (470xg for 5 minutes, 4ºC), the supernatant discarded, and the pellet resuspended in TRIzol to preserve the RNA. Moreover, a 100 µl aliquot was removed from the negative fraction and stored on ice to later check for purity of isolation via flow cytometry, while another aliquot was diluted 1:10 in trypan blue in order to count negatively selected cells using a hemocytometer. Upon determination of the total cell count of the negative fraction, the cell suspension was centrifuged (470xg for 5 minutes, 4ºC), the supernatant discarded and the pellet resuspended in 100 µl MACS buffer per 10^7 cells. The PMN-depleted lung cells were stained with 10 µl of biotinylated monoclonal antibodies (mAbs) against CD31, CD16/32 and CD45 per 10^7 cells to label the remaining cell types (endothelial and hematopoietic cells),

vortexed and incubated for 15 minutes at room temperature. During the incubation time, beads were washed and prepared as described previously in 3.2.6.2. and murine pulmonary epithelial cells were isolated by negative selection using the DynaMag-2, as described in section 3.2.6.2. Upon collection of the negative fraction, a 100 µl aliquot was stored on ice to later check for purity of isolation via flow cytometry, while the rest of the negative fraction was centrifuged (470xg for 5 minutes, 4ºC) and the supernatant discarded. The remaining pellet, enriched in murine pulmonary epithelial cells, was resuspended in TRIzol to preserve the RNA.

3.2.6.4. Bacteria and in vitro stimulation of bone marrow neutrophils

A day prior to stimulation, D39 WT and D39 Δply were grown as previously described in 3.2.2, albeit in the absence of FCS. The following morning, bacteria were grown to mid-log phase, washed and concentration adjusted to 10^9 CFU/ml in cRPMI and kept at 4ºC until isolation of BM-PMN. WT and miR-223$^{-/-}$ BM-PMN were isolated as previously described in 3.2.6.1. and were resuspended in cRPMI medium at a concentration of 4x10^6 cells/ml. BM-PMN were plated on 48 well plates at a seeding density of 10^6 cells per well (250 µl). Within an hour of seeding, BM-PMN were infected with D39 WT, D39 Δply or medium (control). Cells were stimulated at a multiplicity of infection of 1 (MOI1) for 2 hours and 6 hours, while MOI0.1 was utilized for 18 hours of stimulation. At the corresponding time points p.i., cells were centrifuged (470xg for 5 minutes, 4ºC) and the supernatant was collected into RNase-free 1.5 ml microcentrifuge tubes using filter tips. The cellular pellet was resuspended in TRIzol reagent to preserve the RNA and stored in cryotubes. The infected cells and supernatants were stored at -80ºC until future experiments.

3.2.6.5. Exogenous transfer of miR-223 from neutrophils to pulmonary epithelial cells

Murine alveolar epithelial cells were isolated as previously described in 3.2.6.2. and on day 4 post-isolation, cellular supernatants from previously stimulated BM-PMN (isolated and stimulated with D39 WT and D39 Δply as previously described in

3.2.6.4.) were allowed to thaw at 37ºC and then centrifuged (800xg for 5 minutes, at room temperature) to pellet dead cells and debris. The supernatant was carefully collected into a fresh 2 ml microcentrifuge tube and centrifuged again (3300xg for 10 minutes, room temperature) to pellet apoptotic bodies. Meanwhile, murine alveolar epithelial cells were washed with warm 1x PBS in preparation for BM-PMN supernatant stimulation. Following the second centrifugation step to pellet apoptotic bodies, BM-PMN supernatant was carefully removed and transferred onto epithelial cells. Epithelial cells, submerged in stimulated BM-PMN supernatant, were incubated at 37ºC for 5 hours. Following 5 hours of incubation, the supernatant was removed and epithelial cells were washed twice with warm 1x PBS before being resuspended in TRIzol reagent and stored at -80ºC for future analysis of miR-223 transfer from BM-PMN to epithelial cells.

3.2.7. Gentamicin protection assay

In order to compare the capacity of phagocytosis and killing of S. pn. by WT and miR-223$^{-/-}$ BM-PMN, the gentamicin protection assay was utilized. One day prior to cell isolation, WT and GFP-expressing D39 (D39 GFP) were grown as described in 3.2.2, albeit in the absence of FCS. On the day of cell isolation, D39 WT & GFP were grown to mid log phase and the concentrations were adjusted to 10^{10} CFU/ml in HBSS (+Ca^{2+} +Mg^{2+}). WT and miR-223$^{-/-}$ mice were then anesthetized as described in 3.2.4 and upon loss of pedal withdrawal reflexes, blood was drawn into capillary blood collection tubes from the vena cava and allowed to stand vertically for 20 minutes. The tubes were then centrifuged at 13000xg for 3 minutes, the serum was collected without disturbing the clot and stored in 4ºC until needed. Upon collection of blood for generation of sera, mice were sacrificed by exsanguination and bone marrow PMN isolated as previously described in 3.2.6.1. PMN were eluted in HBSS (+Ca^{2+} +Mg^{2+}) and the concentration was adjusted to 4x10^6 cells/ml. 10^6 PMN were seeded in 1.5 ml tubes in a volume of 250 µl. Meanwhile, bacteria were opsonized with the serum generated from WT & miR-223$^{-/-}$ mice for 30 minutes at 37ºC. Following opsonization, WT & miR-223$^{-/-}$ PMN were infected with D39 WT & GFP at MOI10 and MOI100, and incubated for 1 hour at 37ºC for phagocytosis of serum opsonized bacteria (termed time 0 hours; T_0). Next, PMN were treated with

gentamicin (100 µg/ml final concentration) for 5 minutes to eliminate extracellular bacteria, followed by washing twice with HBSS and centrifugation (470xg for 5 minutes, 4ºC). During both washing steps, the supernatant was removed carefully to avoid loss of PMN. PMN at T_0 were resuspended in 100 µl 1x PBS and stained with mAbs for detection of live PMN containing phagocytized bacteria. The remaining PMN, termed time 1 hour (T_1) and time 2 hours (T_2), were incubated further for 1 and 2 hours respectively in HBSS before being washed, centrifuged (470xg for 5 minutes, 4ºC) and resuspended in 1x PBS for cell surface staining with mAbs to detect phagocytosis of bacteria uptaken by live PMN (described further in 3.2.10.5).

3.2.8. RNA isolation, reverse transcription and qPCR

3.2.8.1. Isolation of total RNA from murine lungs

Homogenized lung samples (as described in 3.2.4.4) were thawed at room temperature for 30 minutes before being centrifuged (500xg for 5 minutes, 4ºC) to remove tissue debris. The supernatant was transferred to new RNase-free 1.5 ml microcentrifuge tubes and supplemented with 1/5 volume of chloroform (200 µl) and mixed by manual shaking. Following 5 minutes of incubation at room temperature, the mixture was centrifuged (12000xg for 15 minutes, 4ºC) to obtain phase-separation. The upper aqueous phase was removed and pipetted into a new microcentrifuge tube containing 1/2 volume of isopropanol (500 µl). The mixture was mixed manually and allowed to incubate at room temperature for 10 minutes. The mixture was then centrifuged (12000xg for 15 minutes, 4ºC) and the supernatant discarded. The pellet was washed with chilled 75% ethanol (diluted in DNase/RNase free water) before being centrifuged again (7600xg for 5 minutes, 4ºC). The supernatant was discarded and the microcentrifuge tubes were exposed to a quick spin (maximum speed, 10 seconds) to be able to discard any residual ethanol. Upon careful removal of residual ethanol, pellets were air dried before being resuspended in 20 µl Diethylpyrocarbonate (DEPC)-treated RNase-free water and transferred to a new RNase-free 1.5 ml microcentrifuge tube. The concentration (ng/µl) of RNA was determined from 1 µl isolated RNA samples using Nanodrop 2000.

3.2.8.2. Isolation of total RNA from primary cells

Frozen BM-PMN (section 3.2.6.4) and primary alveolar epithelial cells (section 3.2.6.5) were thawed at room temperature for 30 minutes before being supplemented with 1/5 volume of chloroform (200 µl) and mixed by manual shaking. Following 5 minutes of incubation at room temperature, the mixture was centrifuged (12000xg for 15 minutes, 4ºC) to obtain phase-separation. The upper aqueous phase was removed and pipetted into a new microcentrifuge tube containing 1/2 volume of isopropanol (500 µl), 120 µl of 5 M ammonium acetate and 10 µl of glycogen. The mixture was mixed manually and incubated at -20ºC for 20 minutes. The mixture was then centrifuged (12000xg for 15 minutes, 4ºC) and the supernatant discarded. The pellet was washed with chilled 75% ethanol (diluted in DNase/RNase free water) before being centrifuged again (7600xg for 5 minutes, 4ºC). The supernatant was discarded and the microcentrifuge tubes were exposed to a quick spin (maximum speed, 10 seconds) to be able to discard any residual ethanol. Upon careful removal of residual ethanol, pellets were air dried before being resuspended in 20 µl DEPC-treated RNase-free water and transferred to a new RNase-free 1.5 ml microcentrifuge tube. The concentration (ng/µl) of RNA was determined from 1 µl isolated RNA samples using Nanodrop 2000.

3.2.8.3. Reverse transcription of miR-223 in lung tissue and primary cells

Using pre-designed TaqMan stem loop primers for miR-223-3p, together with pre-designed TaqMan stem loop primers for small nucleolar RNA MBII-202 (snoRNA202; murine endogenous control), 50 ng of RNA extracted from lung tissue or isolated primary cells was reverse transcribed to complementary DNA (cDNA) using the TaqMan MicroRNA Reverse Transcription Kit (Applied Biosystems). A reaction mix composed of 6.41 µl DEPC-treated RNase/DNase free water, 1.5 µl transcription buffer (10X), 0.15 µl dNTPs (25X, 100 mM), 0.375 µl of target (miR-223) and control (snoRNA202) stem loop primers, 0.19 µl RNase inhibitor, and 1 µl MultiScribe reverse transcriptase (RT) was prepared in a 0.5 ml PCR tube on ice and 50 ng of

RNA (5 µl from diluted 10 ng/µl concentration) was added to the reaction mix, pipetted up and down 2-3 times for mixing, and the PCR tube was immediately placed into a thermocycler. The samples were incubated for 30 minutes at 16ºC, followed by 30 minutes at 42ºC and 5 minutes at 85ºC. The cDNA was kept at 4ºC if needed on the same day for qPCR measurements, otherwise stored at -20ºC for future use.

3.2.8.4. qPCR for TaqMan MicroRNA Assays

In order to quantify miR-223 in isolated primary cells or lung homogenates, 50 ng of RNA was reverse transcribed as previously described in 3.2.8.3 and an input of 5 ng of miR-223 cDNA template was quantified using the TaqMan Fast Advanced Master Mix protocol. Separate master mixes were prepared for the target gene (miR-223) and endogenous control (snoRNA202) on ice, consisting of 7.5 µl DEPC-treated water, 1 µl TaqMan MicroRNA Assay (20x) and 10 µl TaqMan Fast Advanced Master Mix (2x). 18.5 µl of each master mix was pipetted into wells of a 0.1 ml MicroAmp™ Fast Optical 96-Well Reaction Plate that was placed on ice. Control assays (snoRNA202) were designated to the top half of the plate, whilst target assays (miR-223) were designated to the bottom half. 1.5 µl of template cDNA was added onto each well (same cDNA template added to control and target wells corresponding to the same sample) in triplicates, mixed and the plate sealed with MicroAmp™ Optical Adhesive Film. The reaction plate was centrifuged shortly (400xg for 3 minutes, 4ºC) to clear any air bubbles and bring the reaction mix to the bottom of the tube. The reaction plate was then run on a StepOnePlus™ Real-Time PCR System. The run program for miR-223 quantification was as follows:

Hold stage: 20 seconds at 95ºC (2.63ºC/s) for polymerase activation

PCR stage (40 cycles): 1 second at 95ºC (2.63ºC/s) for denaturing, 20 seconds at 60ºC (2.42°C/s) for annealing/extending

3.2.8.5. Calculation of relative gene expression

In order to determine the fold-change in gene expression (relative quantification; RQ value), the Delta Delta CT (ddCT) method was utilized. PCR cycle (CT) values of endogenous controls were subtracted from the target gene CT values to obtain a Delta CT (dCT) value for each sample. The mean sham-infected (healthy) dCT values were subtracted from the mean dCT values of infected groups to obtain the ddCT values. The fold-change in gene expression was calculated by 2^{-ddCT}.

3.2.9. Albumin, cytokine, chemokine ELISA

3.2.9.1. Mouse albumin ELISA

Murine alveolar-endothelial barrier integrity was determined using the Mouse Albumin enzyme-linked immunosorbent assay (ELISA) Quantitation Set . BALF and plasma samples were diluted 1:5.000 and 1:500.000 respectively in sample/conjugate diluent and the albumin concentration quantified according to manufacturer's instructions. The degree of alveolar-endothelial barrier integrity was determined by the BALF/plasma ratio, which is an indicator of the degree of leakage of albumin from the plasma into the alveolar space.

3.2.9.2. Inflammatory cytokine multiplex ELISA

Quantification of inflammatory cytokines was carried out using the LEGENDplex™ Mouse Inflammation Panel (13-plex) with V-bottom Plate. Inflammatory cytokine concentrations in BALF (undiluted) and plasma (diluted 1:2) samples were determined by flow cytometry (FACS Canto II) according to manufacturer's instructions.

3.2.9.3. MPO ELISA

Murine MPO concentrations in BALF were quantified using the MPO Mouse ELISA kit according to manufacturer's instructions.

3.2.9.4. CXCL-chemokine ELISA

CXCL1, -2, -5 concentrations in BALF were quantified using Mouse CXCL1/KC DuoSet, Mouse CXCL2/MIP-2 DuoSet, and Mouse LIX DuoSet ELISA kits according to manufacturer's instructions.

3.2.9.5. VEGF ELISA

Vascular endothelial growth factor (VEGF) concentrations in BALF were quantified using the Mouse VEGF DuoSet ELISA kit according to manufacturer's instructions.

3.2.10. Immunofluorescence staining and flow cytometric analysis

3.2.10.1. Cell surface staining of innate leukocyte populations

For quantification and analyses of innate leukocyte populations (AM, PMN, iM), surface antigen staining was performed on isolated BAL cells (gating strategy depicted in Fig. 7). Around $1x10^6$ BAL cells were resuspended in 150 µl FACS buffer and split into three FACS tubes in 50 µl aliquots to analyze different staining panels. BAL cells were incubated in 50 µl FACS buffer solution with mAb against CD16/CD32 (1:200) to block non-specific antibody binding. After 5 minutes, cells were stained with mAbs against CD45 (1:400), CD11c (1:250), CD11b (1:200), F4/80 (1:125), Ly6G (1:200), Ly6C (1:200), Siglec F (1:125) and MHCII (1:666) conjugated to different fluorochromes (see Appendix 1.5) for 20 minutes at 4ºC in darkness. Stained cells were washed with 1x PBS, centrifuged (470xg for 5 minutes, 4ºC) and

then fixed in 150 µl 1% paraformaldehyde (PFA) / PBS fixation buffer and vortexed. Samples were kept at 4ºC overnight in the dark. The following day, samples were washed with 1x PBS, centrifuged (470xg for 5 minutes, 4ºC) and resuspended in 100 µl FACS buffer before analyzing total numbers and frequencies of innate leukocyte populations on the FACS Canto II.

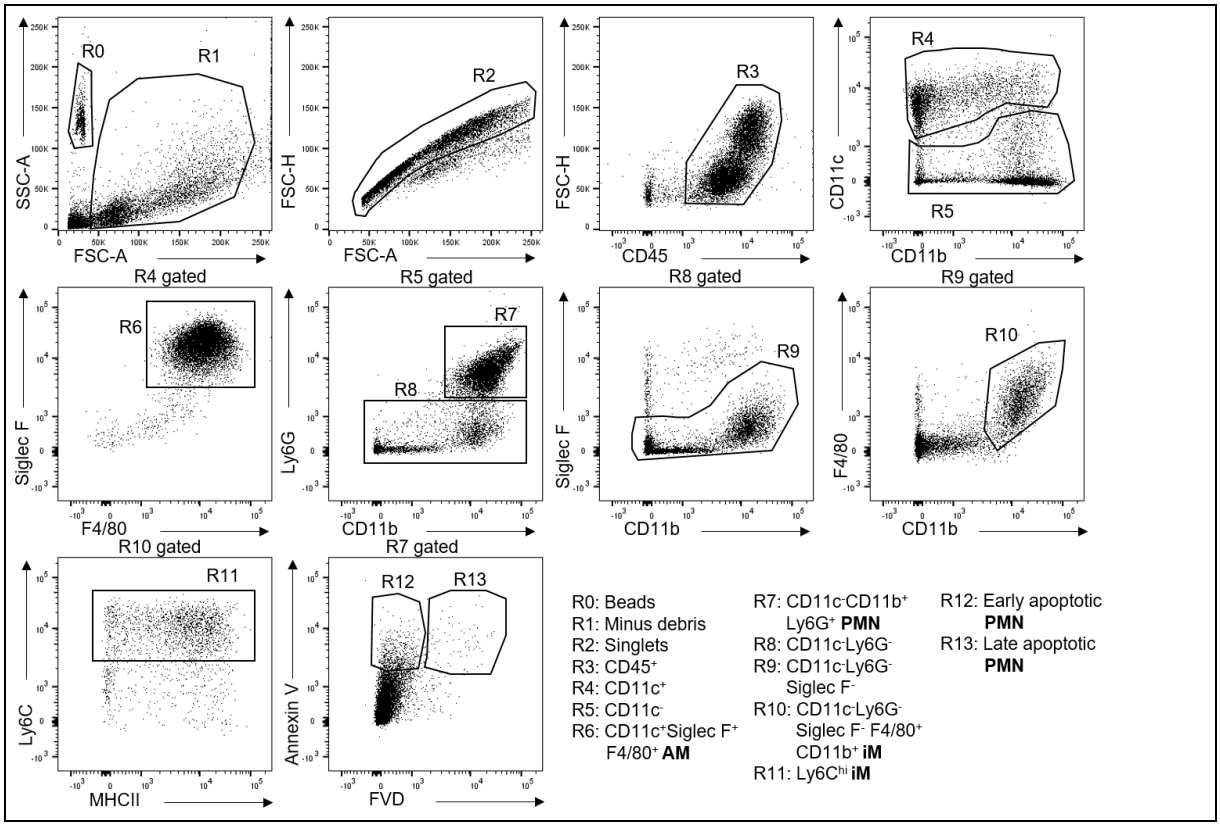

Figure 7. Gating strategy to identify live and apoptotic AM, PMN and Ly6C^{hi} iM.

3.2.10.2. Cell surface staining for analysis of neutrophil activation

In order to determine the extent of PMN activation following infection, BAL cells were incubated in 50 µl FACS buffer solution with mAb against CD16/CD32 (1:200) to block non-specific antibody binding. After 5 minutes, cells were stained with mAbs against CD45 (1:400), CD11b (1:200), Ly6G (1:100), LFA-1 (1:200) and CD14 (1:125) conjugated to different fluorochromes (see Appendix 1.5) for 20 minutes at 4ºC in darkness. Stained cells were washed with 1x PBS, centrifuged (470xg for 5 minutes, 4ºC) and then fixed in 150 µl 1% paraformaldehyde (PFA) / PBS fixation buffer and vortexed. Samples were kept at 4ºC overnight in the dark. The following day, samples were washed with 1x PBS, centrifuged (470xg for 5 minutes, 4ºC) and

resuspended in 100 µl FACS buffer before analyzing the activation state of PMN on the FACS Canto II. PMN were gated as previously described in Fig. 7, followed by analysis of mean fluorescent intensity (MFI) of CD14, LFA-1 and CD11b.

3.2.10.3. Cell surface staining of live and apoptotic innate leukocytes

In order to quantify and analyze live/apoptotic leukocyte populations, Annexin V and Fixable Viability Dye (FVD) staining was utilized together with cell surface staining. First, 1x binding buffer was prepared by diluting 1 part of 10X binding buffer with 9 parts of distilled water. Cell surface staining mix was prepared and BAL cells were incubated in 50 µl FACS buffer with mAb against CD16/CD32 (1:200) to block non-specific antibody binding. After 5 minutes, cells were stained with mAbs against CD11c (1:250), CD11b (1:200), F4/80 (1:125), CD45 (1:125), Ly6G (1:200) and Siglec F (1:125) for 20 minutes at 4ºC in the dark. Cells were then washed twice in cold 1x PBS and centrifuged (470xg for 5 minutes, 4ºC). The supernatant was discarded and pellet resuspended in 50 µl 1x PBS. BAL cells were treated with mAb against FVD (1:800), vortexed immediately and incubated at 4ºC in the dark for 30 minutes. BAL cells were then washed twice in FACS buffer, followed by a single wash with 1x binding buffer and centrifuged (470xg for 5 minutes, 4ºC). BAL cells were resuspended in 1x binding buffer at a concentration of 1-5x10^6 cells/ml. 2.5 µl of Annexin V was added to 50 µl of the cell suspension and incubated for 10-15 minutes at room temperature in the dark. Cells were then washed one final time with 1x binding buffer before centrifugation (470xg for 5 minutes, 4ºC) and resuspension in 100 µl of 1x binding buffer. Live and apoptotic cellular populations were analyzed on the FACS Canto II.

3.2.10.4. Cell surface staining for analysis of reverse migrated neutrophils

For quantification and analysis of reverse migrated PMN, surface antigen staining was performed on isolated spleen cells (gating strategy depicted in Fig. 8). Around 1-5x10^6 BAL cells were resuspended in 50 µl FACS buffer incubated with mAb against

CD16/CD32 (1:200) to block non-specific antibody binding. After 5 minutes, cells were stained with mAbs against CD45 (1:125), CD11b (1:200), Ly6G (1:100), CXCR1 (1:10), and ICAM-1 (1:200) conjugated to different fluorochromes (see Appendix 1.5) for 20 minutes at 4ºC in darkness. Stained cells were washed with 1x PBS, centrifuged (470xg for 5 minutes, 4ºC) and then fixed in 150 µl 1% paraformaldehyde (PFA) / PBS fixation buffer and vortexed. Samples were kept at 4ºC overnight in the dark. The following day, samples were washed with 1x PBS, centrifuged (470xg for 5 minutes, 4ºC) and resuspended in 100 µl FACS buffer before analyzing total numbers and frequencies of reverse migrated PMN on the FACS Canto II. Reverse migrated PMN were identified as a sub-population of ICAM-1^{hi} and $CXCR1^{lo}$ PMN.

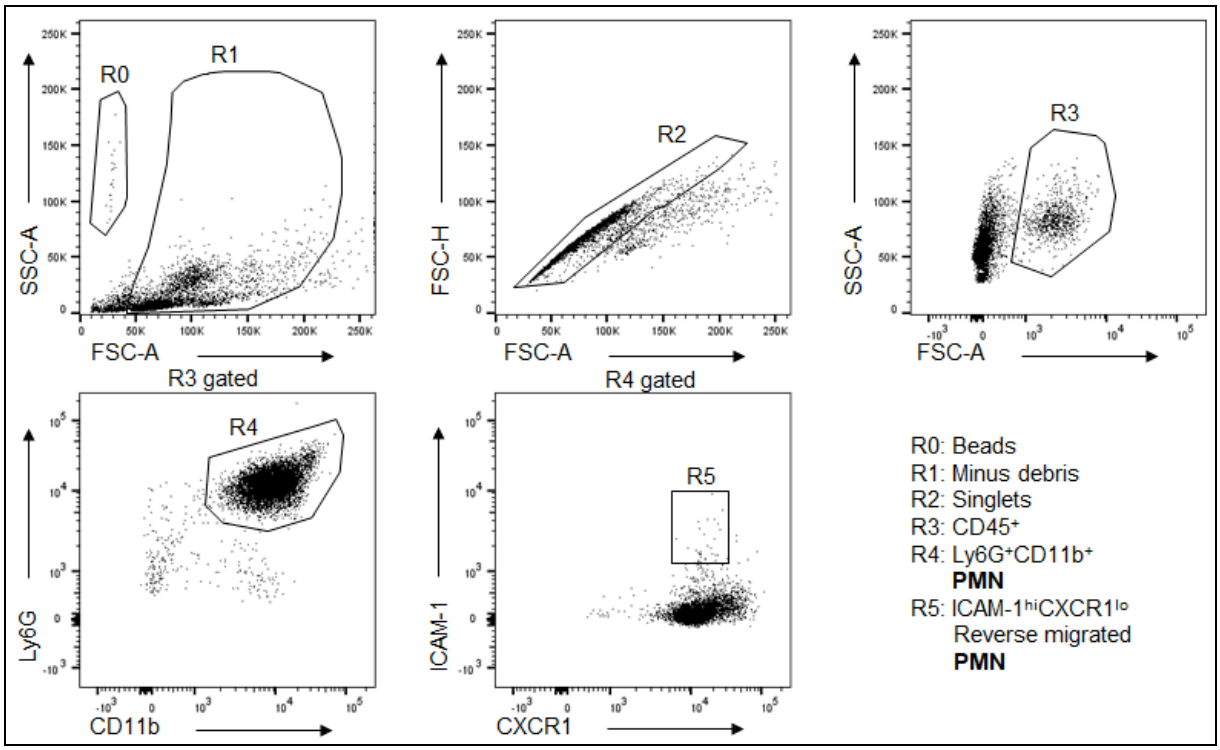

Figure 8. Gating strategy to identify reverse migrated PMN amongst splenic leukocytes.

3.2.10.5. Cell surface staining for analysis of phagocytized bacteria

For the detection of bacterial phagocytosis and killing by BM-PMN (gentamicin protection assay, section 3.2.7), $1x10^6$ BM-PMN were incubated in 100 µl PBS

solution with mAb against CD16/CD32 (1:200) to block non-specific antibody binding. After 5 minutes, cells were stained with mAbs against Ly6G (1:200) and FVD (1:800) for 20 minutes to detect live BM-PMN. Stained cells were washed with FACS buffer, centrifuged (470xg for 5 minutes, 4ºC) and the cellular pellet fixed in 100 µl 2% PFA / PBS fixation buffer and vortexed. The fixed cells were kept in the dark at room temperature for 20 minutes, followed by quenching of fixation with FACS buffer and centrifugation (470xg for 5 minutes, 4ºC). The supernatant was discarded, cells were resuspended in 100 µl FACS buffer and analyzed on the FACS Canto II. Phagocytized D39 GFP were detected through the FITC channel due to overlap of emission spectra, while live BM-PMN that had engulfed D39 GFP identified as double positive for Ly6G and GFP.

3.2.10.6. Calculation of total cell numbers and frequencies

CountBright™ Absolute Counting Beads (Thermo Fisher Scientific) were used to quantify total cell numbers in each staining panel via flow cytometry. Once spleens and lung tissues were processed to a single cell level, stained for desired cell populations and fixed, 50 µl of counting beads were diluted 1:2 in FACS buffer and added to each sample to be measured. For the analysis of BAL cells, 1:10 beads dilution was utilized. The beads gated in gate R0 (Fig. 7) were used to calculate the absolute numbers of leukocytes and lymphocytes in the measured samples based on the ratio of the bead input over beads recorded, while also factoring in the multiplication factor of proportion of lungs used for single cell suspensions (half lung) and amount taken from original pellet (50 µl used for staining from 500 µl original pellet). Absolute numbers of specific cell types and sub-populations were deduced from the ratio of calculated leukocytes/lymphocytes.

3.2.10.7. Flow cytometric analysis

Cells were analyzed using BD FACS Canto II, BD FACS DIVA and FlowJo (v10) software.

3.2.11. Statistical analysis

Statistical analysis was performed using GraphPad Prism software (V7). ROUT test was performed to identify outliers in data sets. D'Agostino-Pearson omnibus test was performed on data sets to determine whether they displayed a normal (Gaussian) distribution or not. Unpaired t test was performed on normally distributed data between two unpaired groups to determine statistical differences of a single parameter. Mann-Whitney U test was performed on nonparametric data between two unpaired groups to determine statistical differences of a single parameter. 2-way ANOVA with Sidak's and/or Tukey's multiple comparisons test was performed on data sets with multiple variables (multiple time points post-infection, multiple mouse strains) to determine statistical differences of multiple parameters (infected vs naïve/sham at different time points).

P values from unpaired t tests and Mann-Whitney U tests were all two-tailed and all statistical tests were set at a confidence level of 95%. */#/§ denotes $P < 0.05$, **/§§ denotes $P < 0.01$, ***/###/ denotes $P < 0.001$, ****/#### denotes $P < 0.0001$.ss

4. Results

4.1. Clinical parameters of WT and miR-223$^{-/-}$ mice following *Streptococcus pneumoniae* infection

Studies conducted in mice showed that in response to S. pn. serotype 3, WT mice exhibited a strong local and systemic inflammation, marked with dramatic weight and temperature loss and high bacterial loads in lungs and secondary lymphoid organs [108]. Hence, we wanted to investigate the pathogenesis of S. pn. serotype 2 and the response of miR-223$^{-/-}$ mice to infection in terms of clinical symptoms.

miR-223$^{-/-}$ mice display deteriorated clinical disease symptoms but similar bacterial burden to WT mice in response to *Streptococcus pneumoniae* infection

WT and miR-223$^{-/-}$ mice were infected intranasally with 5x10^6 CFU S. pn. serotype 2 and monitored at 12-hour intervals starting at 24 hours post-infection (24h p.i.) for changes in body weight (Fig. 9A) and temperature (Fig. 9B). WT mice maintained steady body temperature throughout the infection time course, while miR-223$^{-/-}$ mice exhibited a drop in body temperature at 48h p.i., relative to pre-infection (Fig. 9A). Whilst both groups of mice exhibited a drop in body weight compared to pre-infection, miR-223$^{-/-}$ mice exhibited enhanced weight loss following S. pn. infection 48h p.i. compared to WT mice (Fig. 9B). The bacterial load in the lungs, BAL, spleen and blood were quantified 24h and 48h p.i. (Fig. 9C, Fig. 9D, respectively) and while the bacterial burden recorded at 48h p.i. is generally higher than that of 24h p.i., no significant differences were recorded between WT and miR-223$^{-/-}$ mice at 24h or 48h p.i. (Fig. 9C-D).

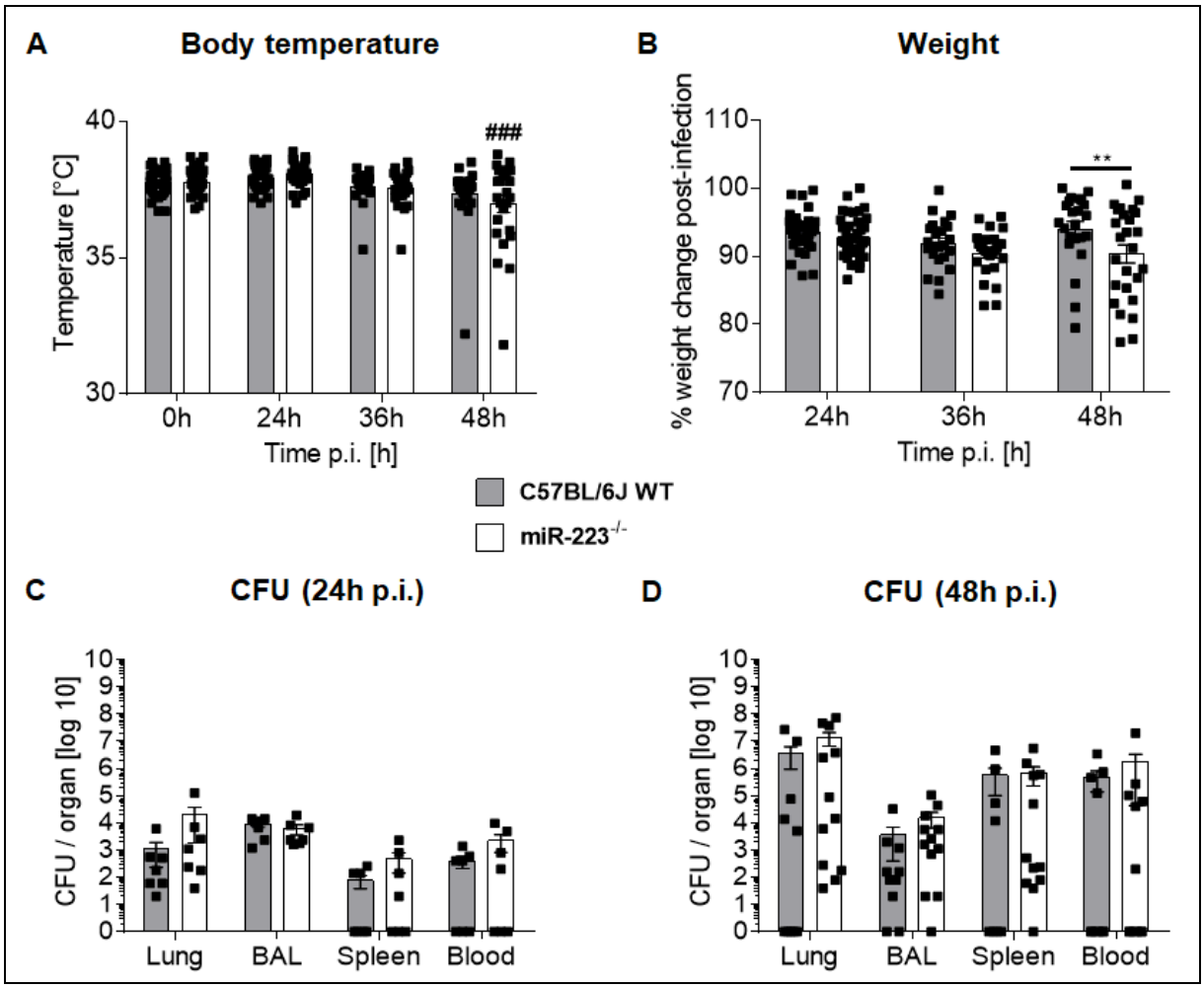

Figure 9. **A** – Body temperature of mice recorded at pre-infection and 24h, 36h, 48h p.i. S. pn. **B** – Changes in body weight relative to pre-infection recorded at 24h, 36h, 48h p.i. S. pn. **C** – Bacterial burden in lungs, BAL, spleen and blood (per µl) 24h p.i. S. pn. **D** – Bacterial burden in lungs, BAL, spleen and blood (per µl) 48h p.i. S. pn.-infected mice (n=7–26) were sacrificed and analyzed at 24h or 48h p.i. S. pn. for the determination of bacterial burden in the associated organs. Each analysis time point was repeated 2-3 independent times respectively. A hash sign (#) denotes statistical difference between S. pn.-infected mice relative to pre-infection, while an asterisk (*) denotes statistical difference between S. pn.-infected mice at the same time point. **C–D**; experiment was repeated 2–3 independent times. **A;** ### denotes $P < 0.001$ (2-way ANOVA/Sidak's multiple comparisons test). **B**; ** denotes $P < 0.01$ (2-way ANOVA/Sidak's multiple comparisons test). Data in **A–D** display means and individual values. Error bars represent SEM. CFU graphs (**C–D**) plotted in logarithmic scale.

4.2. Analysis of cellular migration patterns of leukocytes

4.2.1. miR-223$^{-/-}$ mice exhibit enhanced neutrophilic infiltration into lungs and BAL following *Streptococcus pneumoniae* infection

PMN are recruited to sites of infection very early on after infection, making them crucial in the battle against invading bacterial pathogens (89). In fact, in a previous study we recorded initiation of PMN chemotaxis to the lungs within the first 6 hours following S. pn. infection (unpublished data), while BAL PMN were at their peak in terms of total numbers and frequencies amongst BAL leukocytes 24h p.i. with S. pn. serotype 3 [108]. Hence we aimed to investigate the PMN migration pattern of miR-223$^{-/-}$ mice after S. pn. serotype 2 infection.

Following S. pn. infection, WT and miR-223$^{-/-}$ mice were sacrificed and the BAL, lungs and blood were analyzed for PMN recruitment 24- and 48h p.i. WT and miR-223$^{-/-}$ PMN total numbers and frequencies amongst leukocytes were recorded at similar levels 24h p.i. S. pn. in the BAL and lungs of WT and miR-223$^{-/-}$ mice (Fig. 10A-B). Blood PMN numbers and their frequencies amongst circulating white blood cells (WBCs) were also recorded at comparable levels between WT and miR-223$^{-/-}$ mice 24h p.i. S. pn. (Fig. 10C). However, miR-223$^{-/-}$ mice exhibited a sustained PMN response in the BAL and lungs 48h p.i. S. pn., with frequencies of PMN amongst leukocytes significantly higher in miR-223$^{-/-}$ mice compared to WT controls (Fig. 10D-E). Moreover, higher PMN numbers were recorded in the blood of miR-223$^{-/-}$ mice 48h p.i. S. pn. compared to WT controls (Fig. 10F).

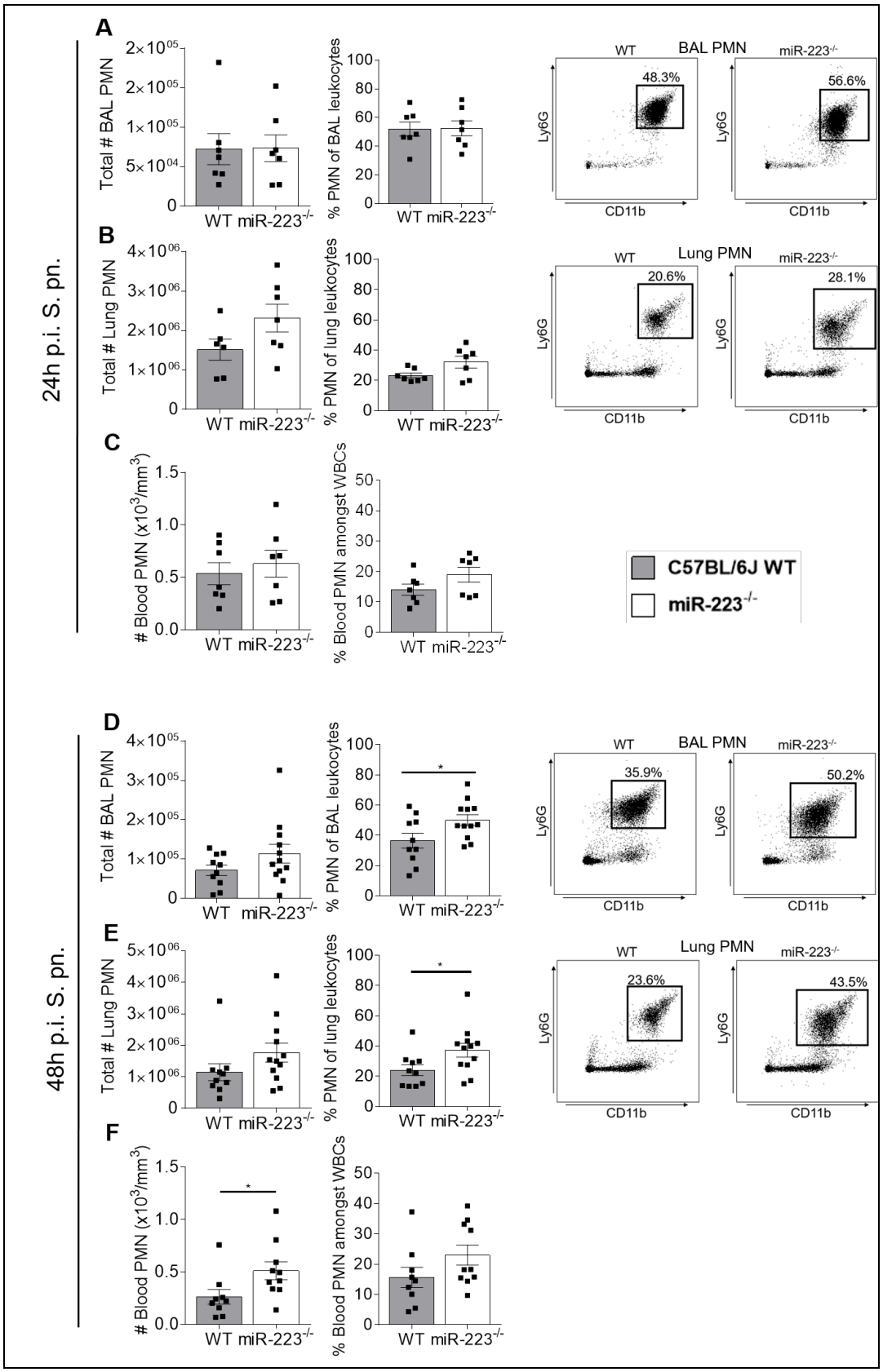

Figure 10. **A** – Total numbers, frequencies and dot blots of BAL PMN 24h p.i. S. pn. **B** – Total numbers, frequencies and dot blots of lung PMN 24h p.i. S. pn. **C** – Total numbers and frequencies of blood PMN 24h p.i. S. pn. **D** – Total numbers, frequencies and dot blots of BAL PMN 48h p.i. S. pn. **E**

– Total numbers, frequencies and dot blots of lung PMN 48h p.i. S. pn. **F** – Total numbers and frequencies of blood PMN 48h p.i. S. pn-infected mice (n=7−12) were sacrificed and the BAL and lungs analyzed at 24h or 48h p.i. S. pn. with flow cytometry for the quantification of PMN influx. Blood PMN were analyzed on the scil Vet ABC Hematology Analyzer. **A–F**; experiment was repeated 2–3 independent times. **D–E;** * denotes $P < 0.05$ (unpaired t-test). **F**; * denotes $P < 0.05$ (Mann-Whitney U test). Data in **A–F** display means and individual values. Error bars represent SEM.

4.2.2. WT mice exhibit enhanced apoptotic neutrophil frequencies in the BAL following *Streptococcus pneumoniae* infection

In light of the sustained PMN response exhibited by miR-223$^{-/-}$ mice 48h p.i. S. pn., BAL and lung cells from WT and miR-223$^{-/-}$ mice at the aforementioned time point were analyzed for early apoptotic and late apoptotic/necrotic PMN populations (Fig. 11A-B), and spleen PMN analyzed for differences in reverse migration (Fig. 11C). Decreased frequencies of early apoptotic PMN were recorded in the BAL of miR-223$^{-/-}$ mice compared to WT mice (Fig. 11A), while late apoptotic/necrotic PMN frequencies were invariant (Fig. 11A). Both early and late apoptotic PMN frequencies were unfluctuating in the lungs of S. pn.-infected mice 48h p.i. (Fig. 11B). Moreover, no differences were recorded between WT and miR-223$^{-/-}$ mice amongst reverse migrated splenic PMN populations (Fig. 11C).

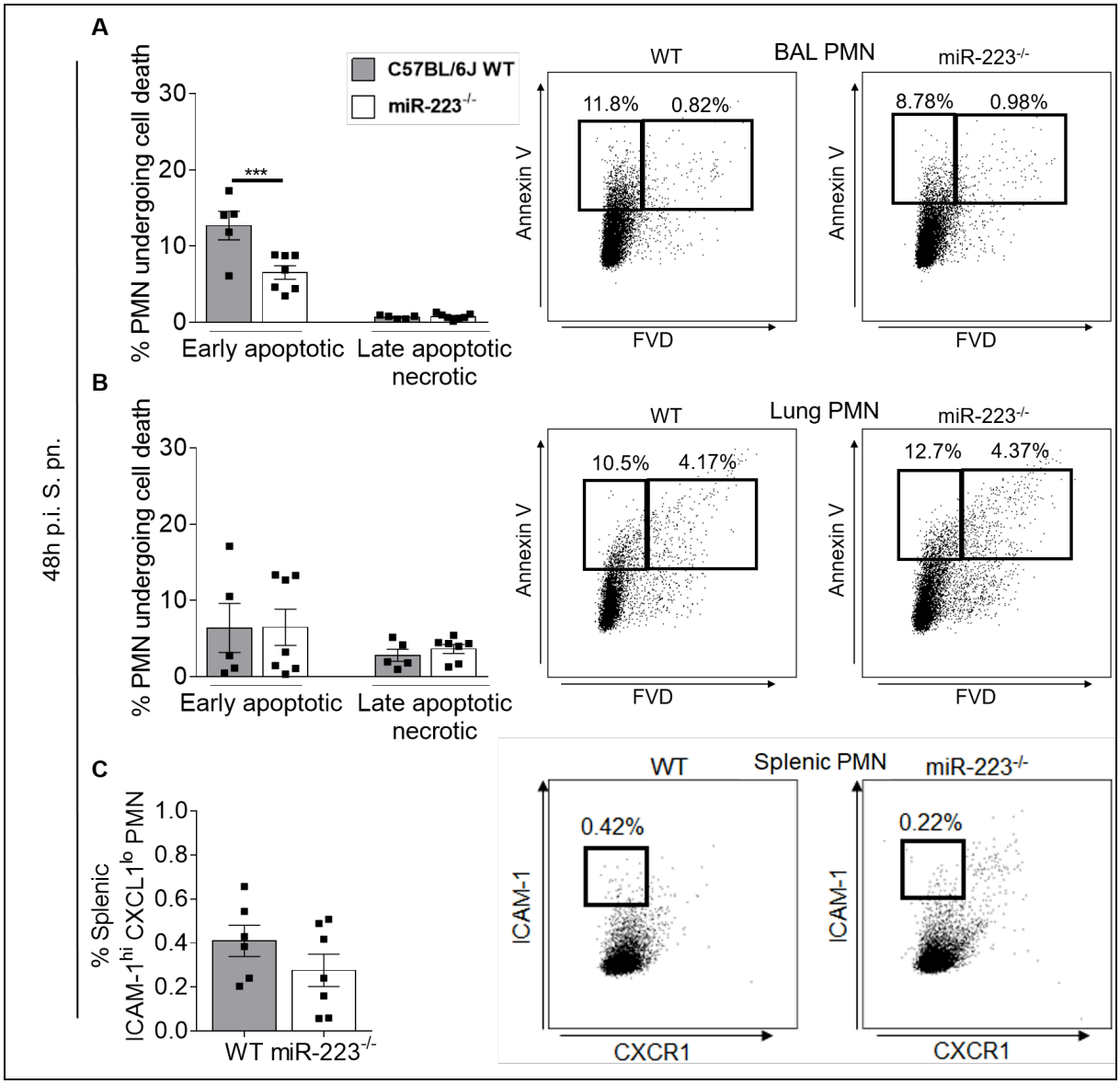

Figure 11. **A** – Frequencies of early apoptotic and late apoptotic/necrotic BAL PMN of WT and miR-223$^{-/-}$ mice 48h p.i. S. pn. **B** – Frequencies of early apoptotic and late apoptotic/necrotic lung PMN of WT and miR-223$^{-/-}$ mice 48h p.i. S. pn. **C** – Reverse migrated PMN frequencies amongst splenic leukocytes of WT and miR-223$^{-/-}$ mice 48h p.i. S. pn.-infected mice (n=5–7) were sacrificed at 48h p.i. S. pn. and the BAL, lungs and spleens analyzed with flow cytometry for evaluation of PMN undergoing cell death and reverse migration (**A–C**). **A–C**; experiment was repeated 2 independent times. **A;** *** denotes $P < 0.001$ (2-way ANOVA/Sidak's multiple comparisons test). Data in **A–C** display means and individual values. Error bars represent SEM.

4.2.3. miR-223$^{-/-}$ mice present decreased alveolar macrophage frequencies in the BAL following *Streptococcus pneumoniae* infection

AM play a crucial role in the response against invading lung pathogens, and while they are unable to contain the growth of pneumococci on their own, they can facilitate PMN recruitment into the lungs through CXCL-chemokines and activate inflammatory cascades through various other cytokine secretion and signaling following infectious stimuli (55, 56, 40). Hence, we aimed to investigate whether altered PMN recruitment had an effect on or was influenced by changes in AM populations.

Following S. pn. infection, WT and miR-223$^{-/-}$ mice were sacrificed and the BAL and lungs were analyzed for AM populations 24- and 48h p.i. WT and miR-223$^{-/-}$ AM total numbers and frequencies amongst leukocytes were recorded at similar levels 24h p.i. S. pn. in the BAL and lungs of WT and miR-223$^{-/-}$ mice (Fig. 12A-B). However, miR-223$^{-/-}$ mice exhibited decreased AM frequencies amongst BAL leukocytes compared to WT controls 48h p.i. S. pn. (Fig. 12C). Total numbers and frequencies of lung AM amongst leukocytes remained unchanged between WT and miR-223$^{-/-}$ mice 48h p.i. S. pn. (Fig. 12D).

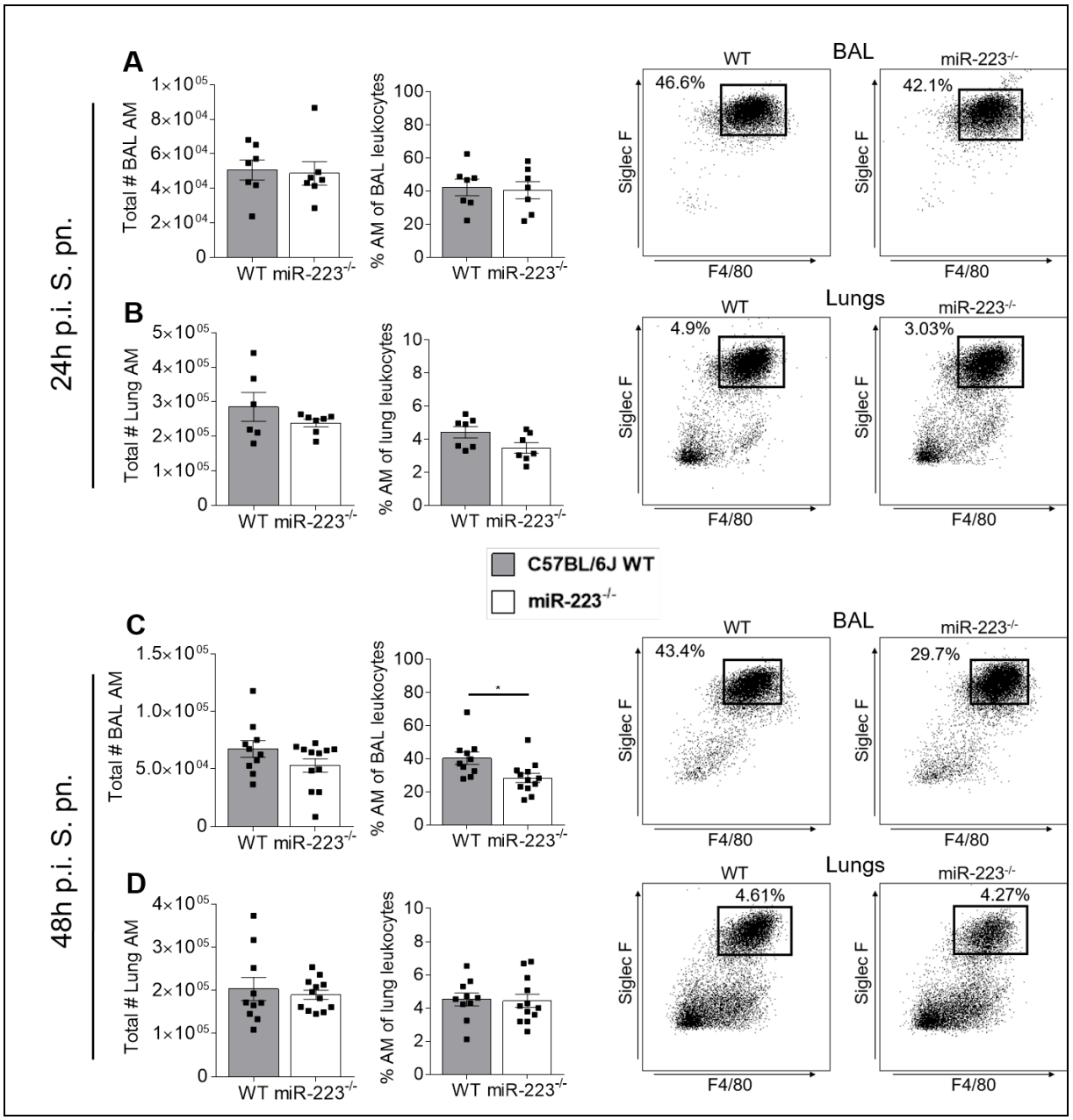

Figure 12. **A** – Total numbers, frequencies and dot blots of BAL AM 24h p.i. S. pn. **B** – Total numbers, frequencies and dot blots of lung AM 24h p.i. S. pn. **C** – Total numbers, frequencies and dot blots of BAL AM 48h p.i. S. pn. **D** – Total numbers, frequencies and dot blots of lung AM 48h p.i. S. pn.-infected mice (n=7–12) were sacrificed and the BAL and lungs analyzed at 24h or 48h p.i. S. pn. with flow cytometry for the quantification of AM and their frequencies amongst leukocytes (**A–D**). **A–D**; experiment was repeated 2–3 independent times. **C;** * denotes $P < 0.05$ (unpaired t-test). Data in **A–D** display means and individual values. Error bars represent SEM.

4.2.4. miR-223$^{-/-}$ mice exhibit decreased inflammatory monocyte/macrophage frequencies in the BAL following *Streptococcus pneumoniae* infection

Monocytes have been described to express low levels of miR-223 relative to bone marrow and peripheral blood PMN (89), while other studies have shown that miR-223 can be released in macrophage-derived microvesicles to facilitate differentiation of a monocytic cell line (THP-1) to a macrophagic phenotype [109]. Hence, we wanted to investigate if the absence of miR-223 affects kinetics of iM populations.

Following S. pn. infection, WT and miR-223$^{-/-}$ mice were sacrificed and the BAL and lungs were analyzed for iM populations 24- and 48h p.i. WT and miR-223$^{-/-}$ iM total numbers and frequencies amongst leukocytes were recorded at similar levels 24h p.i. S. pn. in the BAL and lungs of WT and miR-223$^{-/-}$ mice (Fig. 13A-B). However, miR-223$^{-/-}$ mice exhibited decreased iM frequencies amongst BAL leukocytes compared to WT controls 48h p.i. S. pn. (Fig. 13C). Total numbers and frequencies of lung iM amongst leukocytes remained unchanged between WT and miR-223$^{-/-}$ mice 48h p.i. S. pn. (Fig. 13D).

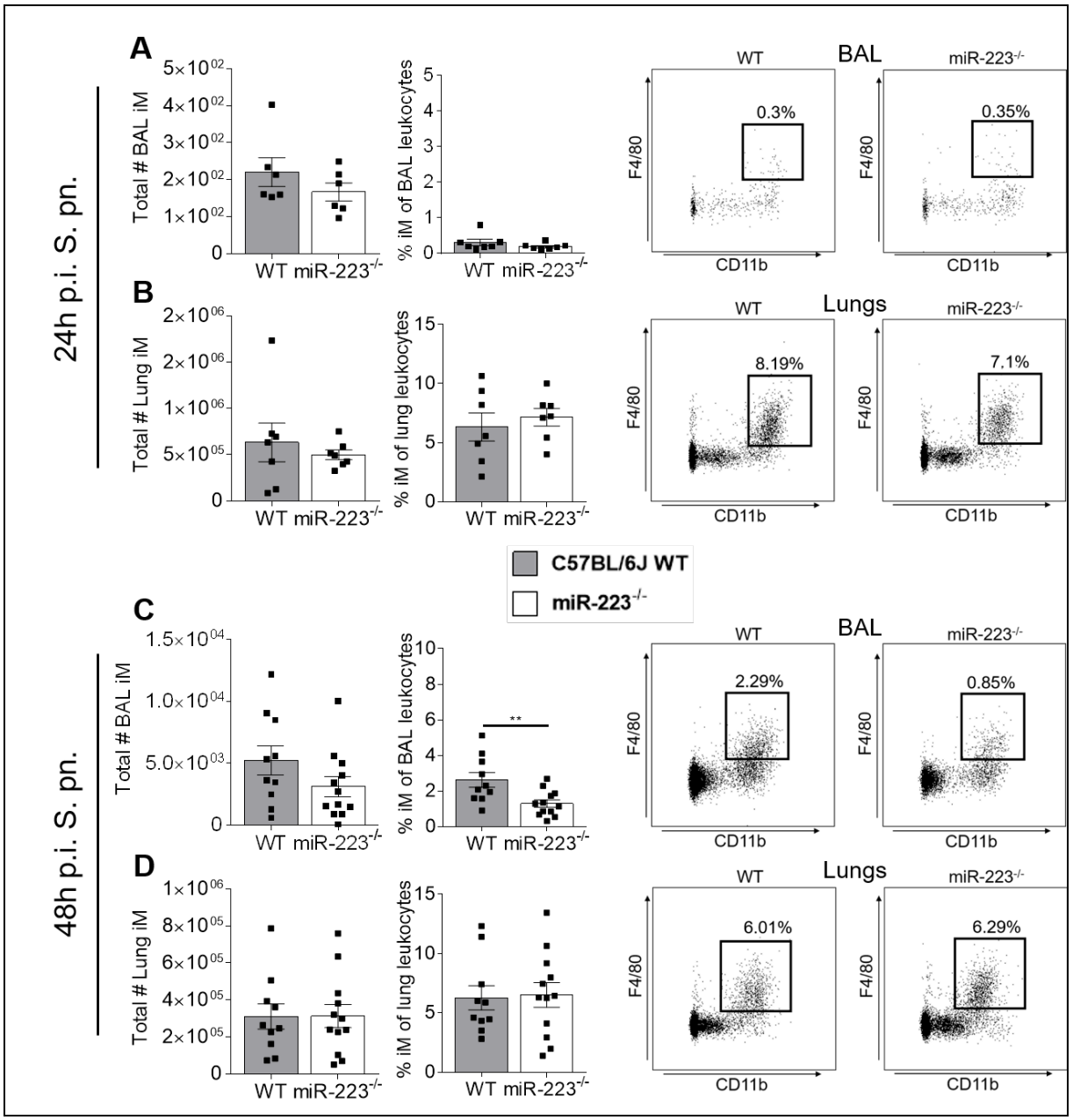

Figure 13. **A** – Total numbers, frequencies and dot blots of BAL iM 24h p.i. S. pn. **B** – Total numbers, frequencies and dot blots of lung iM 24h p.i. S. pn. **C** – Total numbers, frequencies and dot blots of BAL iM 48h p.i. S. pn. **D** – Total numbers, frequencies and dot blots of lung iM 48h p.i. S. pn. S. pn.-infected mice (n=7–12) were sacrificed and the BAL and lungs analyzed at 24h or 48h p.i. S. pn. with flow cytometry for the quantification of iM and their frequencies amongst leukocytes (**A–D**). **A–D**; experiment was repeated 2–3 independent times. **C;** * denotes $P < 0.05$ (unpaired t-test). Data in **A–D** display means and individual values. Error bars represent SEM.

4.2.5. Ly6C^{hi} recruited inflammatory monocyte/macrophage populations remain unchanged between WT and miR-223$^{-/-}$ mice following *Streptococcus pneumoniae* infection

Following S. pn. infection, WT and miR-223$^{-/-}$ mice were sacrificed and the BAL and lungs were analyzed for recruited Ly6C^{hi} iM populations 24- and 48h p.i. WT and miR-223$^{-/-}$ Ly6C^{hi} iM total numbers and frequencies amongst leukocytes were recorded at similar levels 24- and 48h p.i. S. pn. in the BAL and lungs of WT and miR-223$^{-/-}$ mice (Fig. 14A-D).

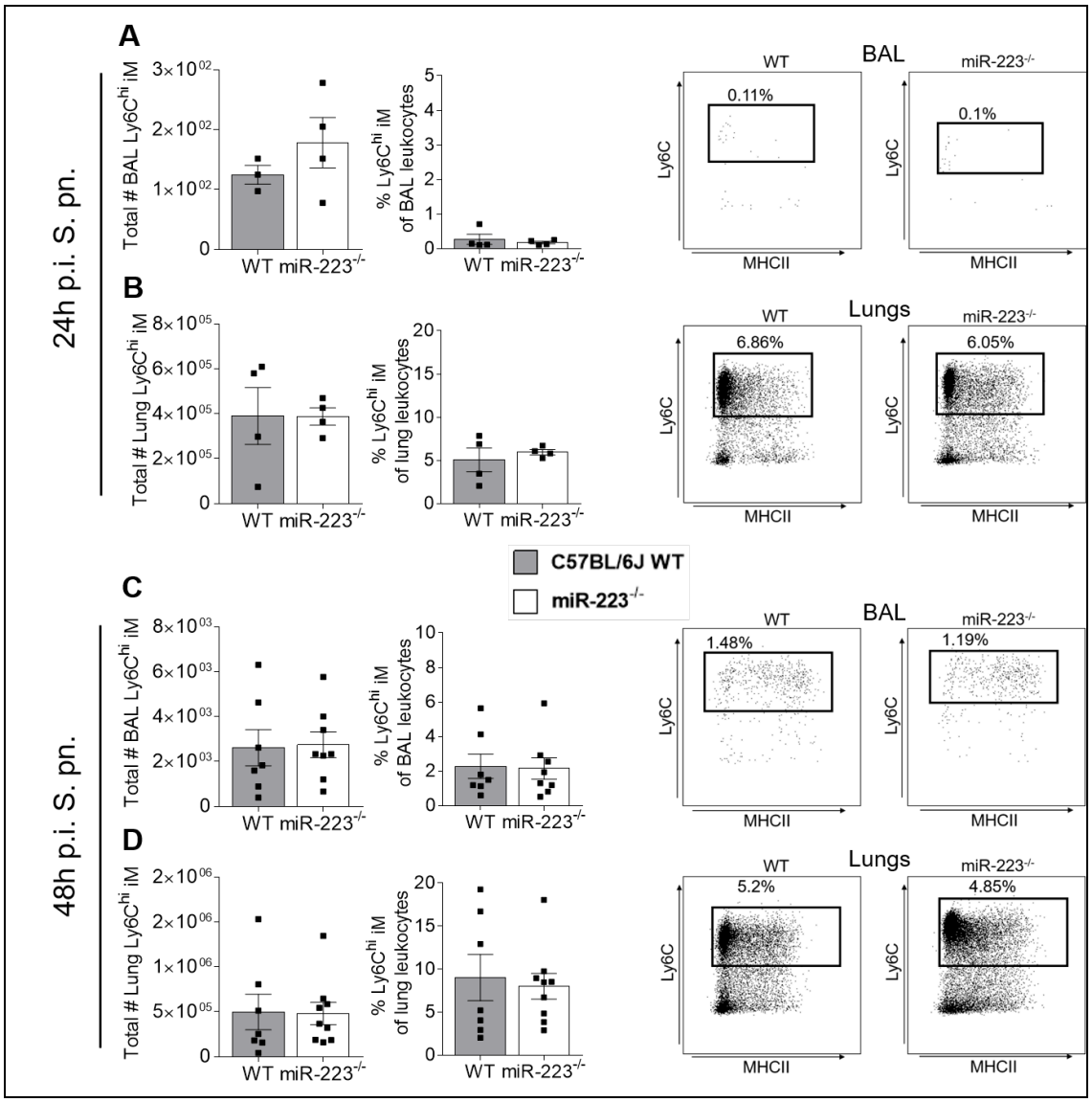

Figure 14. **A** – Total numbers, frequencies and dot blots of BAL Ly6C^{hi} iM 24h p.i. S. pn. **B** – Total numbers, frequencies and dot blots of lung Ly6C^{hi} iM 24h p.i. S. pn. **C** – Total numbers, frequencies

and dot blots of BAL Ly6C^{hi} iM 48h p.i. S. pn. **D** – Total numbers, frequencies and dot blots of lung Ly6C^{hi} iM 48h p.i. S. pn.-infected mice (n=4–9) were sacrificed and the BAL and lungs analyzed at 24h or 48h p.i. S. pn. with flow cytometry for the quantification of Ly6C^{hi} iM and their frequencies amongst leukocytes (**A–D**). **A–D**; experiment was repeated 2 independent times. Data in **A–D** display means and individual values. Error bars represent SEM.

4.2.6. WT and miR-223$^{-/-}$ mice display similar apoptotic/necrotic alveolar macrophage and inflammatory monocyte/macrophage populations following *Streptococcus pneumoniae* infection

miR-223 has been implicated to play a role in cell death pathways including necroptosis in cardiac tissues (110), while miR-223 has also been described to be involved in maintaining viability of THP-1 cells (109). Hence we aimed to investigate if the absence of miR-223 had an impact on apoptotic/necrotic AM and iM populations.

Following S. pn. infection, WT and miR-223$^{-/-}$ mice were sacrificed and the BAL and lungs were analyzed for apoptotic/necrotic AM and iM populations 48h p.i. S. pn. Apoptotic/necrotic AM and iM populations were recorded at similar frequencies in the BAL and lungs of WT and miR-223$^{-/-}$ mice 48h p.i. S. pn. (Fig. 15A-D).

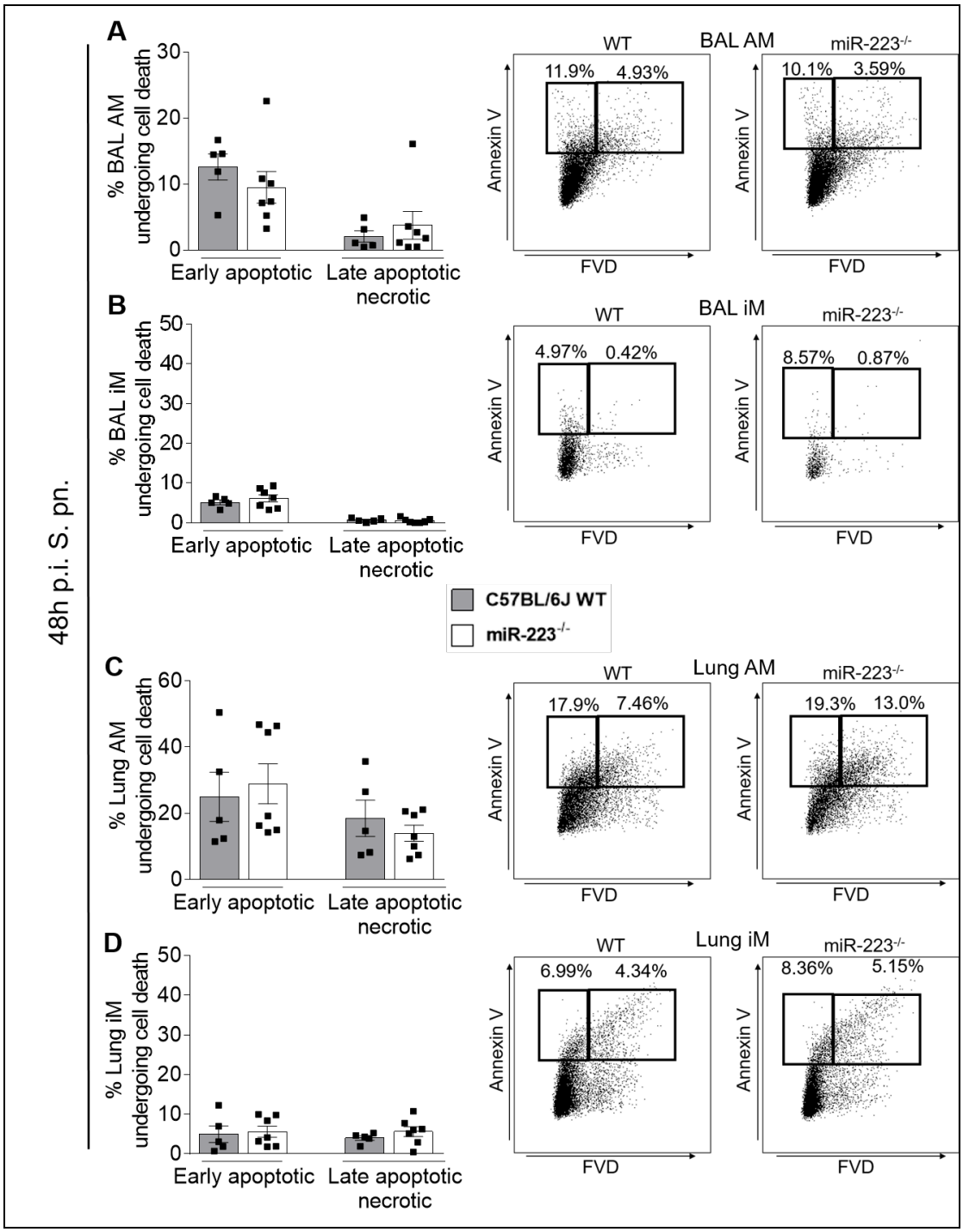

Figure 15. **A** – Frequencies and dot blots of apoptotic/necrotic BAL AM 48h p.i. S. pn. **B** – Frequencies and dot blots of apoptotic/necrotic BAL iM 48h p.i. S. pn. **C** – Frequencies and dot blots of apoptotic/necrotic lung AM 48h p.i. S. pn. **D** – Frequencies and dot blots of apoptotic/necrotic lung iM 48h p.i. S. pn.-infected mice (n=5–7) were sacrificed and the BAL and lungs analyzed at 48h p.i. S. pn. with flow cytometry for the determination of apoptotic/necrotic AM and iM frequencies amongst their respective parent populations. **A–D**; experiment was repeated 2 independent times. Data in **A–D** display means and individual values. Error bars represent SEM.

4.2.7. WT and miR-223$^{-/-}$ neutrophils exhibit similar activation states following *Streptococcus pneumoniae* infection

CD14 has been described to be crucial in the immune response to LPS through TLR4-mediated signaling and is linked to the activation of PMN [111]. LFA-1, on the other hand, is well known for its functions in PMN adhesion and migration [85], however, it has also been suggested to play a role in ROS production in an adhesion-dependent context [112]. Hence, we aimed to investigate if the absence of miR-223 had any bearing on PMN activation state.

Following S. pn. infection, WT and miR-223$^{-/-}$ mice were sacrificed and the BAL and lungs were analyzed for activated PMN populations expressing CD14 and LFA-1 24- and 48h p.i. S. pn. No differences in CD14 or LFA-1 expression were recorded at 24- or 48h p.i. S. pn. (Fig. 16A-D, Fig. 17A-D respectively).

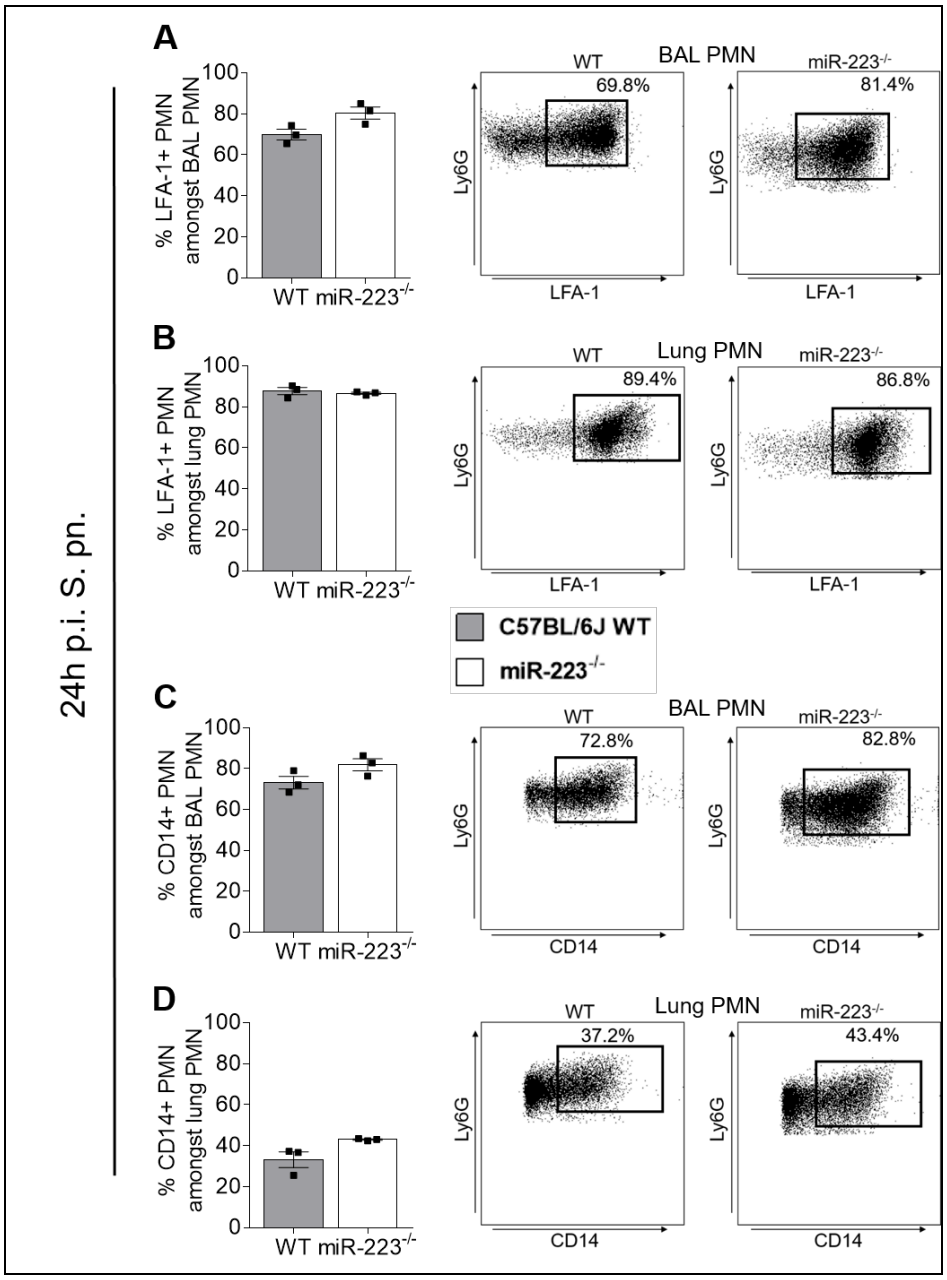

Figure 16. **A** – Frequencies and dot blots of LFA-1+ BAL PMN 24h p.i. S. pn. **B** – Frequencies and dot blots of LFA-1+ lung PMN 24h p.i. S. pn. **C** – Frequencies and dot blots of CD14+ BAL PMN 24h p.i. S. pn. **D** – Frequencies and dot blots of CD14+ lung PMN 24h p.i. S. pn.-infected mice (n=3) were sacrificed and the BAL and lungs analyzed at 24h p.i. S. pn. with flow cytometry for the determination of PMN activation state. **A–D**; experiment was performed once. Data in **A–D** display means and individual values. Error bars represent SEM.

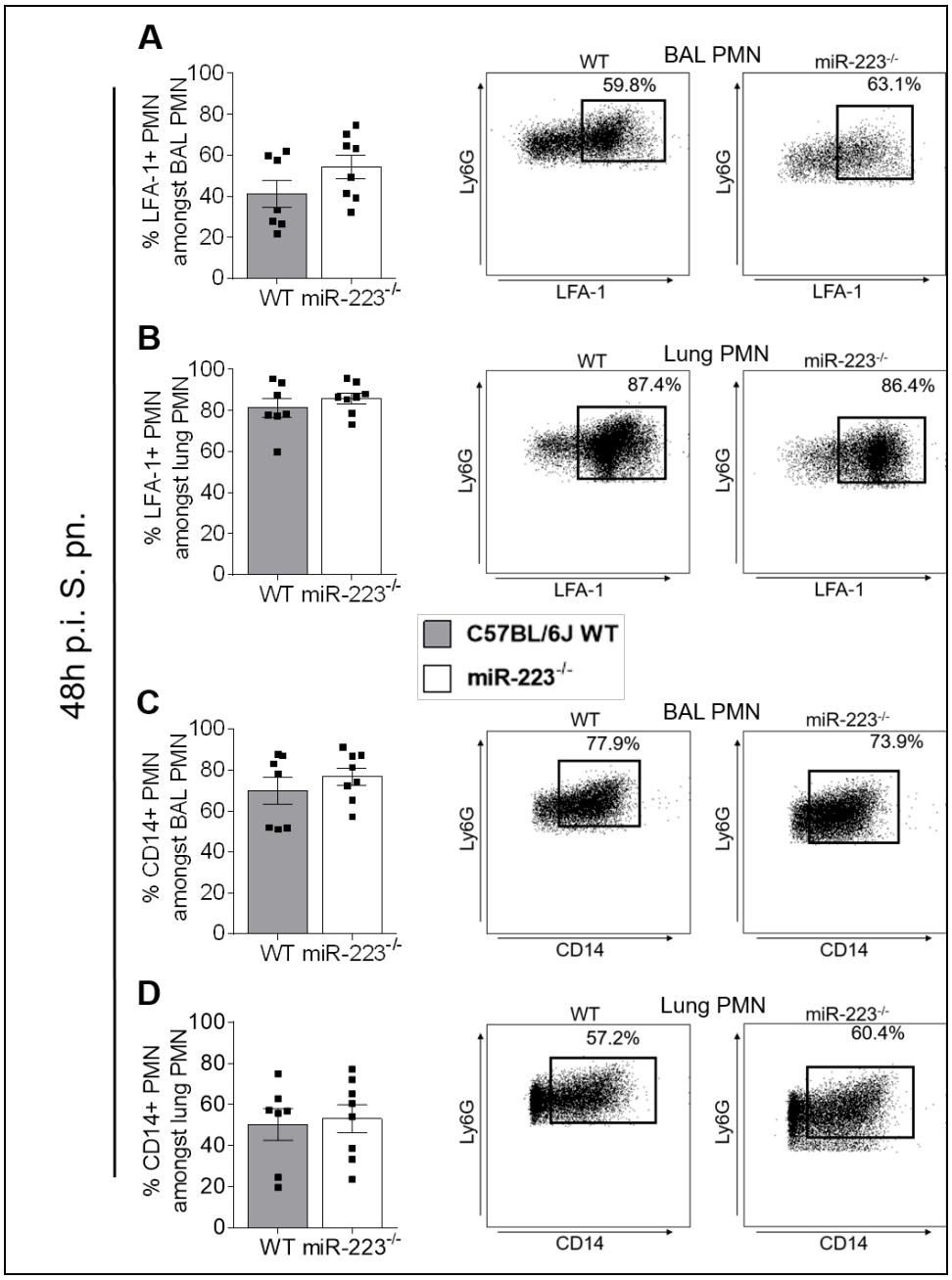

Figure 17. **A** – Frequencies and dot blots of LFA-1+ BAL PMN 48h p.i. S. pn. **B** – Frequencies and dot blots of LFA-1+ lung PMN 48h p.i. S. pn. **C** – Frequencies and dot blots of CD14+ BAL PMN 48h p.i. S. pn. **D** – Frequencies and dot blots of CD14+ lung PMN 48h p.i. S. pn.-infected mice (n=7–8) were sacrificed and the BAL and lungs analyzed at 48h p.i. S. pn. with flow cytometry for the determination of PMN activation state. **A–D**; experiment was performed 2 independent times. Data in **A–D** display means and individual values. Error bars represent SEM.

4.3. miR-223 expression in murine lungs and sorted primary cells following *Streptococcus pneumoniae* infection

In our previous studies, we quantified the fold expression change of miR-223 in murine whole lungs 24- and 48h p.i. S. pn. serotype 3, whereby an approximately 10-fold increase in miR-223 was recorded for both time points relative to sham-infected mice lungs (unpublished data). With mature PMN expressing miR-223 in high levels [89], coupled to the importance of neutrophilic influx in the immune response to pulmonary invading pathogens [66], we aimed at understanding the expression pattern of miR-223 in vivo in murine whole lungs and sorted lung PMN and EpiC 24- and 48h p.i. S. pn. serotype 2, and in vitro in isolated BM-PMN and lung EpiC following 2-, 6-, and 18h S. pn. serotype 2 stimulation.

4.3.1. miR-223 is expressed in vivo in murine whole lungs following *Streptococcus pneumoniae* infection

Following S. pn. or sham (1x PBS) infection, WT mice were sacrificed and a lung lobe was spared for miR-223 expression analysis via qPCR. Relative to sham-infected murine lungs, an approximately 2-fold increase in miR-223 expression was recorded in lungs of S. pn.-infected WT mice 24h p.i., while no differences in miR-223 expression was recorded in lungs of sham- and S. pn.-infected WT mice 48h p.i. miR-223 expression was also significantly higher in murine lungs 24h p.i. compared to 48h p.i. S. pn. (Fig. 18).

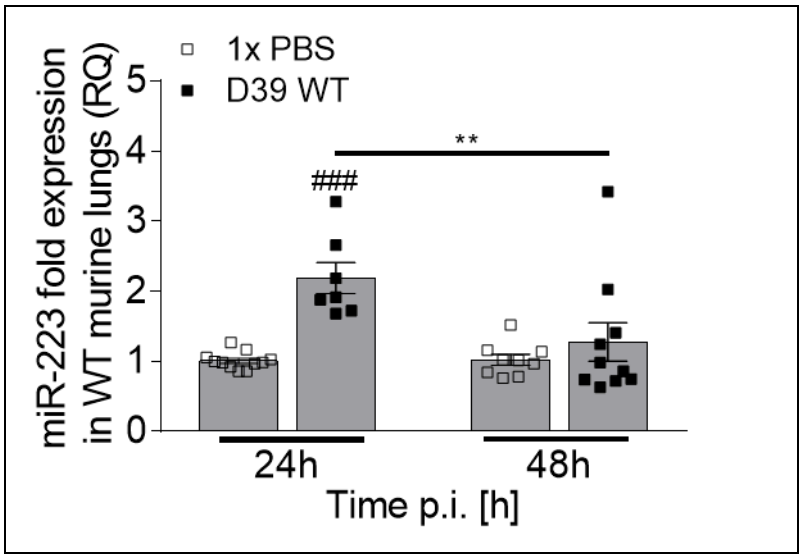

Figure 18. Sham- or S. pn.-infected WT mice (n=7–11) were sacrificed at 24h or 48h p.i. and lungs were harvested, total RNA isolated and reverse transcribed to cDNA for qPCR analysis. miR-223 fold expression in S. pn.-infected lungs (D39 WT) is displayed relative to sham-infected lungs (1x PBS) at the same time point. snoRNA202 was used as a housekeeping gene. A hash sign (#) denotes statistical difference between S. pn.-infected mice relative to the sham-infected group at the same time point, while an asterix (*) denotes statistical difference between S. pn.-infected groups at different time points. Experiment was repeated 2–3 independent times. ### denotes $P < 0.001$ (2-way ANOVA/Sidak's multiple comparisons test), ** denotes $P < 0.01$ (2-way ANOVA/Sidak's multiple comparisons test). Data display means and individual values. Error bars represent SEM.

4.3.2. miR-223 is expressed in magnetically sorted pulmonary neutrophils following *Streptococcus pneumoniae* infection

In order to determine whether the S. pn. virulence factor Ply plays a role in miR-223 expression, naïve, D39 WT- and D39 Δply-infected WT mice were sacrificed and PMN and EpiC were magnetically sorted from whole lungs, followed by qPCR analysis of miR-223 expression. At 24h p.i., sorted PMN from D39 WT-infected mice presented an approximately 3-fold increase in miR-223 expression relative to naïve and D39 Δply-infected sorted PMN, the latter of which displayed similar levels of expression to naïve PMN (Fig. 19A). Furthermore, 24h p.i. sorted PMN from D39 WT-infected mice expressed higher miR-223 than those at 48h p.i. WT PMN that were sorted 24h p.i. did not express miR-223 in the absence of Ply (Fig. 19A), however an approximately 3-fold increase in miR-223 expression was recorded 48h p.i. in D39 Δply-infected WT mice relative to naïve- or D39 WT-infected sorted PMN

(Fig. 19A). With regards to transfer of miR-223 from PMN to lung EpiC, no significant changes were recorded in miR-223 expression in magnetically sorted lung EpiC following sham or S. pn. infection 24- or 48h p.i. (Fig. 19B).

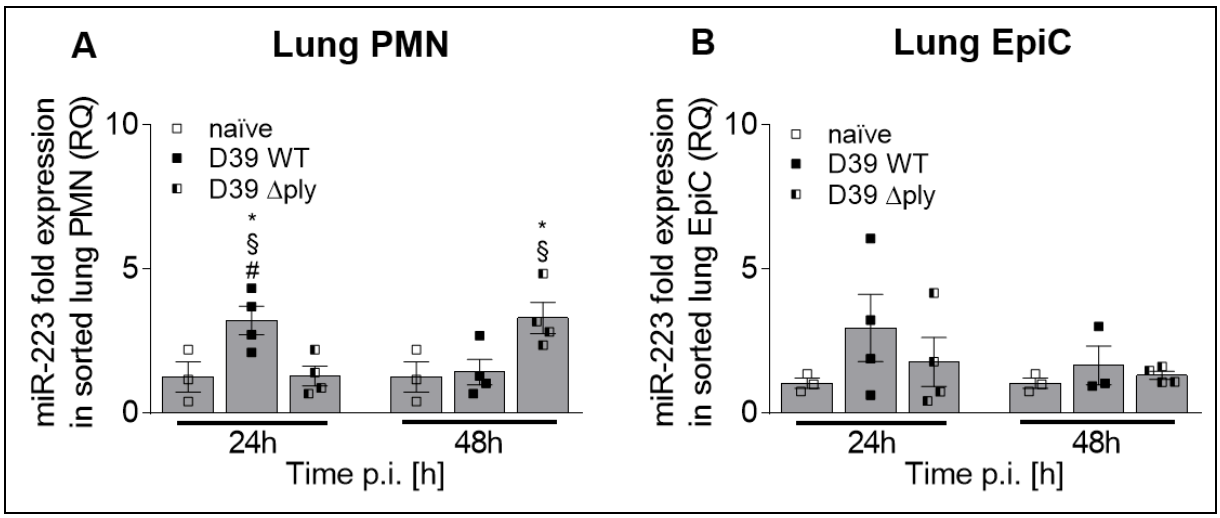

Figure 19. Naïve and S. pn.-infected WT mice (n=3–4) were sacrificed at 24h or 48h p.i. and PMN and lung EpiC were sorted from lungs, total RNA isolated and reverse transcribed to cDNA for qPCR analysis. miR-223 fold expression in (**A**) lung PMN and (**B**) lung EpiC sorted from S. pn.-infected lungs are displayed relative to naïve sorted PMN and lung EpiC. snoRNA202 was used as a housekeeping gene. A hash sign (#) denotes statistical difference between the S. pn.-infected group relative to the naive group, an asterisk (*) denotes statistical difference between adjacent S. pn.-infected groups (bars) at the same time point, while a section sign (§) denotes statistical difference between the S. pn.-infected groups at different time points. **A–B**; experiment was repeated 1–4 independent times. **A;** */#/§ denotes $P < 0.05$ (2-way ANOVA/Sidak's multiple comparisons test/Tukey's multiple comparisons test). Data in **A–B** display means and individual values. Error bars represent SEM.

4.3.3. Absence of pneumolysin delays neutrophil influx into the lungs

Naïve, D39 WT- and D39 Δply-infected WT mice were sacrificed at 24- and 48h p.i. and the lungs processed for magnetic sorting of PMN and EpiC, as previously described in 3.2.6.4. At 24h p.i., D39 WT-infected WT mice presented with approximately 3-fold higher PMN frequencies in the lungs compared to naïve mice, while D39 Δply-infected WT mice presented with milder neutrophilic influx compared to D39 WT-infected mice (Fig. 20). At 48h p.i., D39 WT-infected WT mice exhibited similar levels of lung PMN frequencies to that of 24h p.i., while D39 Δply-infected WT

mice exhibited significantly higher PMN frequencies compared to D39 WT-infected mice 48h p.i. Furthermore, D39 Δply-infected mice presented with enhanced PMN frequencies compared to that of 24h p.i. (Fig. 20).

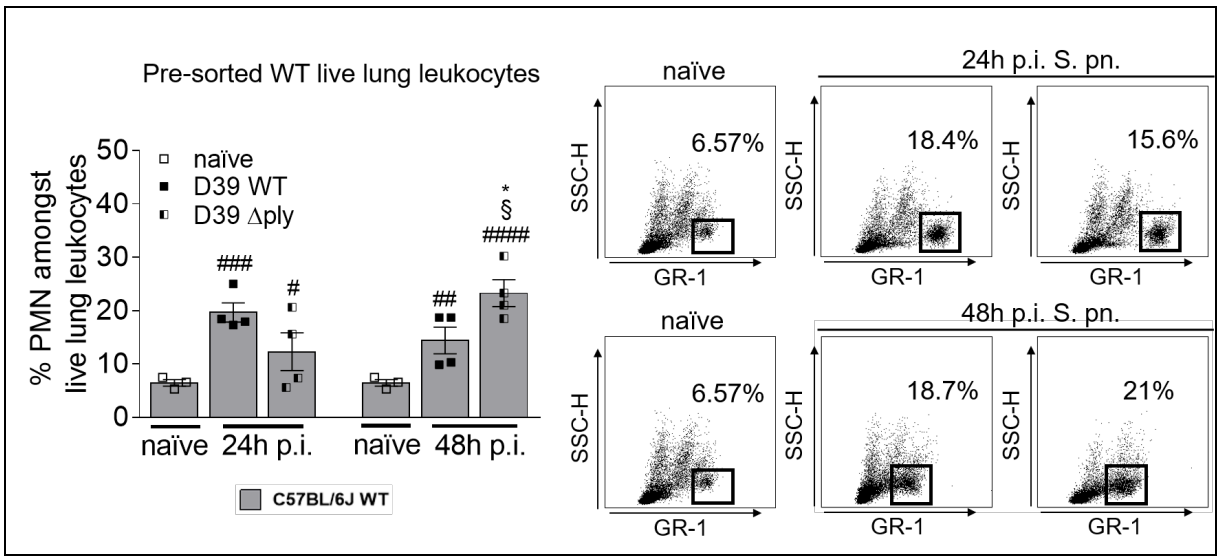

Figure 20. Naïve and S. pn.-infected WT mice (n=3–4) were sacrificed at 24h or 48h p.i. and the lungs were processed for simultaneous sorting of lung PMN and EpiC. Pre-sorted lung suspensions were stained and analyzed with flow cytometry for the determination of PMN frequencies following D39 WT and D39 Δply infection. A hash sign (#) denotes statistical difference between the S. pn.-infected group relative to the naive group, an asterisk (*) denotes statistical difference between adjacent S. pn.-infected groups (bars) at the same time point, while a section sign (§) denotes statistical difference between the S. pn.-infected groups at different time points. Experiment was repeated 1–4 independent times. */#/§ denotes $P < 0.05$ (2-way ANOVA/Sidak's multiple comparisons test/Tukey's multiple comparisons test), ## denotes $P < 0.01$ (2-way ANOVA/Sidak's multiple comparisons test/Tukey's multiple comparisons test), ### denotes $P < 0.001$ (2-way ANOVA/Sidak's multiple comparisons test/Tukey's multiple comparisons test), #### denotes $P < 0.0001$ (2-way ANOVA/Sidak's multiple comparisons test/Tukey's multiple comparisons test). Data display means and individual values. Error bars represent SEM.

4.3.4. Bone marrow neutrophils exhibit delayed upregulation of miR-223 in vitro following *Streptococcus pneumoniae* stimulation

BM-PMN and lung EpiC were isolated from naïve WT mice as previously described in 3.2.6.1 and 3.2.6.2. BM-PMN were stimulated for 2-, 6-, and 18h with 1x PBS

(sham), D39 WT or D39 Δply (illustrated in Fig. 21A), as previously described in 3.2.6.4. Following stimulation, the supernatant was spared and BM-PMN were washed, collected and processed for isolation of RNA and reverse transcription, as previously described in 3.2.8. Isolated lung EpiC were then incubated with the supernatant from stimulated BM-PMN for 5 hours to determine the extent of miR-223 uptake in response to sham- vs WT and Ply-deficient S. pn. stimulation of BM-PMN (illustrated in Fig. 21A). After completion of 5 hours to allow uptake of miR-223 from BM-PMN supernatant, AECII were washed and processed further for the isolation of RNA, reverse transcription, and qPCR analysis as described earlier in 3.2.8.

Following S. pn. stimulation, BM-PMN did not exhibit altered expression of miR-223 2- or 6h p.i., while a 2-fold increase in miR-223 was recorded in BM-PMN stimulated with D39 WT, relative to the sham-infected group (Fig. 21B). No upregulation of miR-223 was observed in BM-PMN following D39 Δply stimulation (Fig. 21B). Upon incubation of AECII with BM-PMN supernatant from Fig. 21B, AECII took up less miR-223 from 6h S. pn.-stimulated BM-PMN supernatant compared to sham-stimulated supernatant (Fig. 21C). Incubation of EpiC with 18h sham- or S. pn.-stimulated BM-PMN supernatant, however, led to a pronounced uptake of miR-223 in lung EpiC incubated with D39 WT-stimulated BM-PMN supernatant, compared to sham- or D39 Δply-stimulated BM-PMN supernatant (Fig. 21C).

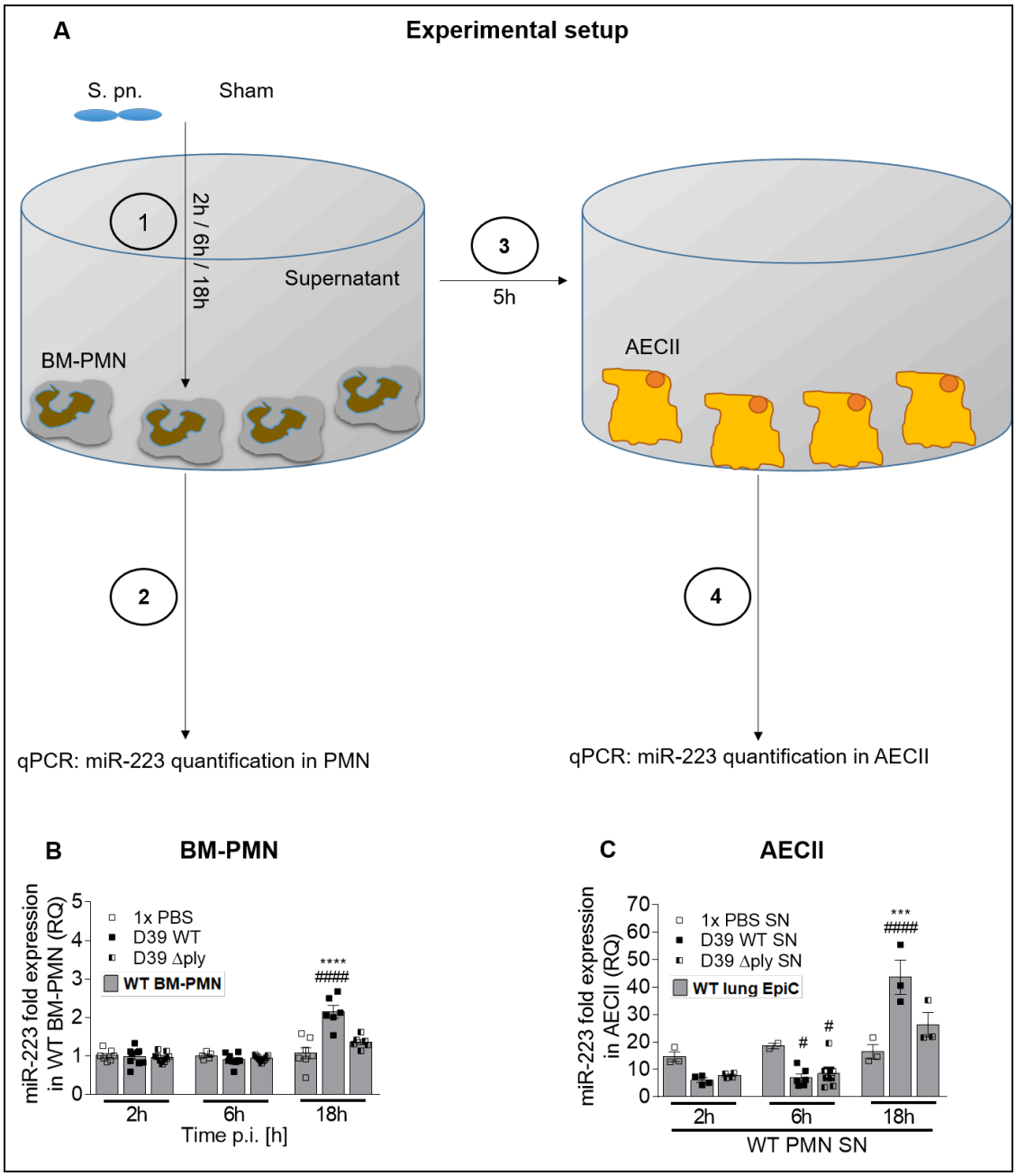

Figure 21. **A** – Experimental setup of miR-223 transfer from stimulated BM-PMN supernatant to AECII. **B** – WT BM-PMN were isolated and stimulated with sham (1x PBS), D39 WT and D39 Δply for 2h, 6h and 18h and analyzed for miR-223 expression via qPCR (n=5–9). **C** – WT AECII were isolated and incubated with stimulated BM-PMN supernatants for 5 hours and analyzed for miR-223 expression via qPCR. miR-223 fold expression in **B** was quantified relative to the sham-stimulated group at each time point. miR-223 fold expression in **C** was quantified relative to untreated lung EpiC. snoRNA202 was used as a housekeeping gene. A hash sign (#) denotes statistical difference between the S. pn.-infected group relative to the sham stimulated or incubated group at the same time point, while an asterisk (*) denotes statistical difference between adjacent S. pn.-infected groups at the same time point. Experiment was repeated 3 independent times. **B**; ****/#### denotes $P < 0.0001$ (2-way ANOVA/Tukey's multiple comparisons test. **C**; # denotes $P < 0.05$ (2-way ANOVA/Tukey's multiple

comparisons test), ** denotes $P < 0.01$ (2-way ANOVA/Tukey's multiple comparisons test), ### denotes $P < 0.001$ (2-way ANOVA/Tukey's multiple comparisons test). Data in **B–C** display means and individual values. Error bars represent SEM.

4.4. Inflammatory mediators and histology

miR-223 has been described to be an anti-inflammatory miRNA in the context of both VILI-associated ALI [96] and chronic lung pathology such as Mtb infection [97]. Hence, we aimed at investigating the role played by miR-223 in regulating lung inflammation through analysis of inflammatory cytokines, chemokines, alveolar-endothelial barrier integrity and lung histopathology.

4.4.1. WT and miR-223$^{-/-}$ mice exhibit comparable levels of inflammation 24h p.i. *Streptococcus pneumoniae*

WT and miR-223$^{-/-}$ mice were infected intranasally with 5x10^6 CFU S. pn. serotype 2 and after 24h, mice were sacrificed and the BAL collected. The BALF was used to quantify inflammatory cytokines (Fig. 22A), inflammatory chemokines (Fig. 22B) and lung barrier integrity parameters (Fig. 22C). Inflammatory cytokines quantified included IL-6, MPO, IL-1α, IL-1β, IL-17A, TNF-α, IFN-γ, GM-CSF and IL-23 (Fig. 22A). The chemokines quantified comprised CXCL1-, 2-, 5 and CCL2 (Fig. 22B). Lung barrier integrity was determined by the ratio of albumin quantified in BALF/plasma and VEGF concentration levels (Fig. 22C). Two-fold less IL-1β concentrations were recorded in the BAL of miR-223$^{-/-}$ mice compared to the BALF of WT mice, however the remainder of the aforementioned inflammatory cytokines were recorded at similar levels between WT and miR-223$^{-/-}$ mice (Fig. 22A). No differences were recorded in CXCL1, -2, -5, and CCL2 concentrations in the BALF of WT and miR-223$^{-/-}$ mice 24h p.i. S. pn. (Fig. 22B). Furthermore, lung barrier integrity was not different between WT and miR-223$^{-/-}$ mice, as evidenced by the ratio of BALF/plasma albumin and BALF VEGF concentrations (Fig. 22C).

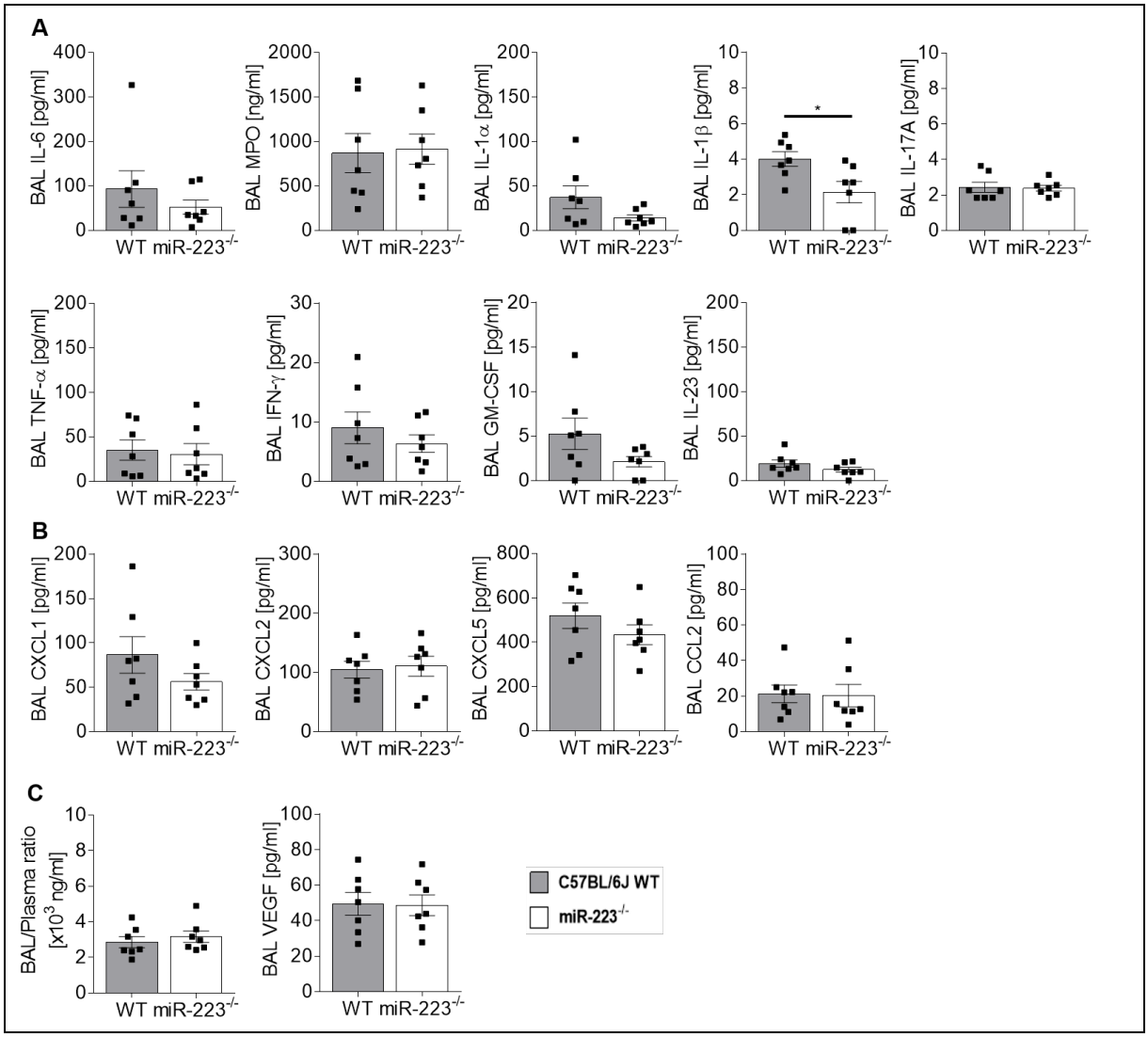

Figure 22. **A** – Concentrations of BALF IL-6, MPO, IL-1α, IL-1β, IL-17A, TNF-α, IFN-γ, GM-CSF and IL-23 recorded in WT and miR-223$^{-/-}$ mice 24h p.i. S. pn. **B** – Concentrations of CXCL1, CXCL2, CXCL5 and CCL2 recorded in WT and miR-223$^{-/-}$ mice 24h p.i. S. pn. **C** – Mouse albumin leakage into BAL from plasma and BAL VEGF concentrations recorded in WT and miR-223$^{-/-}$ mice 24h p.i. S. pn.-infected mice (n=7) were sacrificed and the BAL samples analyzed with ELISA for the determination of inflammatory cytokines, chemokines and barrier integrity parameters. **A–C**; experiment was repeated 2 independent times. **A**; * denotes $P < 0.05$ (unpaired t-test). Data in **A–C** display means and individual values. Error bars represent SEM.

4.4.2. miR-223$^{-/-}$ mice exhibit exacerbated inflammatory cytokine and chemokine concentrations 48h p.i. *Streptococcus pneumoniae*

WT and miR-223$^{-/-}$ mice were infected intranasally with 5x10^6 CFU S. pn. serotype 2 and after 48h, mice were sacrificed and the BAL collected. The BALF was used to quantify inflammatory cytokines (Fig. 23A), inflammatory chemokines (Fig. 23B) and lung barrier integrity parameters (Fig. 23C), as described earlier in 4.4.1. Enhanced concentrations of IL-6, MPO, IL-1α, TNF-α and IFN-γ were recorded in the BALF of miR-223$^{-/-}$ mice 48h p.i. S. pn. (Fig. 23A). Concentrations of IL-1β, IL-17A, GM-CSF and IL-23, however, remained unchanged between WT and miR-223$^{-/-}$ mice 48h p.i. S. pn. (Fig. 23A). BALF CXCL2 concentrations were matching between WT and miR-223$^{-/-}$ mice, however CXCL1, CXCL5 and CCL2 concentrations were elevated in the BALF of miR-223$^{-/-}$ mice compared to WT mice 48h p.i. S. pn. (Fig. 23B). Furthermore, lung barrier integrity was unaltered between WT and miR-223$^{-/-}$ mice, as evidenced by the ratio of BALF/plasma albumin and BALF VEGF concentrations (Fig. 23C).

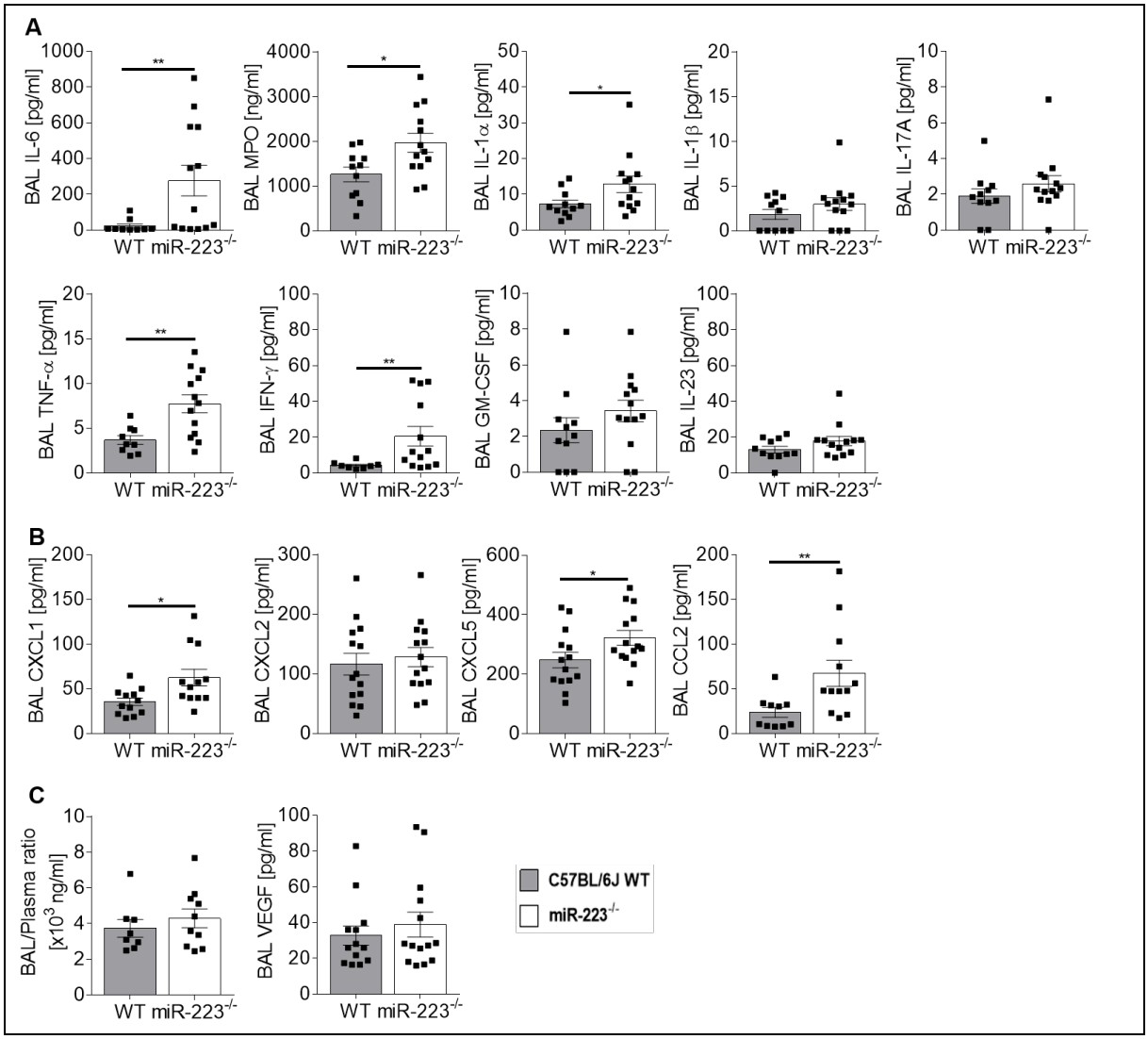

Figure 23. **A** – Concentrations of BALF IL-6, MPO, IL-1α, IL-1β, IL-17A, TNF-α, IFN-γ, GM-CSF and IL-23 recorded in WT and miR-223$^{-/-}$ mice 48h p.i. S. pn. **B** – Concentrations of CXCL1, CXCL2, CXCL5 and CCL2 recorded in WT and miR-223$^{-/-}$ mice 48h p.i. S. pn. **C** – Mouse albumin leakage into BAL from plasma and BAL VEGF concentrations recorded in WT and miR-223$^{-/-}$ mice 48h p.i. S. pn. 11-14 S. pn.-infected mice were sacrificed and the BAL samples analyzed with ELISA for the determination of inflammatory cytokines, chemokines and barrier integrity parameters. **A–C**; experiment repeated 3 independent times. **A–C**; statistical analyses performed using unpaired t-test or Mann-Whitney U test depending on Gaussian distribution as determined by D'Agostino-Pearson omnibus normality test. Outliers were identified and removed following the ROUT test. * denotes $P < 0.05$, ** denotes $P < 0.01$. Data in **A–C** display means and individual values. Error bars represent SEM.

4.4.3. miR-223$^{-/-}$ mice exhibit exacerbated lung pathology 48h p.i. *Streptococcus pneumoniae*

WT and miR-223$^{-/-}$ mice were intranasally infected with 5x10^6 S. pn. and the lungs were examined histologically 48h p.i. (Fig. 24A). Various parameters including purulence, catarrhal purulence, pleuritis, steatitis, perivascular edema, hemorrhages, and percentage of affected lung area were scored from 1-4 (Fig. 24B) (1: minimal, 2: light grade, 3: middle grade, 4: high grade). The overall inflammation score (Fig. 24A) was graded as the sum of the purulence, catarrhal purulence, pleuritis, steatitis, perivascular edema and hemorrhage scores. Upon S. pn. infection, miR-223$^{-/-}$ mice presented with exacerbated lung inflammation characterized by pronounced edema coupled to excessive neutrophilic infiltrates (denoted by * on Fig. 24A, right). WT mice, on the other hand, presented with marginal edema and predominant lymphocytic cuff formation in the lungs (denoted by # on Fig. 24A, left). Furthermore, WT and miR-223$^{-/-}$ mice exhibited similar levels of purulence, catarrhal purulence and area of lungs affected (%), while miR-223$^{-/-}$ mice presented with exacerbated pleuritis, steatitis, hemorrhages and perivascular edema compared to WT mice (Fig. 24B). Hence, the overall inflammation deduced from the aforementioned parameters resulted in an approximately 2-fold higher inflammation score for miR-223$^{-/-}$ mice 48h p.i. S. pn. (Fig. 24).

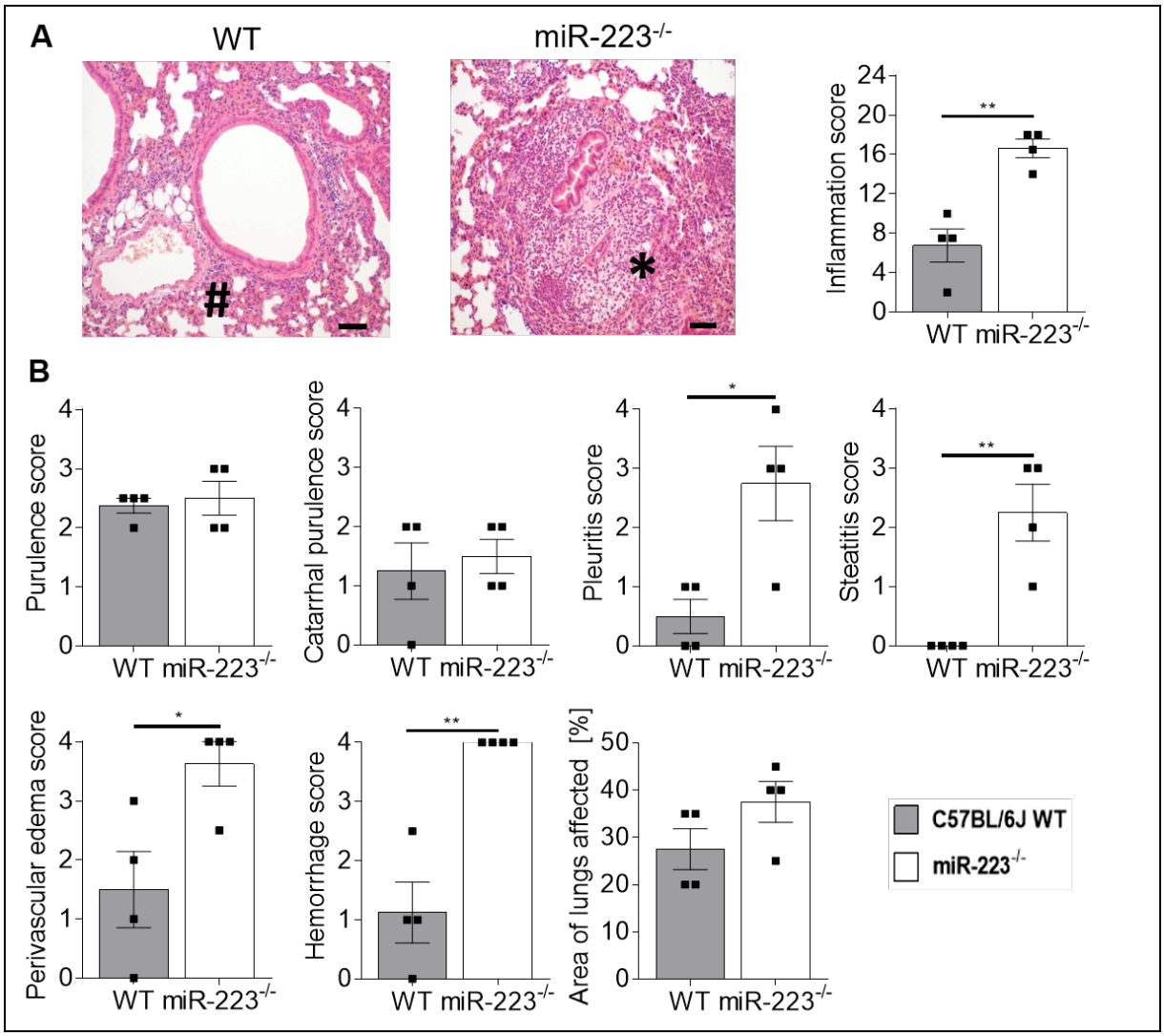

Figure 24. **A** – Histopathological analysis and inflammation score of WT and miR-223$^{-/-}$ murine lungs 48h p.i. S. pn.; **#** (pictured left) – marginal edema coupled to lymphocytic cuff formation, ***** (pictured right) – pronounced edema coupled to excessive neutrophilic infiltrates. **B** – Scores recorded for purulence, catarrhal purulence, pleuritic, steatitis, perivascular edema, hemorrhages and % of affected lung area in WT and miR-223$^{-/-}$ mice 48h p.i. S. pn.-infected mice (n=4) were sacrificed and the lungs analyzed histopathologically for degree of lung inflammation following S. pn. infection. **A–B**; experiment was performed once. **A–C**; experiment was repeated 2 independent times. **A**; ** denotes $P < 0.01$ (unpaired t-test). **B–C**; * denotes $P < 0.05$ (unpaired t-test), ** denotes $P < 0.01$ (unpaired t-test). Data in **A–C** display means and individual values. Error bars represent SEM. Scalebar; 100µm

4.5. Phagocytosis and killing of *Streptococcus pneumoniae* by bone marrow neutrophils

miR-223$^{-/-}$ bone marrow neutrophils exhibit similar capacity for phagocytosis and killing of *Streptococcus pneumoniae* with WT bone marrow neutrophils

WT and miR-223$^{-/-}$ BM-PMN were isolated as previously described in 3.2.6.1 and gentamicin protection assay performed as described in 3.2.7 to determine the extent of phagocytosis and killing of S. pn. BM-PMN were stimulated with serum opsonized D39 GFP and D39 WT for 1 hour at MOI10 and MOI100 to allow for phagocytosis (displayed as 0h on Fig. 25), followed by additional stimulation (displayed as 1h and 2h on Fig. 25) to determine the killing capacity of WT and miR-223$^{-/-}$ BM-PMN via flow cytometry. While close to just 20% of BM-PMN took up D39 GFP at MOI10, around 90% of BM-PMN were recorded to phagocytose D39 GFP at MOI100. WT and miR-223$^{-/-}$ BM-PMN were equally adept at phagocytosis (0h) and killing (1h, 2h) of D39 GFP (Fig. 25).

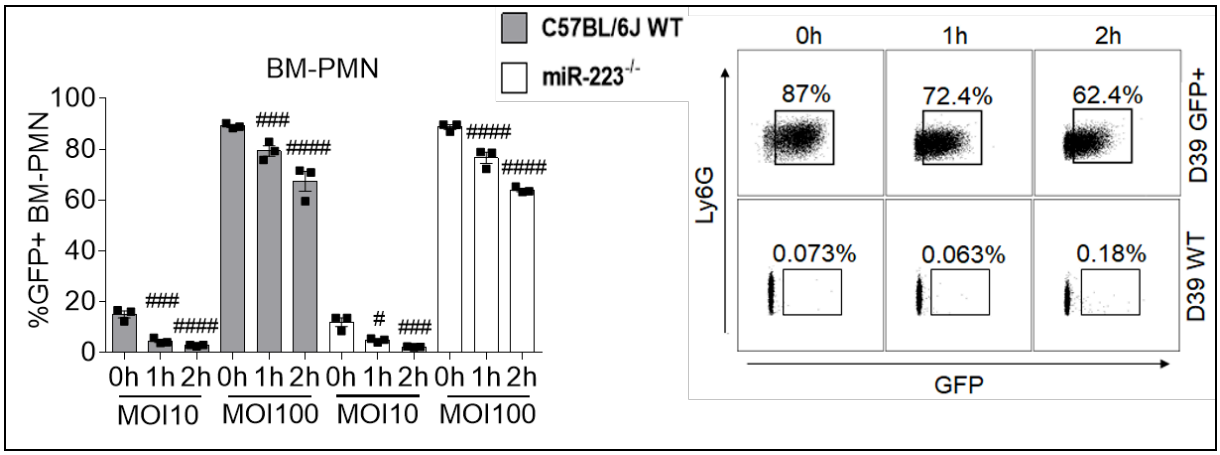

Figure 25. Gentamicin protection assay to determine phagocytosis and killing of S. pn. by WT and miR-223$^{-/-}$ BM-PMN. BM-PMN were stimulated with D39 GFP and D39 WT and analyzed for phagocytosis (0h) and killing (1h, 2h) of S. pn. PMN containing phagocytized D39 GFP were determined as a double positive population for GFP and Ly6G on the flow cytometer. WT and miR-223$^{-/-}$ mice (n=3) were sacrificed and the BM-PMN isolated and plated in triplicate for each condition and time point. A hash sign (#) denotes statistical difference between the S. pn.-infected groups (0h vs 1h and 2h) at the same MOI. # denotes $P < 0.05$ (2-way ANOVA/Sidak's multiple comparisons test), ### denotes $P < 0.001$ (2-way ANOVA/Sidak's multiple comparisons test), #### denotes $P < 0.0001$

(2-way ANOVA/Sidak's multiple comparisons test). Data display means and individual values. Error bars represent SEM.

5. Discussion

The immune response to pneumococci commences in the upper airways, exerted by the production of and entrapment by mucus, clearance by reflexes such as sneezing or coughing, and the presence of immunoglobulins and antimicrobial peptides in the airway lining fluid in order to contain bacterial growth and invasion through the mucus layer [113]. Upon infiltration of bacteria into the lower airways, however, bacterial motifs are sensed by cell surface and intracellular PRRs possessed by epithelia that activate intrinsic signaling pathways, ultimately leading to activation of the cellular immune response through production of leukocyte-attracting chemokines and cytokines [114]. Upon initiation of the cellular immune response, PMN are the first innate phagocytes to mobilize to the lungs and exert effector functions such as phagocytosis, release of intracellular granules and production of reactive oxygen species and elastase [115]. Despite the efficiency of PMN to clear bacteria using the aforementioned mechanisms of action, effector functions such as ROS and elastase production may also be toxic for the host and thus hinder gaseous exchange from taking place freely; demonstrating that bacteria-induced ALI pathology is manifested not only by pathogen-mediated lung tissue exacerbations, but also due to destructive host-mediated inflammation [114]. miR-223 is highly expressed in bone marrow-derived cells [90], with fully mature peripheral blood PMN expressing miR-223 in highest abundance [89]. Furthermore, miR-223 has been described to play vital roles in PMN differentiation, maturation and activation [89], making it crucial to understand the specific role played by miR-223 in the context of acute bacterial lung infection and inflammation.

Generally, pneumonia progression and the cellular immune response were more similar between WT and miR-223$^{-/-}$ mice than initially expected. Clinical parameters such as changes in body temperature and weight loss following S. pn. infection were recorded at similar levels, albeit slightly lower body temperatures exhibited by miR-223$^{-/-}$ mice, coupled to enhanced weight loss 48h p.i. Bacterial burden recorded in the lungs, BAL, spleen and blood were also unvaried, which was supported by a

murine model of ALI utilizing intratracheal *S. aureus* infection, whereby no differences in lung and BAL bacterial burden were recorded between WT and miR-223$^{-/-}$ mice 4h p.i. [96]. These findings were in contrast to a murine model of wound healing, however, as miR-223$^{-/-}$ mice exhibited enhanced clearance of *S. aureus*, inoculated at 1x10^{8} CFU to the wound site, 3 days p.i. [116]. In further contrast, in a murine model of chronic lung inflammation, Mtb-infected miR-223$^{-/-}$ mice exhibited higher bacterial loads in the lungs 21- and 25 days p.i. compared to WT mice, albeit maintaining similar levels 7- and 14 days p.i. [97]. Taken together, the effect of miR-223 on PMN-mediated bacterial clearance depends on the infection model and is organ specific.

Enhanced PMN infiltration in the absence of miR-223 is a hallmark behavior mediated by miR-223$^{-/-}$ mice in the context of acute, chronic or sterile inflammation. In a murine model of wound healing, dorsal skin wounds triggered PMN influx to the wound site, characterized by a slightly delayed influx of miR-223$^{-/-}$ PMN early after injury (1 - 9h post injury) followed by gradual increase in miR-223$^{-/-}$ PMN numbers at the wound site starting 12h post injury [116]. Furthermore, miR-223$^{-/-}$ mice exhibited delayed aseptic skin wound healing characterized by pronounced PMN infiltrates and scar tissue area [116]. In a zebrafish model of wound healing, miR-223$^{-/-}$ zebrafish presented with enhanced neutrophilic inflammation at the wound site compared to WT controls, characterized by higher numbers of miR-223$^{-/-}$ PMN 1- and 6h post injury [117]. In an experimental model of dextran sodium sulfate (DSS)-colitis, miR-223$^{-/-}$ mice exhibited exacerbated acute intestinal inflammation characterized by intestinal infiltrates including high numbers of PMN following induction of colitis [118]. miR-223$^{-/-}$ mice also exhibit pronounced neutrophilic migration patterns in various acute and chronic lung inflammation models. Following S. pn. infection, we recorded mild neutrophilia in the lungs and BAL of miR-223$^{-/-}$ mice compared to WT mice 48h p.i., but not at 24h p.i. While the degree of our recorded PMN influx was in concordance with an ALI model of intratracheal *S. aureus* infection, the degree of PMN influx was inferior to post-VILI in miR-223$^{-/-}$ mice [96]. In a murine model of Mtb-associated chronic lung pathology, which is characterized by accumulation of myeloid cells at the sites of lesions, Mtb-resistant mice became susceptible to Mtb pathology and exhibited dramatic reduction in survival in the absence of miR-223,

triggered by exacerbated PMN migration and PMN-mediated inflammation that could be partially reversed by depletion of PMN [97]. Our analysis of CXCL-chemokines revealed elevated CXCL1- and 5 concentrations in the BAL of miR-223$^{-/-}$ mice 48h p.i. S. pn., while CXCL2 concentrations remained stable between WT and miR-223$^{-/-}$ mice; which helps to explain the enhanced total numbers of blood PMN we recorded in miR-223$^{-/-}$ mice 48h p.i. These findings are in line with the fact that CXCL2, which is predominantly produced by alveolar macrophages [80], is retained in the pulmonary space and acts locally while CXCL1 may selectively transit through the vasculature and into the circulation [80]. Indeed, we previously recorded pronounced CXCL2 production by AM and also by BM-PMN following S. pn. stimulation (unpublished findings), thereby hinting that the enhanced PMN infiltration presented by miR-223$^{-/-}$ mice following S. pn. infection is independent of PMN- or AM-mediated neutrophilic influx. Furthermore, pulmonary CXCL5 has been described to be exclusively produced by epithelial cells [82] and following Mtb infection, CXCL5$^{-/-}$ mice display significantly reduced pulmonary PMN recruitment following both low-dose and high-dose aerosol Mtb infection [36]. Moreover, in an acute lung inflammation setting, we recorded reduced pulmonary PMN infiltration in CXCL5$^{-/-}$ mice compared to WT mice following VILI and also post-S. pn. infection (unpublished data). CXCL1 has been described as a PMN chemoattractant produced by airway epithelia as well as resident lung macrophages [78] and we could confirm in vitro that following S. pn. stimulation, lung EpiC were the predominant sources of CXCL1, followed by AM (unpublished data). Indeed, CXCL1 has been shown to be elevated in miR-223$^{-/-}$ mice following VILI and also after intratracheal *S. aureus* inoculation [96]; collectively suggesting that our findings implicate a mainly epithelial-, rather than macrophage- or PMN-derived, recruitment of PMN into alveolar spaces of miR-223$^{-/-}$ mice following S. pn. infection. In addition to elevated concentrations of chemoattractants, lower frequencies of PMN were recorded to undergo early apoptosis in the BAL of miR-223$^{-/-}$ mice, while apoptotic lung PMN in WT and miR-223$^{-/-}$ mice were recorded at similar frequencies 48h p.i. S. pn. miR-223 has been described to be actively involved in cellular processes such as cell death and proliferation and it has been shown that miR-223 overexpression in hep3B cells − a hepatocellular carcinoma cell line − increased the rate of cells undergoing apoptosis, while cell proliferation was attenuated; an effect linked to the targeting of NLRP3 by miR-223, the former of which has been implicated to have pro-carcinogenic effects

[119]. Moreover, miR-223 has been shown to target NF-κB – a multifunctional transcription factor involved in both pro-inflammatory cytokine production and anti-inflammatory processes such as cell survival and apoptosis during resolution of inflammation [117] - to dampen PMN-mediated inflammation in zebrafish embryos [117]. In recent years, a phenomenon termed “reverse migration” has been described in sterile inflammation models of PMN chemotaxis, which is a process involving migration of PMN away from the site of inflammation and back into circulation instead of undergoing apoptosis [120]. PMN reverse migration in zebrafish larvae was shown to be dependent on initial recruitment into site of inflammation via PMN CXCR1, followed by repulsion of PMN away from the site of inflammation against a gradient of attractant chemokines such as CXCL8, triggered by CXCL8-mediated random migration [121]. PMN reverse migration was also shown to be dependent on reduced expression of junctional adhesion molecule (JAM)-C found on endothelial cells, which was linked to dissemination of systemic inflammation in an ischemia/reperfusion model in mice [122]. Furthermore, reverse migrated PMN were positively correlated with lung injury in acute pancreatitis patients, as determined by enhanced reverse migrated PMN frequencies (ICAM-1^{hi}CXCR1^{lo} PMN) recorded in the peripheral blood of patients with acute pancreatitis, relative to healthy controls and mild acute pancreatitis patients [123]. In light of the findings outlining reverse migration patterns in PMN, we were interested in investigating whether compromised PMN reverse migration could also play a part in the enhanced PMN infiltrates we recorded 48h p.i. S. pn. in the BAL and lungs of miR-223$^{-/-}$ mice. For this, we analyzed splenic leukocytes for differences in ICAM-1^{hi}CXCR1^{lo} PMN via flow cytometry and did not record any differences between reverse migrated PMN populations in WT and miR-223$^{-/-}$ mice. Taken together, our findings imply differential roles of miR-223 in the cellular response to inflammatory triggers; dependent on the presence/absence of pathogens (sterile vs pathogen-triggered inflammation), species of bacteria utilized and the length of disease pathogenesis (chronic vs acute infections), frequencies of PMN undergoing apoptosis and concentrations of CXCL-chemokines, but independent of PMN reverse migration.

Despite recording only mild neutrophilia in the lungs and BAL (relative to WT mice), miR-223$^{-/-}$ mice presented with exacerbated lung inflammation 48h p.i. S. pn. At 24h

p.i., miR-223$^{-/-}$ mice presented with slightly lower concentrations of IL-1β than WT mice, however, the remainder of inflammatory cytokine and chemokine concentrations, together with lung barrier permeability, were recorded at similar levels. At 48h p.i., however, we recorded elevated concentrations of inflammatory cytokines such as IL-6, TNF-α, IFN-γ, IL-1α and neutrophil MPO in miR-223$^{-/-}$ mice, while lung barrier permeability was surprisingly not affected despite the exacerbated pulmonary inflammation exhibited by miR-223$^{-/-}$ mice. Histopathological analysis of miR-223$^{-/-}$ murine lungs following S. pn. infection revealed excessive pleuritis, steatitis, perivascular edema and hemorrhages, resulting in an overall elevated inflammation characterized by neutrophilic infiltrates as opposed to predominant lymphocytic cuff formation in WT mice 48h p.i. S. pn. In support of our findings, it has been shown that miR-223$^{-/-}$ mice also exhibit enhanced IL-6, MPO and CXCL1 concentrations following VILI- and *S. aureus*-mediated ALI, coupled to histopathological exacerbations, albeit in omnipresence of increased lung permeability [96]. Furthermore, miR-223 has been shown to be downregulated in an in vitro model of LPS-induced ALI, which is consistent with our findings, however it was shown that the inflammation was triggered through the targeting of NLRP3 and hence production of higher levels of IL-1β [124], the concentrations of which were recorded to be lower in miR-223$^{-/-}$ mice 24h p.i. and unchanged between WT and miR-223$^{-/-}$ mice 48h p.i. S. pn. in our study; suggesting an NLRP3/IL-1β independent inflammation in our model of pneumococcal pneumonia. IL-6 has also been shown to be a direct target of miR-223, as shown by luciferase assays using HeLa cells transfected with miR-223 mimics [97], which fits with our findings of elevated IL-6 concentrations in miR-223$^{-/-}$ mice 48h p.i. S. pn. Moreover, overexpression of miR-223 in RAW 246.7 cells (a murine macrophage cell line) was shown to reduce NF-κB induction following TNF-α or Mtb stimulation [97]. As IL-6 production is dependent on NF-κB induction [125], and TNF-α is considered a potent inducer of NF-κB [126], our findings of pronounced TNF-α concentrations in the BAL of miR-223$^{-/-}$ mice 48h p.i. S. pn. were in concordance with previous studies investigating NF-κB- and TNF-α-mediated pulmonary inflammation. PMN have been shown to produce IFN-γ in response to S. pn. infection, a process regulated by MyD88 and independent of TLR2/4 signaling, resulting in the activation of transcription of IFN-γ regulated genes important in activation of macrophages and recruitment and activation of leukocytes [127]. It has been shown, however, that elevated IFN-γ can be detrimental in

bacterial lung infections. In a murine superinfection model of pneumonia, persistent IL-13 production up to 3 days p.i. type A influenza (IAV) inhibited production of IFN-γ, which was linked to the reduction of susceptibility to methicillin-resistant *S. aureus* and S. pn. superinfection [128]. Moreover, it was shown that elevated IFN-γ markedly reduces the expression of the class A scavenger receptor macrophage receptor with collagenous structure (MARCO), leading to reduced phagocytosis capacity by AM and hence increased susceptibility to S. pn. superinfection day 7 p.i. influenza virus [129]. Transcriptomic analyses in zebrafish embryos revealed that amongst the abundance of genes upregulated in the absence of miR-223, the top pathways that were modulated included inflammatory response genes, the most enriched of which were interferon and NF-κB pathways [117]. Using clustered regularly interspaced short palindromic repeats (CRISPR) screening, studies identified IFN-γ as a mediator of feedback inhibition of exacerbated inflammation induced by the absence of miR-223, albeit acknowledging the necessity for further characterization [117]. We also recorded enhanced IL-1α concentrations in the BAL of miR-223$^{-/-}$ mice 48h p.i. S. pn. IL-1α has been described as a crucial mediator of innate immunity secreted by stressed alveolar epithelial cells highly relevant in viral aggravation of chronic pulmonary pathologies [130]. Furthermore, it was demonstrated that IL-1α$^{-/-}$ mice exhibited decreased PMN infiltration into the BAL, coupled to lesser collagen deposition in response to bleomycin treatment [130], suggesting further involvement of an enhanced epithelial cell-driven pro-inflammatory response.

We recorded upregulation in miR-223 expression in whole lungs of WT mice 24h p.i., while the expression was reduced to near basal levels 48h p.i. S. pn. This was initially a surprising finding considering PMN frequencies were still elevated in the BAL and lungs of WT mice 48h p.i., coupled to the fact that mature PMN express the highest abundance of miR-223 in hematopoietic cells [89]. However, the simultaneous increase in inflammatory cytokine concentrations 48h p.i. was not a coincidence. Indeed, a similar inflammatory phenotype was exhibited in mice following VILI-associated ALI; a phenotype linked to PARP1-mediated inflammation [96]. Importantly, it was shown that miR-223 can be released from PMN-derived microvesicles and taken up by epithelial cells to directly target PARP1 to dampen inflammation and knocking down PARP1 during pulmonary inflammation relieved the

inflammatory phenotype of miR-223$^{-/-}$ mice following VILI-mediated ALI [96]. In order to assess which cellular populations expressed and transferred miR-223, we simultaneously sorted PMN and EpiC from lungs of mice infected with S.pn. WT and S.pn. Δply. Indeed, sorted PMN from S.pn. WT-infected mice expressed significantly higher miR-223 compared to that of naïve- and S.pn. Δply-infected mice 24h p.i. S. pn., while at 48h p.i., WT PMN sorted from S.pn. WT-infected murine lungs reduced miR-223 expression to near naïve levels, paralleling the expression pattern recorded in whole lungs, while S.pn. Δply infection resulted in a delayed upregulation of miR-223 in sorted lung PMN. The enhanced expression of miR-223 recorded in lung PMN following S. pn. infection was paralleled by the peak point of neutrophilic influx at 24- and 48h p.i. S.pn. WT and S.pn. Δply respectively. However, it cannot be concluded that the enhanced miR-223 expression was solely due to the peak of PMN influx. Sorted lung EpiC also exhibited a mild increase in miR-223 expression 24h p.i. S.pn. WT, albeit without statistical significance in a small sample size. In further characterization steps, in vitro stimulation of BM-PMN with S.pn. WT and S.pn. Δply revealed upregulation of miR-223 only following 18h S.pn. WT stimulation, while supernatant transfer from 1x PBS- and S. pn.-stimulated BM-PMN to lung epithelial cells revealed enhanced uptake of miR-223 from 1x PBS-stimulated BM-PMN. Taken together, it can be concluded that in vitro isolated immature BM-PMN display an altered expression pattern of miR-223 in response to S. pn. compared to fully mature lung infiltrating PMN. However, miR-223 is downregulated in vitro and in vivo by BM-PMN and lung PMN, possibly as a means of endogenously suppressing anti-inflammatory signals in order to execute bactericidal effector functions. This was in line with in vitro findings of miR-223 downregulation in a model of LPS-induced ALI, albeit independently of IL-1β [124]. Hence, we describe for the first time that S. pn. infection results in down regulation of miR-223 despite high presence of PMN in the lungs of mice and also less release of miR-223 into the supernatant of BM-PMN following 2- or 6h S. pn. stimulation, compared to sham stimulation.

While elevated cytokine concentrations and enhanced PMN infiltrates both play major roles in the exacerbated lung inflammation recorded during histopathological examination, we are currently investigating if cell death processes such as necroptosis play a part in dysregulated inflammation in the absence of miR-223.

Necroptosis, a regulated form of necrosis, has been described to play a part in various inflammatory pathologies and illnesses [131]. The most studied axis of necroptosis is that of the TNF/TNFR-1 pathway, which is triggered by binding of the TNF ligand to its cognate receptor. This leads to assembly of the necrosome complex, which is constituted of receptor interacting protein kinase (RIPK)1, RIPK3 and the effector protein mixed-lineage kinase domain like (MLKL), induced by phosphorylation and activation of MLKL by RIPK3 to initiate shuttling of the complex to the cytoplasm. Subsequently, MLKL translocates to the plasma membrane leading to its permeabilization and exertion of necroptotic cell death [131]. Necroptosis has been shown to be a process targeted by miR-223 for suppression in a model of ischemic/reperfused mice [110]. It has been shown that during myocardial ischemia/reperfusion-induced necrosis, miR-223 was dysregulated in murine hearts [110]. Furthermore, overexpression of miR-223 in murine hearts resulted in improved recovery of myocardial contractile performance coupled to reduced myocardial necrosis compared to WT hearts ex vivo and in vivo [110], while miR-223−/− hearts presented with exacerbated myocardial necrosis [110]. In vitro studies utilizing various cell lines demonstrated that TNF-related apoptosis-inducing ligand (TRAIL)-induced necroptosis is triggered by RIPK1/RIPK3-mediated PARP1 activation [132]. Moreover, systemic administration of sublethal LPS into miR-223−/− mice led to presentation of exacerbated clinical distress, delayed recovery and increased liver necrosis markers [89], provoking our interest in investigating the role of miR-223 in necroptotic cell death. We are currently establishing lentiviral overexpression of miR-223 in A549 cells (a lung epithelial cell line) to determine whether the presence of miR-223 reduces necroptosis upon chemical induction, and also if bacterial virulence factors such as Ply play a part in the induction of necroptosis in vivo and in vitro.

Despite miR-223 being described as a master regulator of PMN function and maturation, it is also implicated to be crucial in differentiation of monocytes into macrophages [133]. It has been demonstrated in vitro that during GM-CSF-mediated differentiation of human monocytes to macrophages, miR-223 expression was down regulated, which was linked to enhanced IκB kinase α (IKKα) expression and thus enhanced non-canonical NF-κB signaling [133]; which has been implicated in processes such as survival and maturation of lymphocytes, development of

peripheral lymphoid organs and pathologies such as autoimmunity, inflammation and lymphoid malignancies [134]. Monocytes have been described to express low levels of miR-223 relative to bone marrow and peripheral blood PMN [96] and studies have shown that miR-223 can be released in macrophage-derived microvesicles to facilitate the differentiation of monocytic THP-1 cells to a macrophagic phenotype [109]. Hence, we aimed at understanding whether the absence of miR-223 deregulated cellular numbers, frequencies and rates of apoptosis in mice following S. pn. infection. No differences in Ly6Chi recruited iM were recorded 24h or 48h p.i. S. pn., while only a modest decrease in BAL AM and iM frequencies were recorded 48h p.i. in miR-223−/− mice, likely due to the coincidental enhanced PMN infiltration into the BAL - which occupies the largest share of leukocytes recorded in the BAL following S. pn. infection - rather than the absence of miR-223 affecting cellular frequencies of AM and iM.

CD14 is a crucial mediator of the immune response to LPS through TLR4-mediated signaling and is linked to the activation of PMN [111]. PMN and AM activation by physiological concentrations of LPS can be blocked by mAbs against CD14 [135], indicating its significance in TLR4-mediated signaling. Moreover, Ply has also been reported to signal via TLR4 [33]. Murine macrophages that carry a spontaneous mutation in TLR4 (P712H) were shown to be less responsive to pneumolysin compared to WT macrophages [136]. Moreover, TLR4 has been implicated to play a role in apoptosis of macrophages and epithelial cells, as demonstrated by enhanced pneumolysin-induced apoptosis in WT macrophages compared to TLR4-defective macrophages [137]. In the same study, it was also shown that epithelial cells expressing TLR4 were more prone to undergo apoptosis when stimulated with pneumolysin, compared to epithelial cells expressing TLR2 [137]. Contrasting evidence of TLR4 and its implications in lung infections exist, however. It has been shown in a murine model of pneumococcal pneumonia that TLR4 deficient mice exhibited reduced survival and higher lung bacterial burden only after low dose S. pn. inoculation, whilst during Klebsiella-induced pneumonia, high or low dose bacterial inoculation both led to reduced survival and enhanced bacterial burden in the lungs, suggesting that TLR4-mediated inflammation is more relevant in gram-negative pathogens [138]. LFA-1, on the other hand, is well known for its functions in PMN

adhesion and migration [85], however, it has also been suggested to play a role in ROS production in an adhesion-dependent context [112]. Hence, we aimed to investigate whether the absence of miR-223 had any bearing on PMN activation in the BAL and lungs. No differences were recorded in CD14+ or LFA-1+ PMN frequencies in the BAL and lungs 24- or 48h p.i. S. pn., indicating that the pathology exhibited by miR-223$^{-/-}$ mice was independent of CD14 or LFA-1. In light of the absence of any alterations in PMN activation markers, we performed in vitro functional assays to determine whether WT and miR-223$^{-/-}$ BM-PMN displayed any defective or enhanced phagocytosis and killing of bacteria. No differences in phagocytosis or killing of S.pn.-GFP were recorded between WT and miR-223$^{-/-}$ BM-PMN, hence miR-223 could be regarded as redundant with regards to phagocytosis or killing of S. pn. It was shown in a previous study that miR-223$^{-/-}$ BM-PMN exhibited enhanced killing of *Candida albicans* by approximately 10-15% compared to WT BM-PMN [89], however mechanisms of recognition and effector functions against fungal and bacterial pathogens differ [139]. Additionally, peripheral blood PMN express 4-fold higher levels of miR-223 relative to BM-PMN [89], hence it would be more descriptive and accurate to measure phagocytosis and killing capacity in fully mature circulating PMN as opposed to relatively immature BM-PMN. An optimal alternative to understand PMN functional capacity to phagocytose and kill bacteria would be to perform an in vivo phagocytosis and killing assay following intranasal S.pn.-GFP inoculation, however, as seen in Fig. 25, an MOI of more than 10 would have to be achieved in order to accurately pick up and analyze the GFP signal within PMN via flow cytometry; making the necessary infectious dose multitudes higher than our infectious dose of $5x10^6$ CFU.

6. Summary of results

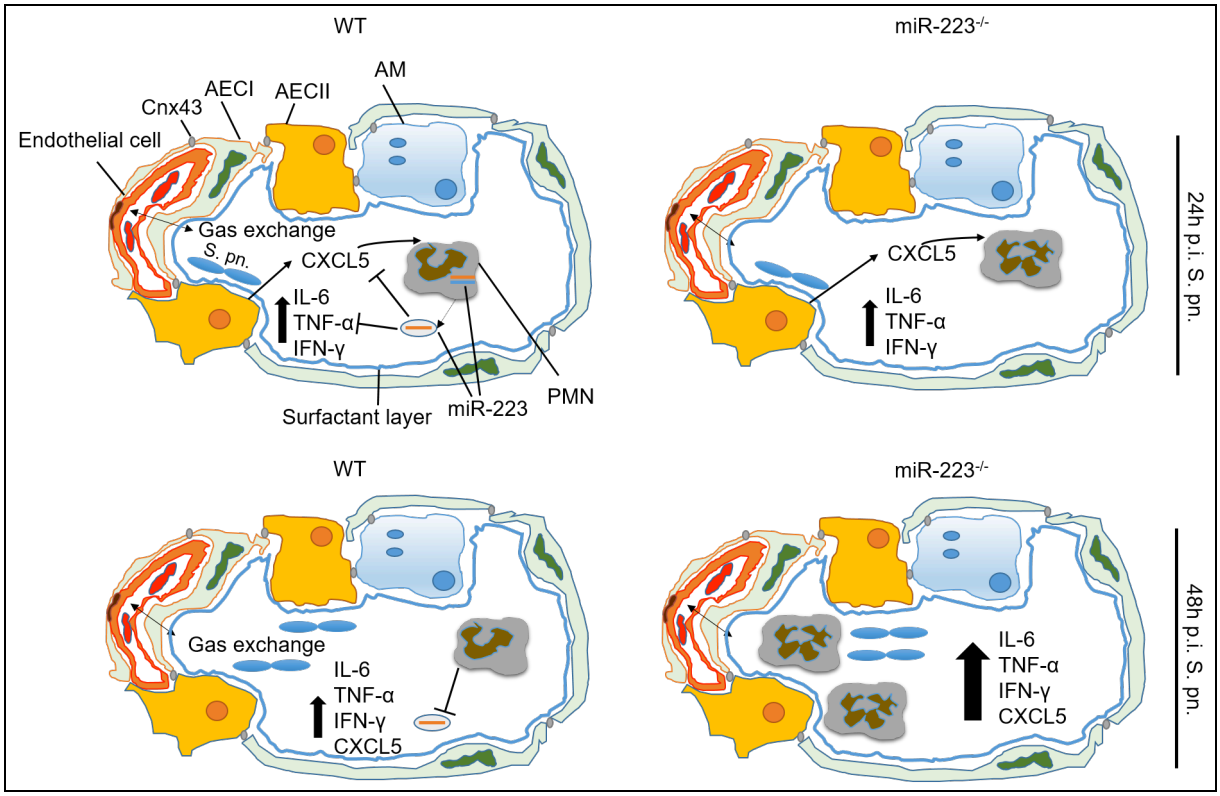

Figure 26. Summarized illustration of miR-223 mediated regulation of lung inflammation in pneumococcal pneumonia. WT; wild-type, miR-223$^{-/-}$; microRNA-223 knockout, Cnx43; connexin 43, AEC; alveolar epithelial cell, AM; alveolar macrophage, PMN; neutrophil, IL; interleukin, TNF; tumor necrosis factor, IFN; interferon, CXCL; CXC chemokine ligand.

WT and miR-223$^{-/-}$ mice initiate pulmonary inflammation upon S. pn. infection which is characterized by PMN influx orchestrated by local release of CXCL-chemokines. At 24h p.i., miR-223 expression is upregulated in WT murine lungs and PMN, which acts by targeting of inflammatory cytokines and chemokines, thereby limiting the degree of lung inflammation 48h p.i. In the absence of miR-223, PMN migration is enhanced and lung inflammation is exacerbated; as characterized by higher PMN frequencies, higher concentrations of inflammatory cytokines and chemokines, and pronounced perivascular edema, steatitis and pleuritis. Moreover, WT and miR-223$^{-/-}$ mice exhibit similar pulmonary bacterial loads, which indicates that the destructive inflammation in miR-223$^{-/-}$ mice is driven not by failure to clear bacteria, but by the lack of an anti-inflammatory signal coupled to an enhanced PMN response.

6. Zusammenfassung der Ergebnisse

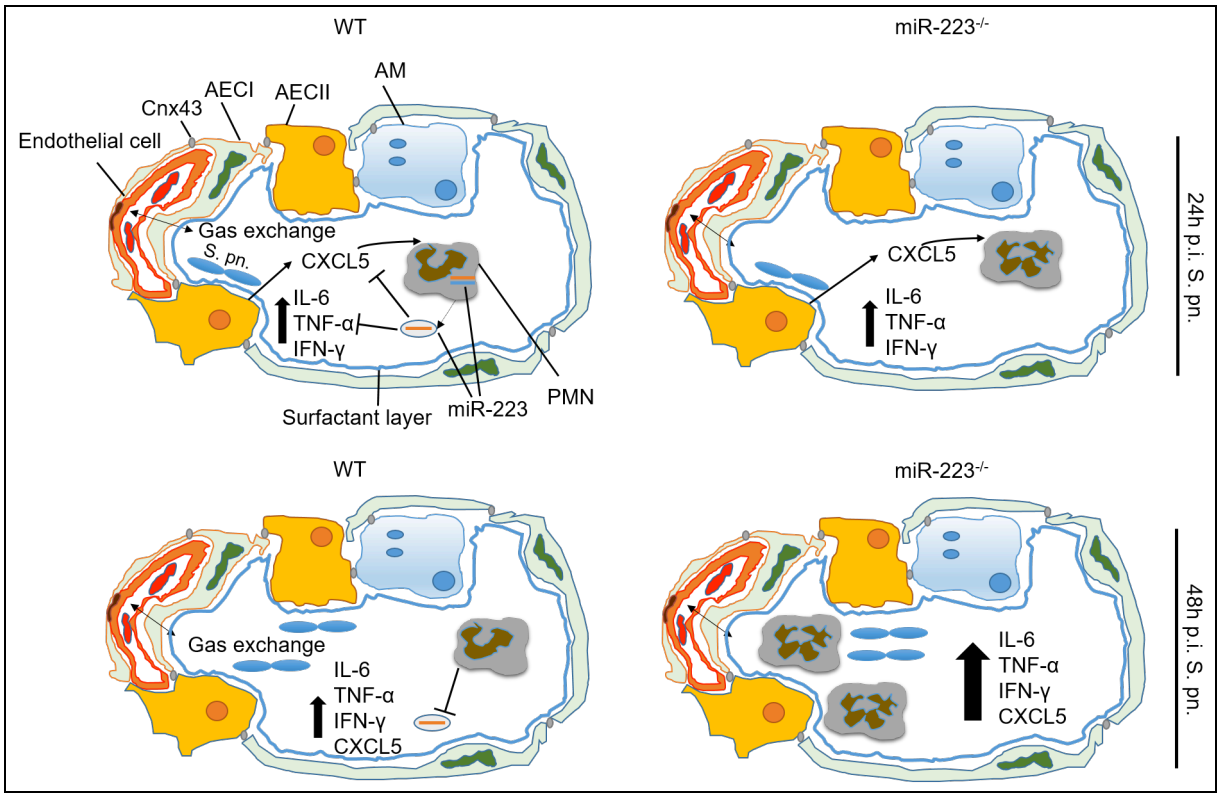

Abbildung 26. Zusammenfassende Darstellung der miR-223-vermittelten Regulation der pulmonalen Inflammation bei Pneumokokken-Pneumonie. WT; wild-type, miR-223$^{-/-}$; microRNA-223 knockout, Cnx43; connexin 43, AEC; alveolar epithelial cell, AM; alveolar macrophage, PMN; neutrophil, IL; interleukin, TNF; tumor necrosis factor, IFN; interferon, CXCL; CXC chemokine ligand.

WT und miR-223$^{-/-}$ Mäuse initiieren nach S. pn. Infektion eine klassische pulmonale Entzündungsreaktion, welche durch Rekrutierung Neutrophiler Granulozyten gekennzeichnet ist, die durch lokale Freisetzung von CXCL-Chemokinen orchestriert wird. In WT Mäusen lässt sich 24h p.i. eine vemehrte miR-223 Expression in den Lungen sowie den rekrutierten pulmonalen Neutrophilen feststellen. miR-223 senkt das Niveau vieler inflammatorischer Zytokine und Chemokine, wodurch das Ausmaß der pulmonalen Entzündungsreaktion in WT Mäusen zum Zeitpunkt 48h p.i. limitiert wird. In Abwesenheit von miR-223 wird die pulmonale Neutrophilenrekrutierung verstärkt und die Entzündung exazerbiert; dies ist gekennzeichnet durch höhere Neutrophilen-Frequenzen, höhere Konzentrationen an inflammatorischen Zytokinen und Chemokinen sowie ausgeprägten perivaskulären Ödemen, Steatitis und

Pleuritis. WT- und miR-223$^{-/-}$ Mäuse weisen eine ähnliche pulmonale Bakterienlast auf, was darauf hinweist, dass die erhöhte Entzündungsreaktion der miR-223$^{-/-}$ Mäuse nicht auf das Versagen der Bakterien-Elimination, sondern auf das Fehlen eines antiinflammatorischen Signals, gekoppelt mit einer verstärkten Neutrophilen-Antwort, zurückzuführen ist.

.

7. Bibliography

1. Blaschke AJ. Interpreting Assays for the Detection of Streptococcus pneumoniae. *Clin Infect Dis* (2011); **52** (S4): S331–S337
2. Institute for Health Metrics and Evaluation (IHME). *Rethinking Development and Health: Findings from the Global Burden of Disease Study* (2016); Seattle, WA: IHME, 2016
3. GBD 2013 Mortality and Causes of Death Collaborators. Global, regional and national age-sex specific all-cause and cause-specific mortality for 240 causes of death, 1990-2013: a systematic analysis for the Global Burden of Disease Study 2013. *Lancet* (2015); **385**: 117-71
4. Steel HC, Cockeran R, Anderson R, Feldman C. Overview of community-acquired pneumonia and the role of inflammatory mechanisms in the immunopathogenesis of severe pneumococcal disease. *Mediators Inflamm* (2013); **2013**: 490346.
5. Herrero FS, Olivas JS. Microbiology and Risk Factors for Community-Acquired Pneumonia. *Semin Respir Crit Care Med* (2012); **33**: 220-31
6. Hoare Z, Lim WS. Pneumonia: update on diagnosis and management. *BMJ* (2006); **332** (7549): 1077-9
7. Schirm S, Ahnert P, Wienhold S, Mueller-Redetzky H, Nouailles-Kursar G, Loeffler M, Witzenrath M, Scholz M. A Biomathematical Model of Pneumococcal Lung Infection and Antibiotic Treatment in Mice. *PLoS ONE* (2016); **11** (5): doi:10.1371/journal.pone.0156047
8. Brown LA, Mitchell AM, Mitchell TJ. *Streptococcus pneumonia* and lytic antibiotic therapy: are we adding insult to injury during invasive pneumococcal disease and sepsis? *J Med Microbiol* (2017); **66**: 1253-56
9. Mandell LA, Wunderink RG, Anzueto A, Bartlett JG, Campbell GD, Dean NC, Dowell SF, File Jr. TM, Musher DM, Niederman MS, Torres A, Whitney CG. Infectious Diseases Society of America/American Thoracic Society Concensus Guidelines on the Management of Community-Acquired Pneumonia in Adults. *Clin Infect Dis* (2007); **44** (2): 27-72

10. Houck PM, Bratzler DW, Nsa W, Ma A, Bartlett JG. Timing of antibiotic administration and outcomes for Medicare patients hospitalized with community-acquired pneumonia. *Arch Intern Med* (2004); **164** (6): 637-44
11. Daniel P, Rodrigo C, Mckeever TM, Woodhead M, Welham S, Lim WS, British Thoracic Society. Time to first antibiotic and mortality in adults hospitalised with community-acquired pneumonia: a matched-propensity analysis. Thorax (2016); 71 (6): 568-70
12. Obaro SK, Monteil MA, Henderson DC. The pneumococcal problem. *BMJ* (1996); **312**: 1521-5
13. Catterall JR. Streptococcus pneumoniae. *Thorax* (1999); **54** (10): 929.
14. Harboe ZB, Thomsen RW, Riis A, Valentiner-Branth P, Christensen JJ, Lambertsen L, Krogfelt KA, Konradsen HB, Benfield TL. Pneumococcal serotypes and mortality following invasive pneumococcal disease: a population based cohort study. *PLoS Med* (2009); **6** (5): e1000081
15. CDC. Surveillance and Reporting - Trends (2017). www.cdc.gov/pneumococcal/surveillance
16. van der Poll T, Opal SM. Pathogenesis, treatment, and prevention of pneumococcal pneumonia. Lancet (2009); 374 (9700): 1543-56
17. Nelson AL, Roche AM, Gould JM, Chim K, Ratner AJ, Weiser JN. Capsule Enhances Pneumococcal Colonization by Limiting Mucus-Mediated Clearance. *Infect Immun* (2007); **75** (1): 83-90
18. Weiser JN, Austrian R, Sreenivasan PK, Masure HR. Phase variation in pneumococcal opacity: relationship between colonial morphology and nasopharyngeal colonization. *Infect Immun* (1994); **62** (6): 2585-9
19. Wartha F, Beiter K, Albiger B, Fernebro J, Zychlinsky A, Normark S, Henriques-Normark B. Capsule and D-alanylated lipoteichoic acids protect *Streptococcus pneumonia* against neutrophil extracellular traps. *Cell Microbiol* (2007); **9** (5): 1162-71
20. Kristian SA, Datta V, Weidenmaier C, Kansal R, Fedtke I, Peschel A, Gallo RL, Nizet V. D-alanylation of teichoic acids promotes group a streptococcus antimicrobial peptide resistance, neutrophil survival, and epithelial cell invasion. *J Bacteriol* (2005); **187** (19): 6719-25

21. Jedrzejas MJ, Lamani E, Becker RS. Characterization of selected strains of pneumococcal surface protein A. *J Biol Chem* (2001); **276** (35): 33121-8
22. Tu AH, Fulgham RL, McCrory MA, Briles DE, Szalai AJ. Pneumococcal surface protein A inhibits complement activation by Streptococcus pneumoniae. *Infect Immun* (1999); **67** (9): 4720-4
23. McDaniel LS, Ralph BA, McDaniel DO, Briles DE. Localization of protection-eliciting epitopes on PspA of Streptococcus pneumonia between amino acid residues 192 and 260. *Microb Pathog* (1994); **17** (5): 323-37
24. Kerr AR, Paterson GK, McCluskey J, Iannelli F, Oggioni MR, Pozzi G, Mitchell TJ. The contribution of PspC to pneumococcal virulence varies between strains and is accomplished by both complement evasion and complement-independent mechanisms. *Infect Immun* (2006); **74** (9): 5319-24
25. Johnston JW, Myers LE, Ochs MM, Benjamin WH Jr, Briles DE, Hollingshead SK. Lipoprotein PsaA in virulence of Streptococcus pneumoniae: surface accessibility and role in protection from superoxide. *Infect Immun* (2004); **72** (10): 5858-67
26. Marra A, Lawson S, Asundi JS, Brigham D, Hromockyj AE. In vivo characterization of the psa genes from Streptococcus pneumoniae in multiple models of infection. *Microbiology* (2002); **148** (Pt 5): 1483-91
27. McCluskey J, Hinds J, Husain S, Witney A, Mitchell TJ. A two-component system that controls the expression of pneumococcal surface antigen A (PsaA) and regulates virulence and resistance to oxidative stress in Streptococcus pneumoniae. *Mol Microbiol* (2004); **51** (6): 1661-75
28. Berry AM, Paton JC. Sequence heterogeneity of PsaA, a 37-kilodalton putative adhesion essential for virulence of Streptococcus pneumoniae. *Infect Immun* (1996); **64** (12): 5255-62
29. Bergmann S, Rohde M, Chhatwal GS, Hammerschmidt S. Alpha-Enolase of Streptococcus pneumoniae is a plasmin(ogen)-binding protein displayed on the bacterial cell surface. *Mol Microbiol* (2001); **40** (6): 1273-87
30. Manco S, Hernon F, Yesilkaya H, Paton JC, Andrew PK, Kadioglu A. Pneumococcal neuraminidases A and B both have essential roles during infection of the respiratory tract and sepsis. *Infect Immun* (2006); **74** (7): 4014-20

31. Berry AM, Lock RA, Hansman D, Paton JC. Contribution of autolysin to virulence of Streptococcus pneumoniae. *Infect Immun* (1989); **57** (8): 2324-30
32. Balachandran P, Hollingshead SK, Paton JC, Briles DE. The autolytic enzyme LytA of Streptococcus pneumoniae is not responsible for releasing pneumolysin. *J Bacteriol* (2001); **183** (10): 3108-16
33. Koppe U, Suttorp N, Opitz B. Recognition of *Streptococcus Pneumoniae* by the innate immune system. *Cell Microbiol* (2012); **14** (4): 460-66.
34. Anderson R, Nel JG, Feldman C. Multifaceted Role of Pneumolysin in the Pathogenesis of Myocardial Injury in Community-Acquired Pneumonia. *Int J Mol Sci* (2018); **19** (4): 1147
35. Novick S, Shagan M, Blau K, Lifshitz S, Givon-Lavi N, Grossman N, Bodner L, Dagan R, Nebenzahl YM. Adhesion and invasion of *Streptococcus pneumonia* to primary and secondary respiratory epithelial cells. *Mol Med Rep K* (2017); **15** (1): 65-74
36. Nouailles G, Dorhoi A, Koch M, Zerrahn J, Weiner J 3rd, Faé KC, Arrey F, Kuhlmann S, Bandermann S, Loewe D, Mollenkopf HJ, Vogelzang A, Meyer-Schwesinger C, Mittrücker HW, McEwen G, Kaufmann SH. CXCL5-secreting pulmonary epithelial cells drive destructive neutrophilic inflammation in tuberculosis. *J Clin Invest* (2014); **124** (3): 1268-82.
37. Kawai T, Akira S. The roles of TLRs, RLRs and NLRs in pathogen recognition. *Int Immunol* (2009); **21** (4): 317-37
38. Hoebe K, Georgel P, Rutschmann S, Du X, Mudd S, Crozat K, Sovath S, Shamel L, Hartung T, Zähringer U, Beutler B. CD36 is a sensor of diacylglycerides. *Nature* (2005); **433** (7025): 523-7
39. Akira S, Uematsu S, Takeuchi O. Pathogen recognition and innate immunity. *Cell* (2006); **124** (4): 783-801
40. McNeela EA, Burke A, Neill DR, Baxter C, Fernandes VE, Ferreira D, Smeaton S, El-Rachkidy R, McLoughlin RM, Mori A, Moran B, Fitzgerald KA, Tschopp J, Pétrilli V, Andrew PK, Kadioglu A, Lavelle EC. Pneumolysin activates the NLRP3 inflammasome and promotes proinflammatory cytokines independently of TLR4. *PLoS Pathog* (2010); **6** (11): e1001191

41. Kadioglu A, Weiser JN, Paton JC, Andrew PW. The role of *Streptococcus pneumoniae* virulence factors in host respiratory colonization and disease. *Nat Rev Microbiol* (2008); **6** (4): 288-301.
42. Henriques-Normark B & Tuomanen EI. The Pneumococcus: Epidemiology, Microbiology, and Pathogenesis. *Cold Spring Harb Perspect Med* (2013); **3**: a010215
43. Whitsett JA, Alenghat T. Respiratory epithelial cells orchestrate pulmonary innate immunity. *Nat Immunol* (2015); **16** (1): 27-35
44. Greeley MA. Atlas of Histology of the Juvenile Rat; Chapter 4 – Respiratory System (2016): https://doi.org/10.1016/B978-0-12-802682-3.00004-5
45. Davis E. Equine Internal Medicine (Fourth Edition); Chapter 8 – Disorders of the Respiratory System (2018): https://doi.org/10.1016/B978-0-323-44329-6.00008-5
46. Polosukhin VV, Richmond BW, Du RH, Cates JM, Wu P, Nian H, Massion PP, Ware LB, Lee JW, Kononov AV, Lawson WE, Blackwell TS. Secretory IgA Deficiency in Individual Small Airways Is Associated with Persistent Inflammation and Remodeling. *Am J Respir Crit Care Med* (2017); **195** (8): 1010-1021
47. Sears PR, Davis CW, Chua M, Sheehan JK. Mucociliary interactions and mucus dynamics in ciliated human bronchial epithelial cell cultures. *Am J Physiol Lung Cell Mol Physiol* (2011); **301** (2): L181-6
48. Westphalen K, Gusarova GA, Islam MN, Subramanian M, Cohen TS, Prince AS, Bhattacharya J. Sessile alveolar macrophages modulate immunity through connexin 43-based epithelial communication. *Nature* (2014); **506** (7489): 503-6
49. Martin FJ, Prince AS. TLR2 regulates gap junction intercellular communication in airway cells. *J Immunol* (2008); **180** (7): 4986-93
50. Godleski JJ, Brain JD. The origin of alveolar macrophages in mouse irradiation chimeras. *J Exp Med* (1972); **136** (3): 630-43
51. Guilliams M, De Kleer I, Henri S, Post S, Vanhoutte L, De Prijck S, Deswarte K, Malissen B, Hammad H, Lambrecht BN. Alveolar macrophages develop from fetal monocytes that differentiate into long-lived cells in the first week of life via GM-CSF. *J Exp Med* (2013); **210** (10): 1977-92

52. Burgess AW, Camakaris J, Metcalf D. Purification and properties of colony-stimulating factor from mouse lung-conditioned medium. *J Biol Chem* (1977); **252** (6): 1998-2003

53. Stanley E, Lieschke GJ, Grail D, Metcalf D, Hodgson G, Gall JAM, Maher DW, Cebon J, Sinickas V, Dunn AR. Granulocyte/macrophage colony-stimulating factor-deficient mice show no major perturbation of hematopoiesis but develop a characteristic pulmonary pathology. *Proc Natl Acad Sci USA* (1994); 91: 5592-6

54. Pittet LA, Quinton LJ, Yamamoto K, Robson BE, Ferrari JD, Algül H, Schmid RM, Mizgerd JP. Earliest Innate Immune Responses Require Macrophage RelA during Pneumococcal Pneumonia. *Am J Respir Cell Mol Biol* (2011); **45** (3): 573-81

55. Aberdein JD, Cole J, Bewley MA, Marriott HM, Dockrell DH. Alveolar macrophages in pulmonary host defense – the unrecognized role of apoptosis as a mechanism of intracellular bacterial killing. *Clin Exp Immunol* (2013); **174** (2): 193-202

56. Sawant KV, Xu R, Cox R, Hawkins H, Sbrana E, Kolli D, Garofalo RP, Rajarathnam K. Chemokine CXCL1-mediated neutrophil trafficking in the lung: Role of CXCR2 activation. *J Innate Immun* (2015); **7** (6): 647-58

57. Byrne AJ, Mathie SA, Gregory LG, Lloyd CM. Pulmonary macrophages: key players in the innate defence of the airways. *Thorax* (2015); **70** (12): 1189-96

58. Kratofil RM, Kobes P, Deniset JF. Monocyte Conversion During Inflammation and Injury. *Arterioscler Thromb Vasc Biol* (2017); **37** (1): 35-42

59. Chen Q, Snapper CM. Inflammatory monocytes are critical for induction of a polysaccharide-specific antibody response to an intact bacterium. *J Immunol* (2012); **190** (3):1048-55.

60. Deshmane SL, Kremlev S, Amini S, Sawaya BE. Monocyte Chemoattractant Protein-1 (MCP-1): An Overview. *J Interferon Cytokine Res* (2009); **29** (6): 313-26

61. Yang J, Zhang L, Yu C, Yang XF, Wang H. Monocyte and macrophage differentiation: circulation inflammatory monocyte as biomarker for inflammatory diseases. *Biomark Res* (2014); 2(1): 1.

62. Chen K, Kolls JK. T cell-mediated host immune defenses in the lung. *Annu Rev Immunol* (2013); **31**: 605-33.

63. Zelante T, Wong AYW, Ping TJ, Chen J, Sumatoh HR, Vigano E, Bing YH, Lee B, Zolezzi F, Fric J, Newell EW, Mortellaro A, Poidinger M, Puccetti P, Ricciardi-Castagnoli P. $CD103^+$ Dendritic Cells Control Th17 Cell Function in the Lung. *Cell Rep* (2015); **12** (11): 1789-801

64. Van Maele L, Carnoy C, Cayet D, Ivanov S, Porte R, Deruy E, Chabalgoity JA, Renauld JC, Eberl G, Benecke AG, Trottein F, Faveeuw C, Sirard JC. Activation of Type 3 Innate Lymphoid Cells and Interleukin 22 Secretion in the Lungs During *Streptococcus pneumoniae* Infection. *J Infect Dis* (2014); **210** (3): 493-503

65. Kolls JK. $CD4^+$ T-cell subsets and host defense in the lung. *Immunol Rev* (2013); **252** (1):156-63.

66. Herbold W, Maus R, Hahn I, Ding N, Srivastava M, Christman JW, Mack M, Reutershan J, Briles DE, Paton JC, Winter C, Welte T, Maus UA. Importance of CXC Chemokine Receptor 2 in Alveolar Neutrophil and Exudate Macrophage Recruitment in Response to Pneumococcal Lung Infection. *Infect Immun* (2010); **78** (6): 2620-30

67. Dancey JT, Deubelbeiss KA, Harker LA, Finch CA. Neutrophil kinetics in man. *J Clin Invest* (1976); **58** (3): 705-15

68. Pillay J, den Braber I, Vrisekoop N, Kwast LM, de Boer RJ, Borghans JA, Tesselaar K, Koenderman L. In vivo labeling with $^2H_20$ reveals a human neutrophil lifespan of 5.4 days. *Blood* (2010); **116** (4): 625-7

69. Lahoz-Beneytez J, Elemans M, Zhang Y, Ahmed R, Salam A, Block M, Niederalt C, Asguith B, Macallan D. Human neutrophil kinetics: modeling of stable isotope labeling data supports short blood neutrophil half-lives. *Blood* (2016); **127** (26): 3431-8

70. Summers C, Rankin SM, Condliffe AM, Singh N, Peters AM, Chilvers ER. Neutrophil kinetics in health and disease. *Trends Immunol* (2010); **31** (8): 318-24

71. Sasmono RT, Ehrnsperger A, Cronau SL, Ravasi T, Kandane R, Hickey MJ, Cook AD, Himes SR, Hamilton JA, Hume DA. Mouse neutrophilic granulocytes express mRNA encoding the macrophage colony-stimulating

factor receptor (CSF-1R) as well as many other macrophage-specific transcripts and can transdifferentiate into macrophages in vitro in response to CSF-1. *J Leukoc Biol* (2007); **82** (1): 111-23

72. Basu S, Hodgson G, Katz M, Dunn AR. Evaluation oft he role of G-CSF in the production, survival, and release of neutrophils from bone marrow into circulation. *Blood* (2002); **100** (3): 854-61
73. Bronchud MH, Scarffe JH, Thatcher N, Crowther D, Souza LM, Alton NK, Testa NG, Dexter TM. Phase I/II study of recombinant human granulocyte colony-stimulating factor in patients receiving intensive chemotherapy for small cell lung cancer. *Br J Cancer* (1987); **56**: 809-13
74. Demetri GD, Griffin JD. Granulocyte Colony-Stimulating Factor and Its Receptor. *Blood* (1991); **78** (11): 2791-808
75. Boettcher S, Gerosa RC, Radpour R, Bauer J, Ampenberger F, Heikenwalder M, Kopf M, Manz MG. Endothelial cells translate pathogen signals into G-CSF-driven emergency granulopoiesis. *Blood* (2014); **124** (9): 1393-403)
76. Disteldorf EM, Krebs CF, Paust HJ, Turner JE, Nouailles G, Tittel A, Meyer-Schwesinger C, Stege G, Brix S, Velden J, Wiech T, Helmchen U, Steinmetz OM, Peters A, Bennstein SB, Kaffke A, Llanto C, Lira SA, Mittrücker HW, Stahl RAK, Kurts C, Kaufmann SHE, Panzer U. CXCL5 Drives Neutrophil Recruitment in T_H17-Mediated GN. *J Am Soc Nephrol* (2015); **26** (1): 55-66
77. Sawant KV, Poluri KM, Dutta AK, Sepuru KM, Troshkina A, Garofalo RP, Rajarathnam K. Chemokine CXCL1 mediated neutrophil recruitment: Role of glycosaminoglycan interactions. *Sci Rep* (2016); **14** (6): 33123
78. Becker S, Quay J, Koren HS, Haskill JS. Constitutive and stimulated MCP-1, GRO alpha, beta and gamma expression in human airway epithelium and bronchoalveolar macrophages. *Am J Physiol* (1994); **266** (3 Pt 1): L278-86
79. Hornick EE, Banoth B, Miller AM, Zacharias ZR, Jain N, Wilson ME, Gibson-Corley KN, Legge KL, Bishop GA, Sutterwala FS, Cassel SL. Nlrp12 Mediates Adverse Neutrophil Recruitment during Influenza Virus Infection. *J Immunol* (2018); **200** (3): 1188-97
80. Quinton LJ, Nelson S, Zhang P, Boe DM, Happel KI, Pan W, Bagby GJ. *Am J Physiol Lung Cell Mol Physiol* (2004); **286**: L465-72
81. Hoth JJ, Wells JD, Hiltbold EM, McCall CE, Yoza BK. Mechanism of neutrophil recruitment to the lung after pulmonary contusion. *Shock* (2011); **35** (6): 604-9

82. Mei J, Liu Y, Dai N, Hoffmann C, Hudock KM, Zhang P, Guttentag SH, Kolls JK, Oliver PM, Bushman FD, Worthen GS. Cxcr2 and Cxcl5 regulate the IL-17/G-CSF axis and neutrophil homeostasis in mice. *J Clin Invest* (2012); **122** (3): 974-86

83. Kadioglu A, De Filippo K, Bangert M, Fernandes VE, Richards L, Jones K, Andrew PK, Hogg N. The integrins Mac-1 and alpha4beta1 perform crucial roles in neutrophil and T cell recruitment to lungs during Streptococcus pneumoniae infection. *J Immunol* (2011); **186** (10): 5907-15

84. Sreeramkumar V, Adrover JM, Ballesteros I, Cuartero MI, Rossaint J, Bilbao I, Nácher M, Pitaval C, Radovanovic I, Fukui Y, McEver RP, Filippi MD, Lizasoain I, Ruiz-Cabello J, Zarbock A, Moro MA, Hidalgo A. Neutrophils scan for activated platelets to initiate inflammation. *Science* (2014); **346** (6214): 1234-8

85. Zarbock A, Polanowska-Grabowska RK, Ley K. Platelet-neutrophil-interactions: linking hemostasis and inflammation. *Blood Rev* (2007); **21** (2): 99-111

86. Marriott HM, Jackson LE, Wilkinson TS, Simpson AJ, Mitchell TJ, Buttle DJ, Cross SS, Ince PG, Hellewell PG, Whyte MKB, Dockrell DH. Reactive Oxygen Species Regulate Neutrophil Recruitment and Survival in Pneumococcal Pneumonia. *Am J Respir Crit Care Med* (2008); **177** (8): 887-95

87. Cieutat AM, Lobel P, August JT, Kieldsen L, Sendeløv H, Borregaard N, Bainton DF. Azurophilic granules of human neutrophilic leukocytes are deficient in lysosome-associated membrane proteins but retain the mannose 6-phosphate recognition marker. *Blood* (1998); **91** (3): 1044-58

88. Brinkmann V, Reichard U, Goosmann C, Fauler B, Uhlemann Y, Weiss DS, Weinrauch Y, Zychlinsky A. Neutrophil extracellular traps kill bacteria. *Science* (2004); **303** (5663): 1532-5

89. Johnnidis JB, Harris MH, Wheeler RT, Stehling-Sun S, Lam MH, Kirak O, Brummelkamp TR, Fleming MD, Camargo FD. Regulation of progenitor cell proliferation and granulocyte function by microRNA-223. *Nature* (2008); **451** (7182): 1125-9

90. Chen CZ, Li L, Lodish HF, Bartel DP. MicroRNAs modulate hematopoietic lineage differentiation. *Science* (2004); **303** (5654): 83-6

91. Guo H, Ingolia NT, Weissman JS, Bartel DP. Mammalian microRNAs predominantly act to decrease target mRNA levels. *Nature* (2010); **466** (7308): 834-40
92. Ardekani AM, Naeini MM. The Role of MicroRNAs in Human Diseases. *Avicenna J Med Biotechnol* (2010); **2** (4): 161-79
93. Fukao T, Fukuda Y, Kiga K, Sharif J, Hino K, Enomoto Y, Kawamura A, Nakamura K, Takeuchi T, Tanabe M. An evolutionarily conserved mechanism for microRNA-223 expression revealed by microRNA gene profiling. *Cell* (2007); **129** (3): 617-31
94. Fazi F, Rosa A, Fatica A, Gelmetti V, De Marchis ML, Nervi C, Bozzoni I. A minicircuitry comprised of microRNA-223 and transcription factors NFI-A and C/EBPalpha regulates human granulopoiesis. *Cell* (2005); **123** (5): 819-31
95. Mehta A, Baltimore D. MicroRNAs as regulatory elements in immune system logic. *Nat Rev Immunol* (2016); **16** (5): 279-94
96. Neudecker V, Brodsky KS, Clambey ET, Schmidt EP, Packard TA, Davenport B, Standiford TJ, Weng T, Fletcher AA, Barthel L, Masterson JC, Furuta GT, Cai C, Blackburn MR, Ginde AA, Graner MW, Janssen WJ, Zemans RL, Evans CM, Burnham EL, Homann D, Moss M, Kreth S, Zacharowski K, Henson PM, Eltzschig HK. Neutrophil transfer of *miR-223* to lung epithelial cells dampens acute lung injury in mice. *Sci Transl Med* (2017); **9** (408): pii: eaah5360
97. Dorhoi A, Iannaccone M, Farinacci M, Faé KC, Schreiber J, Moura-Alves P, Nouailles G, Mollenkopf HJ, Oberbeck-Müller D, Jörg S, Heinemann E, Hahnke K, Löwe D, Del Nonno F, Goletti D, Capparelli R, Kaufmann SHE. MicroRNA-223 controls susceptibility to tuberculosis by regulating lung neutrophil recruitment. *J Clin Invest* (2013); **123** (11): 4836-48
98. Taïbi F, Metzinger-Le Meuth V, Massy ZA, Metzinger L. miR-223: An inflammatory oncomiR enters the cardiovascular field. *Biochim Biophys Acta* (2014); **1842** (7): 1001-9
99. Liu L, Zhang C, Li X, Sun W, Qin S, Qin L, Wang X. miR-223 promotes colon cancer by directly targeting p120 catenin. *Oncotarget* (2017); **8** (38): 63764-79
100. Yang Y, Jiang Z, Ma N, Wang B, Liu J, Zhang L, Gu L. MicroRNA-223 Targeting STIM1 Inhibits the Biological Behavior of Breast Cancer. *Cell Physiol Biochem* (2018); **45** (2): 856-66

101. Pulikkan JA, Dengler V, Peramangalam PS, Peer Zada AA, Müller-Tidow C, Bohlander SK, Tenen DG, Behre G. Cell-cycle regulator E2F1 and microRNA-223 comprise an autoregulatory negative feedback loop in acute myeloid leukemia. *Blood* (2010); **115**: 1768-78
102. Mitchell PS, Parkin RK, Kroh EM, Fritz BR, Wyman SK, Pohosova-Agadjanyan EL, Peterson A, Noteboom J, O'Briant KC, Allen A, Lin DW, Urban N, Drescher CW, Knudsen BS, Stirewalt DL, Gentleman R, Vessella RL, Nelson PS, Martin DB, Tewari M. Circulating microRNAs as stable blood-based markers for cancer detection. *Proc Natl Acad Sci USA* (2008); **105** (30): 10513-8
103. Hunter MP, Ismail N, Zhang X, Aguda BD, Lee EJ, Yu L, Xiao T, Schafer J, Lee ML, Schmittgen TD, Nana-Sinkam SP, Jarjoura D, Marsh CB. Detection of microRNA expression in human peripheral blood microvesicles. *PLoS One* (2008); **3** (11): e3694
104. Arroyo JD, Chevillet JR, Kroh EM, Ruf IK, Pritchard CC, Gibson DF, Mitchell PS, Bennett CF, Pohosova-Agadjanyan EL, Stirewalt DL, Tait JF, Tewari M. Argonaute2 complexes carry a population of circulating microRNAs independent of vesicles in human plasma. *Proc Natl Acad Sci USA* (2011); **108** (12): 5003-8
105. Bhattacharya S, Steele R, Shrivastava S, Chakraborty S, Di Bisceglie AM, Ray RB. Serum miR-30e and miR-223 as Novel Noninvasive Biomarkers for Hepatocellular Carcinoma. *Am J Pathol* (2016); **186** (2): 242-7
106. Aiso T, Ohtsuka K, Ueda M, Karita S, Yokoyama T, Takata S, Matsuki N, Kondo H, Takizawa H, Okada AA, Watanabe T, Ohnishi H. Serum levels of candidate microRNA diagnostic markers differ among the stages of non-small-cell lung cancer. *Oncol Lett* (2018); **16** (5): 6643-51
107. Mo MH, Chen L, Fu Y, Wang W, Fu SW. Cell-free Circulating miRNA Biomarkers in Cancer. *J Cancer* (2012); **3**: 432-48
108. Berger S, Goekeri C, Gupta SK, Vera J, Dietert K, Behrendt U, Lienau J, Wienhold SM, Gruber AD, Suttorp N, Witzenrath M, Nouailles G. Delay in antibiotic therapy results in fatal disease outcome in murine pneumococcal pneumonia. *Crit Care* (2018); **22** (1): 287
109. Ismail N, Wang J, Dakhlallah D, Moldovan L, Agarwal K, Batte K, Shah P, Wisler J, Eubank TD, Tridandapani S, Paulaitis ME, Piper MG, Marsh CB.

Macrophage microvesicles induce macrophage differentiation and *miR-223* transfer. *Blood* (2013); **121**: 984-95

110. Qin D, Wang X, Li Y, Yang L, Wang R, Peng J, Essandoh K, Mu X, Peng T, Han Q, Yu KJ, Fan GC. MiR-223-5p and -3p Cooperatively Suppress Necroptosis in Ischemic/Reperfused Hearts. *J Biol Chem* (2016); **291** (38): 20247-59
111. Soler-Rodriguez AM, Zhang H, Lichenstein HS, Qureshi N, Niesel DW, Crowe SE, Peterson JW, Klimpel GR. Neutrophil Activation by Bacterial Lipoprotein Versus Lipopolysaccharide: Differential Requirements for Serum and CD14. *J Immunol* (2000); **164** (5): 2674-83
112. Woodfin A, Beyrau M, Voisin MB, Ma B, Whiteford JR, Hordijk PL, Hogg N, Nourshargh S. ICAM-1-expressing neutrophils exhibit enhanced effector functions in murine models of endotoxemia. *Blood* (2016); **127**: 898-907
113. Clement CG, Evans SE, Evans CM, Hawke D, Kobayashi R, Reynolds PR, Moghaddam SJ, Scott BL, Melicoff E, Adachi R, Dickey BF, Tuvim MJ. Stimulation of Lung Innate Immunity Protects against Lethal Pneumococcal Pneumonia in Mice. *Am J Respir Crit Care Med* (2008); **177** (12): 1322-30
114. Gómez MI, Prince A. Airway epithelial cell signaling in response to bacterial pathogens. *Pediatr Pulmonol* (2008); **43** (1): 11-9
115. Balamayooran G, Batra S, Fessler MB, Happel KI, Jeyaseelan S. Mechanisms of neutrophil accumulation in the lungs against bacteria. *Am J Respir Cell Mol Biol* (2010); **43** (1): 5-16
116. de Kerckhove M, Tanaka K, Umehara T, Okamoto M, Kanematsu S, Hayashi H, Yano H, Nishiura S, Tooyama S, Matsubayashi Y, Komatsu T, Park S, Okada Y, Takahashi R, Kawano Y, Hanawa T, Iwasaki K, Nozaki T, Torigoe H, Ikematsu K, Suzuki Y, Tanaka K, Martin P, Shimokawa I, Mori R. Targeting *miR-223* in neutrophils enhances the clearance of *Staphylococcus aureus* in infected wounds. *EMBO Mol Med* (2018); **10** (10): pii: e9024
117. Zhou W, Pal AS, Hsu AYH, Gurol T, Zhu X, Wirbisky-Hershberger SE, Freeman JL, Kasinski AL, Deng Q. MicroRNA-223 Suppresses the Canonical NF-κB Pathway in Basal Keratinocytes to Dampen Neutrophilic Inflammation. *Cell Rep* (2018); **22** (7): 1810-23
118. Neudecker V, Haneklaus M, Jensen O, Khailova L, Masterson LC, Tye H, Biette K, Jedlicka P, Brodsky KS, Gerich ME, Mack M, Robertson AAB,

Cooper MA, Furuta GT, Dinarello CA, O'Neill LA, Eltzschig HK, Masters SL, McNamee EN. Myeloid-derived miR-223 regulates intestinal inflammation via repression of the NLRP3 inflammasome. *J Exp Med* (2017); **214** (6): 1737-52

119. Wan L, Yuan X, Liu M, Xue B. miRNA-223-3p regulates NLRP3 to promote apoptosis and inhibit proliferation of hep3B cells. *Exp Ther Med* (2018); **15** (3): 2429-35
120. de Oliveira S, Rosowski EE, Huttenlocher A. Neutrophil migration in infection and wound repair: going forward in reverse. *Nat Rev Immunol* (2016); **27** (16): 378-91
121. Powell D, Tauzin S, Hind LE, Deng Q, Beebe DJ, Huttenlocher A. Chemokine Signaling and the Regulation of Bidirectional Leukocyte Migration in Interstitial Tissues. *Cell Rep* (2017); **19** (8): 1572-85
122. Woodfin A, Voisin MB, Beyrau M, Colom B, Caille D, Diapouli FM, Nash GB, Chavakis T, Albelda SM, Rainger GE, Meda P, Imhof BA, Nourshargh S. Junctional adhesion molecule-C (JAM-C) regulates polarized neutrophil transendothelial cell migration *in vivo*. *Nat Immunol* (2012); **12** (8): 761-9
123. Wu D, Zeng Y, Fan Y, Mulatibieke T, Ni J, Yu G, Wan R, Wang X, Hu G. Reverse-migrated neutrophils regulated by JAM-C are involved in acute pancreatitis-associated lung injury. *Sci Rep* (2016); **6**: 20545
124. Yan Y, Lu K, Ye T, Zhang Z. MicroRNA-223 attenuates LPS-induced inflammation in an acute lung injury model via the NLRP3 inflammasome and TLR4/NF-κB signaling pathway via RHOB. *Int J Mol Med* (2019); **43** (3): 1467-77
125. Peng SC, Wong DS, Tung KC, Chen YY, Chao CC, Peng CH, Chuang YJ, Tang CY. Computational modeling with forward and reverse engineering links signaling network and genomic regulatory responses: NF-kappaB signaling-induced gene expression responses in inflammation. *BMC Bioinformatics* (2010); **11**: 308
126. Schütze S, Wiegmann K, Machleidt T, Krönke M. TNF-induced activation of NF-kappa B. *Immunobiology* (1995); **193** (2-4): 193-203
127. Gomez JC, Yamada M, Martin JR, Dang H, Brickey WJ, Bergmeier W, Dinauer MC, Doerschuk CM. Mechanisms of Interferon-γ Production by Neutrophils and Its Function during *Streptococcus pneumoniae* Pneumonia. *Am J Respir Cell Mol Biol* (2015); **52** (3): 349-64

128. Rynda-Apple A, Harmsen A, Erickson AS, Larson K, Morton RV, Richert LE, Harmsen AG. Regulation of IFN-γ by IL-13 dictates susceptibility to secondary postinfluenza MRSA pneumonia. *Eur J Immunol* (2014); **44** (11): 3263-72
129. Sun K, Metzger DW. Inhibition of pulmonary antibacterial defense by interferon-gamma during recovery from influenza infection. *Nat Med* (2008); **14** (5): 558-64
130. Suwara MI, Green NJ, Borthwick LA, Mann J, Mayer-Barber KD, Barron L, Corris PA, Farrow SN, Wynn TA, Fisher AJ, Mann DA. IL-1α released from damaged epithelial cells is sufficient and essential to trigger inflammatory responses in human lung fibroblasts. *Mucosal Immunol* (2014); **7** (3): 684-93
131. Weber K, Roelandt R, Bruggeman I, Estornes Y, Vandenabeele P. Nuclear RIPK3 and MLKL contribute to cytosolic necrosome formation and necroptosis. *Commun Biol* (2018); doi: 10.1038/s42003-017-0007-1
132. Jouan-Lanhouet S, Arshad MI, Piquet-Pellorce C, Martin-Chouly C, Le Moigne-Muller G, Van Herreweghe F, Takahashi N, Sergent O, Lagadic-Gossmann D, Vandenabeele P, Samson M, Dimanche-Boitrel MT. TRAIL induces necroptosis involving RIPK1/RIPK3-dependent PARP-1 activation. *Cell Death Differ* (2012); **19** (12): 2003-14
133. Li T, Morgan MJ, Choksi S, Zhang Y, Kim YS, Liu ZG. MicroRNAs modulate the noncanonical NF-κB pathway by regulating IKKα expression during macrophage differentiation. *Nat Immunol* (2010); **11** (9): 799-805
134. Sun SC. The non-canonical NF-κB pathway in immunity and inflammation. *Nat Rev Immunol* (2017); **17** (9): 545-58
135. Wright SD, Ramos RA, Tobias PS, Ulevitch RJ, Mathison JC. CD14, a receptor for complexes of lipopolysaccharide (LPS) and LPS binding protein. *Science* (1990); **249** (4975): 1431-3
136. Malley R, Henneke P, Morse SC, Cieslewicz MJ, Lipsitch M, Thompson CM, Kurt-Junes E, Paton JC, Wessels MR, Golenbock DT. Recognition of pneumolysin by Toll-like receptor 4 confers resistance to pneumococcal infection. *Proc Natl Acad Sci USA* (2003); **100** (4): 1966-71
137. Srivastava A, Henneke P, Visintin A, Morse SC, Martin V, Watkins C, Paton JC, Wessels MR, Golenbock DT, Malley R. The apoptotic response to pneumolysin is Toll-like receptor 4 dependent and protects against pneumococcal disease. *Infect Immun* (2005); **73** (10): 6479-87

138. Branger J, Knapp S, Weijer S, Leemans JC, Pater JM, Speelman P, Florquin S, van der Poll T. Role of Toll-like receptor 4 in gram-positive and gram-negative pneumonia in mice. *Infect Immun* (2004); **72** (2): 788-94

139. Roeder A, Kirschning CJ, Rupec RA, Schaller M, Weindl G, Korting HC. Toll-like receptors as key mediators in innate antifungal immunity. *Med Mycol* (2004); **42** (6): 485-98

8. List of publications

Berger S, **Goekeri C**, Gupta SK, Vera J, Dietert K, Behrendt U, Lienau J, Wienhold SM, Gruber AD, Suttorp N, Witzenrath M, Nouailles G. Delay in antibiotic therapy results in fatal disease outcome in murine pneumococcal pneumonia. *Crit Care* (2018); **22** (1): 287

9. Acknowledgements

First and foremost, I would hereby like to thank Prof. Dr. Martin Witzenrath for providing me with the opportunity to join his group to work on projects that have been nothing short of interesting and stimulating. His support, both scientifically and financially, has always been in favor of his students and has without a doubt created a collaborative working atmosphere that advocates critical and outside-the-box thinking that is a fundamental of scientific research. I would also like to thank the ZIBI Graduate School for granting me the chance to be part of their graduate program and financing my first year as a PhD student. With the regular seminars, retreats and various training courses on offer, being part of the graduate school has undoubtedly boosted my scientific knowledge, collaboration opportunities with fellow scientists, and provided an opportunity to voice my opinions for changes and improvements needed in the scientific field together with fellow PhD students also part of the graduate school.

I owe a special thank you to my one and only supervisor Dr. Geraldine Nouailles, who has been my role model not only in terms of becoming a fearless scientist, but also as a wonderful, compassionate human being. She has helped me develop a strong work ethic and has always been there for me, through thick and thin. I'm sure that she will continue being a strong and positive influence on me after my studies. I would also like to acknowledge Ulrike Behrendt, Luiz Gustavo Teixeira Alves, Kim Lyons Hernandez, Dr. Sarah Berger, Dr. Birgitt Gutbier, Dr. Katrin Reppe and Dr. Sandra Wienhold for their tireless help with experiments, consultations and managing the animal house.

Despite not being physically present in the lab, my family, partner and friends have been supporting me endlessly in the background and have always reminded me that at the end of the storm, there's a golden sky. Their support and motivation cannot be understated. Finally, I would like to acknowledge Prof. Dr. Rupert Mutzel for being my internal supervisor and for reviewing and grading my thesis. An eternal thank you to everyone.

Abbreviations

−/−	Knockout
$^{2}H_20$	Heavy water
AEC	Alveolar epithelial cell
AM	Resident alveolar macrophage
AML	Acute myeloid leukemia
AMP	Antimicrobial peptide
ANOVA	Analysis of variance
BAL	Bronchoalveolar lavage
BALC	BAL cells
BALF	BAL fluid
BM-PMN	Bone marrow neutrophil
BSA	Bovine serum albumin
CAP	Community Acquired Pneumonia
CCL	C-C chemokine ligand
CCR	C-C chemokine receptor
C/EBP	CCAAT enhancer binding protein
CD	Cluster of differentiation
CDC	Centers for Disease Control and Prevention
CFU	Colony forming unit
Cnx	Connexin
COPD	Chronic obstructive pulmonary disease
CRISPR	Clustered regularly interspaced short palindromic repeats
cRPMI	Complete Roswell Park Memorial Institute
CXCL	C-X-C motif chemokine cigand

CXCR	C-X-C motif chemokine receptor
D39 WT	Wild-type S. pn. serotype 2
D39 GFP	GFP-expressing S. pn. serotype 2
D39 Δply	Pneumolysin-deficient S. pn. serotype 2
DC	Dendritic cell
DEPC	Diethylpyrocarbonate
DGCR	DiGeorge syndrome critical region
DMEM	Dulbecco's modified eagle medium
DSS	Dextran sodium sulfate
E2F	E2F transcription factor
EDTA	Ethylenediaminetetraacetic acid
eMACS	Epithelial MACS buffer
EMT	Epithelial-mesenchymal transition
Eno	Alpha-enolase
EpiC	Epithelial cell
FACS	Fluorescence associated cell sorting
FCS	Fetal calf serum
Fig.	Figure
FVD	Fixable viability dye
GFP	Green fluorescent protein
G-CSF	Granulocyte colony-stimulating factor
GM-CSF	Granulocyte-macrophage colony-stimulating factor
HBSS	Hank's balanced salt solution
HEPES	4-(2-hydroxyethyl)-1-piperazineethanesulfonic acid
HIV	Human immunodeficiency virus
IAV	Type A influenza virus
ICAM	Intercellular adhesion molecule
IFN	Interferon
Ig	Immunoglobulin
IKK	IκB kinase
IL	Interleukin

ILC	Innate lymphoid cell
iM	Inflammatory monocyte/macrophage
IPD	Invasive pneumococcal disease
IRF	Interferon regulatory factor
JAM	Junctional adhesion molecule
K. pneumoniae	*Klebsiella pneumoniae*
kDa	Kilodalton
L-glu	L-glutamine
LFA	Lymphocyte function-associated antigen
LPS	Lipopolysaccharide
LTA	Lipoteichoic acid
$Ly6C^{hi}$ iM	Recruited inflammatory monocyte
LytA	Autolysin
mAb	Monoclonal antibody
Mac-1	Macrophage-1 antigen
MACS	Magnetic associated cell sorting
MARCO	Macrophage receptor with collagenous structure
Mef2c	Myocyte enhancer factor-2c
MHC	Major histocompatibility complex
miRNA	MicroRNA
miR-223	MicroRNA-223
MIP-2	Macrophage inflammatory protein 2
MOI	Multiplicity of infection
MLKL	Mixed-lineage kinase domain like
MPO	Myeloperoxidase
mRNA	Messenger RNA
Mtb	*Mycobacterium tuberculosis*
MyD88	Myeloid differentiation primary response 88
NADPH	Nicotinamide adenine dinucleotide phosphate reduced
NanA	Neuraminidase

NETs	Neutrophil extracellular traps
NF-κB	Nuclear factor 'kappa-light-chain-enhancer' of activated B cells
NFI-A	Nuclear factor 1 A-type
NK	Natural killer cell
NLR	Nucleotide oligomerization domain (NOD)-like receptor
NLRP	NLR family, pyrin domain-containing
NSCLC	Non-small cell lung carcinoma
OD	Optical density
oncomiR	Oncogenic microRNA
p.i.	Post-infection
P/S	Penicillin streptomycin
PAMP	Pathogen-associated molecular pattern
PARP	Poly (ADP-Ribose) polymerase
PBS	Phosphate-buffered saline
PCV	Pneumococcal conjugate vaccine
PFA	Paraformaldehyde
pIgR	Polymeric immunoglobulin receptor
Ply	Pneumolysin
PMA	Phorbol myristate acetate
PMN	Polymorphonuclear neutrophil
Pol	Polymerase
PPCV	Pneumococcal polysaccharide conjugate vaccine
PRR	Pathogen recognition receptor
Psa	Pneumococcal surface antigen
PSGL	P-selectin glycoprotein ligand
Psp	Pneumococcal surface protein
PU.1	Spi-1 transcription factor
RIPK	Receptor interacting protein kinase
RISC	RNA-induced silencing complex
RLR	Retinoic acid-inducible gene-I (RIG-I)-

	like receptor
ROS	Reactive oxygen species
RQ	Relative quantification
S. aureus	*Staphylococcus aureus*
S. pn.	*Streptococcus pneumoniae*
SEM	Standard error of mean
SPF	Specific pathogen free
STIM	Stromal interaction molecule
TGF	Transforming growth factor
Th	T helper
THY	Todd Hewitt Browth medium supplemented with 0.5% yeast
TIGR4	S. pn. serotype 4
TLR	Toll-like receptor
TNF	Tumor necrosis factor
TRAIL	TNF-related apoptosis-inducing ligand
TRAM	TRIF-related adaptor molecule
TRIF	TIR-domain-containing adapter-inducing interferon-β
UTR	Untranslated region
VEGF	Vascular endothelial growth factor
VILI	Ventilator-induced lung injury
WT	Wild-type

Appendix 1: Materials

Appendix 1.1: Instruments

Instrument	Specification	Company
Autoclave	Tuttnauer Systec 2540 EL	Systec GmbH (Germany)
Balance	Sartorius, MC 5 (-OCE)	Sartorius AG (Germany)
Flow cytometer	BD FACSCanto II	BD (Germany)
Homogenizer	gentleMACS™ Dissociator	Miltenyi Biotec (Germany)
Incubator	Heraeus Type BB 6220 O^2	Kendro Laboratory Products (Germany)
Incubator	TH 30	Edmund Bühler (Germany)
Laminar flow hood	Hera Safe Type HS 12	Kendro Laboratory Products (Germany)
pH-Meter	FiveEasy™ pH/mV Meter	Mettler-Toledo (USA)
Microplate reader	Multiskan™ FC Microplate Photometer	Thermo Fisher Scientific (USA)
Real-Time PCR System	StepOnePlus	Applied Biosystems (USA)
Red light	Bosotherm 4000	Bosch + Sohn GmbH (Germany)
Spectrophotometer	Multiskan™ Mikrotiterplatten-Photometer	Thermo Fisher Scientific (USA)
Spectrophotometer	Scanning Spectrophotometer, Uvikon XL	BioTek Instruments (USA)
Surgical instruments		Fine Science Tools GmbH (Germany)
Thermometer	BAT-12 MicroprobeThermometer	Physitemp Instruments, Inc. (USA)
Tracheal cannula		Hugo Sachs Elektronic (Germany)
Vortexer	Vortex-Genie 2® Model G-560E	Scientific Industries, Inc. (USA)
Water bath	SW23 Schüttelwasserbad	Julabo GmbH (Germany)
Water bath	WBT 6	Carl Roth (Germany)

Appendix 1.2: Consumables

Product	Specification	Company
Adhesive plate covers	Optical Adhesive Covers (DNA/RNase/PCR Inhibitors free)	Applied Biosystems (USA)
Cannula 18 G	Sterican® G 18 x 1/2”	B. Braun (Germany)
Cannula 20 G	Sterican® G 20 x 1/2”	B. Braun (Germany)
Cannula 26 G	Sterican® G 26 x 1/2”	B. Braun (Germany)
Cannula 27 G	BD Microlance™ 3	BD (Germany)
Capillary blood collection tube	Microvette® 500	Sarstedt (Germany)
Cell strainer (70 µm)	EASYstrainer™ cell strainer	Greiner Bio-One (Austria)
Cell strainer (100 µm)	EASYstrainer™ cell strainer	Greiner Bio-One (Austria)
Centrifuge tubes (15, 50 ml)	Falcon® conical centrifuge tube	Corning (USA)
Cuvette	Semi-micro cuvette, PS	Sarstedt (Germany)
Disposable cup (100 ml)	Disposable cup, PP	Sarstedt (Germany)
FACS tube (5 ml)	Falcon® 5 ml round bottom high clarity PP test tube	Corning (USA)
Gloves		B. Braun (Germany)
Homogenizer tubes	gentleMACS™ M Tubes	Miltenyi Biotec (Germany)
Inoculation loop		Sarstedt (Germany)
Microtiter plate	96 wells	Bethyl Laboratories, Inc. (USA)
Pipet tips (0.1-10 µl)	ClearLine filter tips	Dutscher (France)
Pipet tips (100 µl)	ClearLine filter tips	Dutscher (France)
Pipet tips (200 µl)	Filter tips	Biozym Scientific GmbH (Germany)
Pipet tips (1000 µl)	ClearLine filter tips	Dutscher (France)
Pre-Separation Filters (30 µm)		Miltenyi Biotec (Germany)
Reaction tubes (0.5, 1.5, 2.0 ml)	SafeSeal reaction tube, PP	Sarstedt (Germany)

Reaction tubes (1.5 ml)	Biosphere™ SafeSeal, DNase/RNase free	Sarstedt (Germany)
Reaction plate (96 wells, 0.1 ml)	MicroAmp® Fast 96-Well Reaction Plate (DNA/RNA/RNase free)	Applied Biosystems (USA)
Serological pipet (5, 10, 25 ml)	Falcon™, PS	Corning (USA)
Syringe (1 ml)	Omnifix® F Solo (1 ml)	B. Braun (Germany)
Syringe (2, 5, 10 ml)	BD Discardit™ II	BD (Germany)
Tissue culture dish	TC dish 35, PS	Sarstedt (Germany)
Tissue culture dish	TC dish 60, PS	Sarstedt (Germany)
Tissue culture plate	TC plate, 48 wells	VWR (USA)
Vacuum Filter/Storage Bottle System (500 ml)	Vacuum Filter, PS, nonpyrogenic	Corning (USA)

Appendix 1.3: Reagents

Reagent	**Company**
Ammonium acetate (5M)	Invitrogen (USA)
Bovine Serum Albumin (BSA)	Sigma-Aldrich Chemie GmbH (Germany)
cOmplete™, Mini Protease Inhibitor Cocktail	Roche Diagnostics GmbH (Germany)
CountBright™ Absolute Counting Beads	Thermo Fisher Scientific (USA)
DEPC Treated Water (Pyrogen-free)	Invitrogen (USA)
Ethanol, Absolute	Merck (Germany)
Ethanol, Absolute (Analytical Reagent Grade)	Fisher Scientific (USA)
FACSFlow™	BD (Germany)
FACS™ Shutdown Solution	BD (Germany)
TaqMan™ Fast Advanced Master Mix	
Formaldehyde solution, buffered (4%)	AppliChem (Germany)
Glycogen (5 mg/ml)	Invitrogen (USA)
Isopropanol	Serva (Germany)
MagniSort™ Streptavidin Negative Selection Beads	Sigma-Aldrich Chemie GmbH (Germany)
TaqMan™ Fast Advanced Master Mix	Applied Biosystems (USA)

TaqMan™ MicroRNA Assay (hsa-miR-223, Assay ID 002295)	Applied Biosystems (USA)
TaqMan™ MicroRNA Control Assay (snoRNA202, Assay ID 001232)	Applied Biosystems (USA)
Thilo Tears Eye Gel	Alcon Pharma GmbH (Germany)
TRIzol™ Reagent	Invitrogen (USA)
UltraPure™ LMP Agarose	Invitrogen (USA)
UltraPure™ Distilled Water (DNase/RNase free)	Invitrogen (USA)

Appendix 1.4: Enzymes

Enzyme	Company
Collagenase II	Biochrom (Germany)
DNase I	AppliChem (Germany)
Dispase	Corning (USA)

Appendix 1.5: Antibodies for flow cytometry

Epitope	Clone	Fluorochrome	Concentration	Company
CD11b	M1/70	PE-Cy7	0.2 mg/ml	BD (Germany)
CD11c	N418	Cy5	1 mg/ml	ATCC (USA)
CD11c	N418	APC	0.2 mg/ml	BioLegend (USA)
CD14	Sa14-2	APC	0.5 mg/ml	BioLegend (USA)
CD16/CD32	2.4G2	Biotin	0.5 mg/ml	BD (Germany)
CD16/CD32	2.4G2	Unconjugated	0.2 mg/ml	BD (Germany)
CD31	MEC 13.3	Biotin	0.5 mg/ml	BD (Germany)
CD326 (Ep-CAM)	G8.8	PE	0.2 mg/ml	BioLegend (USA)
CD45	30-F11	Biotin	0.5 mg/ml	BD (Germany)
CD45	30-F11	FITC	0.5 mg/ml	BD (Germany)
CD45	30-F11	V500	0.2 mg/ml	BD (Germany)
CD54 (ICAM-1)	YN1/1.7.4	FITC	0.5 mg/ml	BioLegend (USA)
CD62L	MEL-14	APC	0.2 mg/ml	eBioscience

CXCR1/IL-8 RA	1122A	PE	-	R&D Systems (USA)
CXCR2	TG11/CXCR2	PerCP-Cy5.5	0.2 mg/ml	BioLegend (USA)
GR-1	RB6-8C5	FITC	1 mg/ml	ATCC (USA)
LFA-1	H155-78	PE	0.2 mg/ml	BioLegend (USA)
Ly6C	AL-21	V450	0.2 mg/ml	BD (Germany)
Ly6G	1A8	Biotin	0.5 mg/ml	BioLegend (USA)
Ly6G	1A8	PerCP-Cy5.5	0.2 mg/ml	BD (Germany)
Ly6G	1A8	V450	0.2 mg/ml	BD (Germany)
Ly6C	HK1.4	BV510	100 µg/ml	BioLegend (USA)
MHCII	M5/114.15.2	AlexaFluor 700	0.2 mg/ml	eBioscience
Siglec F	E50-2440	BV421	0.5 mg/ml	BD (Germany)

Appendix 1.6: Buffers

Buffer	**Constituents**	**Company**
1x PBS	Phosphate-buffered Saline	Thermo Fisher Scientific (USA)
FACS Buffer	1x PBS 0.2% BSA	Thermo Fisher Scientific (USA) Sigma-Aldrich Chemie GmbH (Germany)
eMACS buffer	1x PBS 3% FCS (heat inactivated) 10 mM EDTA	Thermo Fisher Scientific (USA) CAPRICORN Scientific (Germany) Thermo Fisher Scientific (USA)
HBSS (+Ca^{2+} +Mg^{2+})	Hank's Balanced Salt Solution	Thermo Fisher Scientific (USA)
HBSS (-Ca^{2+} -Mg^{2+})	Hank's Balanced Salt Solution	Thermo Fisher Scientific (USA)
MACS buffer	1x PBS 0.5% BSA	Thermo Fisher Scientific (USA) Sigma-Aldrich Chemie GmbH (Germany)
Red Blood Cell Lysis Buffer	0.01 M $KHCO_3$ 0.155 M NH_4Cl	Merck (Germany) Merck (Germany)

	0.1 mM EDTA in distilled water, pH 7.5	Thermo Fisher Scientific (USA) B. Braun (Germany)
Annexin V Binding Buffer (1x)	Distilled Water (9 parts) 10x Binding Buffer (1 part)	B. Braun (Germany) eBioscience

Appendix 1.7: Media

Medium	**Constituents**	**Company**
cRPMI	RPMI 1640 10% FCS (heat inactivated) 1% HEPES buffer (1M) 1% L-Glutamine (200 mM, 100x) 1% Penicillin/Streptomycin (10.000 U/ml)	PAA Laboratories GmbH (Austria) CAPRICORN Scientific (Germany) Life Technology (USA) Life Technology (USA) Life Technology (USA)
Bacterial Growth Medium	Distilled H_2O 0.5% yeast extract 3% Todd Hewitt Bouillon	B. Braun (Germany) BD (Germany) BD (Germany)
Bacterial Freezing Medium	20% Glycerin 80% Bacterial Growth Medium	Merck (Germany) Self-produced

Appendix 1.8: Kits

Kit	**Company**
Annexin V Apoptosis Detection Kit APC	eBioscience
FoxP3/Transcription Factor Staining Buffer Set	Thermo Fisher Scientific (USA)
LEGENDplex™ Mouse Inflammation Panel (13-plex) with V-bottom Plate	BioLegend
Mouse Albumin ELISA Quantitation Set	Bethyl Laboratories, Inc. (USA)
Mouse CXCL1/KC DuoSet ELISA	R&D Systems (USA)
Mouse CXCL2/MIP-2 DuoSet ELISA	R&D Systems (USA)
Mouse LIX DuoSet ELISA	R&D Systems (USA)
Mouse VEGF DuoSet ELISA	R&D Systems (USA)
MPO Mouse ELISA kit	Hycult Biotech (The Netherlands)

TaqMan™ MicroRNA Reverse Transcription Kit	Applied Biosystems™ (USA)

Appendix 1.9: Narcosis

Narcosis	Constituents	Company
For Infection of Mice	3 ml 0.9% NaCl 3 ml 10% Ketamine 2.4 ml Xylazin (20 mg/ml)	B. Braun (Germany) CP-pharma (Germany) CP-pharma (Germany)
For Preparation of Mice	2.25 ml 0.9% NaCl 0.5 ml 10% Ketamine 0.25 ml Xylazin (20 mg/ml)	B. Braun (Germany) Bela-pharm (Germany) CP-Pharma (Germany)

Appendix 1.10: Software

Software	Company
GraphPad Prism, V7	GraphPad (USA)
FACS Diva	BD (Germany)
FlowJo, V10	FlowJo, LLC (USA)
LEGENDplex™, V8	BioLegend (USA)
SkanIt RE, 4.1	Thermo Fisher Scientific (USA)
StepOnePlus Software	Applied Biosystems (USA)